Active Knit Actuation Architectures

by

Julianna M. Abel

A dissertation submitted in partial fulfillment
of the requirements for the degree of
Doctor of Philosophy
(Mechanical Engineering)
in the University of Michigan
2014

Doctoral Committee:

Professor Diann Erbschole Brei, Co-Chair
Associate Research Scientist Jonathan E. Luntz, Co-Chair
Assistant Professor Samantha Hayes Daly
Professor John A. Shaw

To Josh

ACKNOWLEDGMENTS

I would like to thank my advisors, Diann Brei and Jon Luntz, for their guidance, support, and encouragement throughout my Ph.D. research at the University of Michigan. I have learned so much from Diann and Jon and could not have completed this work without them. Also, my committee members, John Shaw and Sam Daly, provided significant guidance and support in this process, especially at the very end of this work, for which I am thankful.

I would also like to thank my lab mates, both past and present, Brent Utter, WonHee Kim, Tizoc Cruz-Gonzalez, Suhant Ranga, Clover Aguayo, John Redmond, Anupam Pathak, Brian Barnes, Isabel Czarnocki, Clare McNamara, Shishira Nagesh, Monica Toma, Poorna Mane, Josh Radice, Paul Alexander, Jim Otten, and Joe Shaktman. Their support was pivotal to the completion of this work. I was also lucky to have the opportunity to work with great undergraduate students – Miquella Trujillo, Anilash Panikulangara, Pete Gomes, and Ben Pascoe – who contributed to this work.

Most importantly, I would like to thank my family and friends for their love and support. My husband, Josh, who has provided me with emotional support through this entire process. My entire family – Jay, Donna, MaryAnn, Les, Jason, Jen, Willie, Val, Anna, Alyssa, Isaac, Hannah, Mike, Leah, Max, Granny, Pa, Gloria, Lee, Patty, and Ruth – has always encouraged me to pursue my goals. My local friends – Mike, Alison, Jill, Jason, Jeff, and all my friends at volleyball – have made Ann Arbor feel like home. I would like to thank Jess, Sarah, and Noeet, who are always there for me even when I haven't seen them in years.

Finally, I am thankful to all those who have invested in my education and career by supporting this work – the Air Force Office of Scientific Research for support under grant FA9550-09-1-0217, the National Science Foundation through the Graduate Research Fellowship Program, the NASA Harriett G. Jenkins Predoctoral Fellowship Project, the GM-UM Smart Materials and Structures Collaborative Research Laboratory, Rackham Graduate School and the Mechanical Engineering Department at the University of Michigan.

TABLE OF CONTENTS

Dedication ii

Acknowledgments iii

List of Tables ix

List of Figures x

Abstract xii

Chapter 1. Introduction 1

1.1. GROWING ACTUATION NEED 1

1.2. CURRENT ACTUATOR STATE OF THE ART 2
1.2.1. Conventional Actuators 2
1.2.2. Smart Material Actuators 3
1.2.3. Smart Material Actuator Architectures 3
1.2.3.1. Frequency Leveraged Actuation Architectures 4
1.2.3.2. Combinatorial (Building Block) Actuation Architectures 4
1.2.3.3. Externally Leveraged Actuation Architectures 5
1.2.3.4. Internally Leveraged Actuation Architectures 5

1.3. ACTIVE KNITS 7
1.3.1. Active Knits Architecture 7
1.3.2. Active Knits Operation 9
1.3.3. Research Issues 10
1.3.3.1. Hierarchical Architecture Classification 11
1.3.3.2. Active Knit Modeling 11
1.3.3.3. Experimental Validation 12
1.3.3.4. Case Study 12

1.4. RESEARCH GOALS AND OBJECTIVES 12

1.5. RESEARCH APPROACH 13
1.5.1. Active Knit Hierarchy 13
1.5.2. Two-Dimensional Analytical Knitted Loop Model 15

1.5.3. Three-Dimensional Analytical Reduced Order Knit Pattern Model 16
1.5.4. Feasibility Demonstration Study 17

1.6. Outcomes and Contributions 18

Chapter 2. Active Knit Hierarchical Architecture 21

2.1. Materials and Methods 23

2.2. Level 1: Knitted Loops 24

2.3. Level 2: Knit Patterns 25
2.3.1. Solid Knit Pattern – Stockinette 26
2.3.2. Horizontally Striped Patterns – Garter and Welt 27
2.3.3. Vertically Striped Patterns – Rib 30
2.3.4. Diagonally Striped Patterns – Seed 31

2.4. Level 3: Grid Patterns 32

2.5. Level 4: Restructured Grids 34
2.5.1. Post-Knitting Connection 34
2.5.2. Course-Wise Restructuring 37
2.5.3. Grid Cell Merging 38
2.5.4. Re-Ordered Grids 40

2.6. Active Knit Hierarchy Conclusions 41

Chapter 3. Two-Dimensional Analytical Model of Planar Active Knitted Loops 44

3.1. Two-Dimensional Planar Loop Model Nomenclature 46

3.2. Garter Knit Pattern Architecture and Operation 47
3.2.1. Garter Knit Pattern Architecture 47
3.2.2. Garter Knit Pattern Operation 48
3.2.2.1. Austenite Free State 49
3.2.2.2. Austenite Extended State 50
3.2.2.3. Martensite Extended State 50
3.2.2.4. Austenite Contracted State 50

3.3. Analytical Garter Knit Pattern Model 51
3.3.1. Assumptions 52
3.3.2. Geometric Relations 53
3.3.3. Austenite Free Reference State 55
3.3.3.1. Force Equilibrium Interactions 56

3.3.3.2. Analysis of Governing Differential Equations 57
3.3.3.2.1. Lower Loop Segment AB 57
3.3.3.2.2. Upper Loop Segment BC 60
3.3.3.3. Kinematic Relations 62
3.3.3.4. Kinetic Relations 63
3.3.4. Austenite and Martensite Extended States 63
3.3.4.1. Kinematic Relations 64
3.3.4.2. Kinetic Relations 65
3.3.5. Austenite Contracted State 66
3.3.5.1. Kinematic Relations 66
3.3.5.2. Kinetic Relations 67
3.3.6. Textile Actuation Prediction 68

3.4. GARTER KNIT PATTERN EXPERIMENTAL VALIDATION 68
3.4.1. SMA Material Properties 69
3.4.2. Active Knit Prototype 70
3.4.3. Experimental Method 71
3.4.4. Austenite and Martensite Extended States 72
3.4.5. Austenite Contracted State 74
3.4.6. Net Actuation 75

3.5. TWO-DIMENSIONAL ANALYTICAL MODEL CONCLUSIONS 77

Chapter 4. Three-Dimensional Segment Superposition Analytical Modeling Approach ... 80

4.1. SEGMENT SUPERPOSITION MODELING APPROACH 81
4.1.1. Identify Unit Cell 82
4.1.2. Segment Unit Cell 83
4.1.3. Enumerate Simple Mechanical Effects Models 83
4.1.4. Predict Force-Deflection Performance of Simple Effect Models 84
4.1.5. Superimpose Force-Deflection Model 84

4.2. SEGMENT MODEL OF 2X2 RIB KNIT ACTUATOR ARCHITECTURE 85
4.2.1. 2x2 Rib Knit Actuator Architecture and Operation 86
4.2.1.1. 2x2 Rib Knit Architecture 86
4.2.1.2. Rib Knit Pattern Operation 87
4.2.1.2.1. Martensite Compressed State 88
4.2.1.2.2. Austenite Expanded State 88
4.2.2. Identify Unit Cell of 2x2 Rib Knit Actuator Architecture 89
4.2.3. Segment Unit Cell of 2x2 Rib Knit Actuator Architecture 89
4.2.4. Enumerate Simple Effect Model of 2x2 Rib Knit Actuator Architecture 92
4.2.5. Predict Force-Deflection Performance of Simple Effect Model of 2x2 Rib Knit Actuator Architecture 93
4.2.5.1. Assumptions 93
4.2.5.2. Force Equilibrium Interactions 94

4.2.5.2.1. Torsional Spring Representation 94
4.2.5.2.2. Austenite and Martensite Free States 95
4.2.5.2.3. Loaded State Heights 96
4.2.5.2.4. Textile Performance Prediction 96

4.3. Rib Knit Pattern Experimental Validation 97
4.3.1. SMA Material Properties 97
4.3.2. Active Knit Prototypes 98
4.3.3. Experimental Method 100
4.3.3.1. Martensite Compressed and Austenite Expanded 101
4.3.3.2. Net Actuation 103

4.4. Segment Superposition Three-Dimensional Model Conclusions 106

Chapter 5. Feasibility Demonstration Study 109

5.1. Rib Knit pattern Architecture, Operation, and Configurations 111
5.1.1. Architecture 111
5.1.2. Operation 112
5.1.2.1. Martensite Compressed State 113
5.1.2.2. Austenite Expanded State 114
5.1.3. Rib Knit pattern Architectural Configurations 114
5.1.3.1. Stacking 115
5.1.3.2. Nestling 116

5.2. Rib Knit Pattern Experimental Evaluation 116
5.2.1. Contour Bump Specifications 116
5.2.2. Rib Knit Pattern Prototype Fabrication 117
5.2.3. Experimental Setup and Procedure 118
5.2.4. Experimental Results 119
5.2.4.1. Single Rib Knit Pattern Prototypes 120
5.2.4.2. Stacked Rib Knit Pattern Prototype 123
5.2.4.3. Nestled Rib Knit Pattern Prototype 123
5.2.4.4. Stacked-Nestled Rib Knit Pattern Prototypes 125

5.3. Feasibility Demonstration Study Conclusions 127

Chapter 6. Conclusions 130

6.1. Research Overview 131
6.1.1. Active Knit Hierarchy 131
6.1.2. Two-Dimensional Analytical Knitted Loop Model 133
6.1.3. Three-Dimensional Analytical Reduced Order Knit Pattern Model 134
6.1.4. Feasibility Design Study 136

6.2. CONTRIBUTIONS 137

6.3. CLOSING 139

References 141

LIST OF TABLES

Table 1. Summary of Prototypes and Experimental Results. 42
Table 2. Impact of Hierarchical Level on Actuation Behavior. 43
Table 3. Garter Knit Pattern Prototype Geometric Parameters. 71
Table 4. Nomenclature for Segment Model of 2x2 Rib Knit Actuator Architecture 85
Table 5. Geometric Parameters of 2x2 Rib Knit Pattern Prototypes 98
Table 6. Predictive Capabilities of 2x2 Rib Knit Actuator Architecture Segment Model 104
Table 7. Rib Knit Pattern Prototype Parameters. 118
Table 8. Rib Knit Pattern Experimental Results. 127

LIST OF FIGURES

Figure 1. Active Knit Architecture. 8
Figure 2. Active Knit Operation. 10
Figure 3. Hierarchical Knit Architecture. 22
Figure 4. Knitted Loops. 24
Figure 5. Solid Knit Pattern – Stockinette. 26
Figure 6. Horizontally Striped Knit Pattern – Garter. 28
Figure 7. Horizontally Striped Knit Pattern – Welt. 29
Figure 8. Vertically Striped Knit Pattern – Rib. 30
Figure 9. Diagonally Striped Knit Pattern – Seed. 32
Figure 10. Grid Pattern. 33
Figure 11. Restructured Grid – Post-Knitting Connection. 35
Figure 12. Restructured Grid – Course-Wise Restructuring. 37
Figure 13. Restructured Grid – Grid Cell Merging. 39
Figure 14. Restructured Grid – Re-Ordered Grids. 40
Figure 15. Basic Garter Knit Pattern Architecture. 48
Figure 16. Active Garter Knit Pattern Operational States. 49
Figure 17. Planar Knit Unit Cell. 52
Figure 18. Garter Knit Unit Cell Free Body Diagram. 54
Figure 19. Loop Segment Free Body Diagrams. 59
Figure 20. Experimental Material Properties of SMA Wire. 69
Figure 21. Garter Knit Pattern Active Knit Prototype. 70
Figure 22. Garter Knit Pattern Experimental Setup. 72
Figure 23. Austenite Extended State. 74
Figure 24. Martensite Extended State. 74
Figure 25. Austenite Contracted State. 75
Figure 26. Garter Knit Actuation Results. 75

Figure 27. Rib Knit Pattern Architecture. 86
Figure 28. Rib Knit Pattern Operation. 87
Figure 29. Unit Cell Identification for 2x2 Rib Knit Actuator Architecture. 89
Figure 30. Segmented Unit Cell of 2x2 Rib Knit Actuator Architecture. 91
Figure 31. Geometry of segmented 2x2 rib knit unit cell. 92
Figure 32. Rib Constraint Regions. 93
Figure 33. Free body diagram of 2x2 rib knit pattern unit cell. 94
Figure 34. Experimental Material Properties of SMA Wire. 98
Figure 35. 2x2 Rib Knit Pattern Prototype. 99
Figure 36. Experimental Setup for Rib Prototypes. 100
Figure 37. 2x2 Rib Knit Actuator Architecture Experimental Procedure. 101
Figure 38. Experimental Results of 2x2 Rib Knit Actuation Architecture. 102
Figure 39. Net Actuation of 2x2 Rib Knit Actuation Architecture. 103
Figure 40. Constant Load Actuation Strain of 2x2 Rib Knit Actuator Architecture. 105
Figure 41. Rib Knit Architecture. 112
Figure 42. Rib Knit Pattern Operation. 114
Figure 43. Rib Knit Pattern Actuation Mechanism. 115
Figure 44. Architectural Configurations. 116
Figure 45. Rib Knit Pattern Prototype. 118
Figure 46. Experimental Setup for Rib Knit Pattern Prototypes. 119
Figure 47. Rib Knit Pattern Experimental Procedure. 120
Figure 48. Experimental Results of the Single Rib Knit Pattern Prototype. 121
Figure 49. Experimental Results of Rib Knit Pattern Architectural Configurations. 122
Figure 50. Experimental Results of Rib Knit Pattern Actuators for Flow Control Application. 125

ABSTRACT

Actuators move our world. While conventional and smart material actuators have enabled myriad applications, many advanced applications (e.g., morphing aircraft, deployable space structures, and medical devices) require complex, distributed, three-dimensional motions that are limited by current actuation capabilities. This dissertation explores a new cellular architectural actuator, active knits, and provides the fundamental scientific understanding of the active knit actuation architecture to enable the design, analysis, and synthesis of simultaneous large force and strain actuators that produce complex three-dimensionally distributed motions. The active knit architecture leverages a smart material fiber through a continuous network of hierarchically organized loops that generate complex motions (contraction, scrolling, coiling, accordion, arching, etc.), while simultaneously delivering high strain (10-600%) and force (1-100 N). This dissertation defines a four level active knit hierarchy (knitted loops, knit patterns, grid patterns, and restructured grids), establishing a language to design, synthesize, and analyze new actuators and a framework to explore the breadth of actuator motions. To provide high fidelity predictive capabilities of planar active knit actuators, a two-dimensional analytical model is derived using Euler-Bernoulli beam bending and Elastica theory assuming dual stiffness material behavior. To provide predictive capabilities of three-dimensional knit patterns early in the design process, a segment superposition modeling approach is developed that segments the unit cell and creates simple mechanical models that are superimposed to yield coarse prediction of the textile's global performance. All models were experimentally validated against shape memory alloy (SMA) active knit prototypes with strong correlation of the force-deflection and actuation performance, confirming predictive capabilities for this simultaneous large strain and force actuation architecture. To further demonstrate the actuation potential, an active flow control case study was conducted using rib pattern actuators. The study verified that active knits can generate the simultaneous large displacements (23 mm/75%) and forces (4.4 kPa/44.4 N) that are necessary for extreme applications. While further research will be necessary to bring active knits into practice, this research established the necessary language, models, and experimental techniques to provide the scientific understanding essential for design, analysis, and synthesis of this novel cellular actuator architecture – opening the door to applications not yet imagined.

Chapter 1. INTRODUCTION

Actuators move our world. While actuators have enabled myriad technologies, there are still countless applications that are limited by available actuation approaches. For example, there is a strong need in several application fields for simultaneous large force and displacement actuators that create complex, three-dimensional actuation motions distributed through a structure in a small package size. While conventional and smart material based technologies cannot fulfill this need, new cellular smart material architectures show great promise. The goal of this research was to develop the fundamental scientific understanding of the active knit actuation architecture, which has the ability to deliver simultaneous radical forces and strains in variety of complex, distributed actuation motions.

This chapter establishes the need for this new set of actuation capabilities and assesses different actuation approaches to meet the need. A promising approach, active knits, is identified and briefly described. The related research issues are discussed leading to goals and objectives to establish the foundation for this cellular actuation architecture.

1.1. GROWING ACTUATION NEED

There is a growing need for actuators capable of concurrent radical forces and strains that produce three-dimensionally complex motions, distributed throughout a structure in a small package size. This need is particularly evident in the aerospace sector, which has an interest in configurable multifunctional structures that have the ability to dramatically alter their shape, functionality or mechanical properties in response to environmental or operational conditions to improve aircraft efficiency [1]-[2]. One such multifunctional structure is morphing aircraft that can adjust their wing geometry to expand the aircrafts operational platform and allow it to efficiently maneuver over a large range of flight regimes [3]. Another application, active flow control, requires the implementation of a multifunctional structure to create a controlled and varied texture across a surface to delay or reattach a separated boundary layer in order to reduce surface drag and improve flight efficiency [4]-[8]. Additionally, deployable space structures such as

stabilization booms, solar arrays, communication reflectors, and telescopes need to be compactly stowed in launch vehicles then undergo radical deformations to recover the large structures in space [9]-[14].

Other areas, such as the medical device and automotive fields, would also greatly benefit from actuator advancements. For example, the medical field needs actuators that can produce large distributed strains that can be used in or on the human body to realize technologies that diagnosis, repair, and rehabilitate, such as field bandages and contracture tissue expanders that contract of expand over a large surface area [15], guided catheters that can navigate the complex curved conduits of the body [16], and implantable devices that can provide large mechanotransductive strains [17]. Similar needs arise in the automotive field to advance technologies that improve vehicle efficiency and customer satisfaction such as active air dams [18] and louvers [19] that provide flow control over the surface of the vehicle body and through the engine, morphing bumpers [19] that reshape areas of the body after an accident, and seat belts [20] that supply distributed restraint during rapid deceleration. These diverse applications illustrate a common need for actuators capable of simultaneous large forces and strains in the form of complex three-dimensionally distributed actuation motions.

1.2. CURRENT ACTUATOR STATE OF THE ART

Myriad applications (including medical devices, automotive, deployable structures, and aircraft) require advanced actuators that are capable of concurrent radical forces and strains while creating complex multi-dimensional actuation motions that are distributed throughout a structure. Substantial research has been conducted on actuator technologies; however, actuators capable of producing enhanced characteristics simultaneously have remained elusive.

1.2.1. Conventional Actuators

The proliferation of conventional actuators (electromagnetic, hydraulics, and pneumatics) has enabled countless applications. However, as demand for new applications increases a different genre of actuators are required to meet the application needs. There is a growing need for actuators capable of producing large three-dimensionally complex distributed actuation motions in a small package. Conventional actuators are established technologies that are capable of balancing force, stroke, and speed. However, they have difficulties providing more than point actuation. Because conventional actuators are typically point actuators they are not capable of producing distributed

actuation motions or complex out-of-plane motions without incorporating additional mechanism. Even if conventional actuators could create the desired motions they do not to meet the packaging requirement, which requires a high energy density. Most conventional actuators have energy densities orders of magnitude less than smart materials [21]. One exception is hydraulic actuators, which have similar energy density to that of Shape Memory Alloys (SMAs). While hydraulic actuators are energy dense, they have complex supporting infrastructure such as pumps and hydraulic lines that are large and difficult to package, making the system less than optimal.

1.2.2. Smart Material Actuators

Smart materials (materials that have the ability to transform energy from one domain to another) are energy dense actuators that have long held the promise of increasing the actuation authority and decreasing weight/size by an order of magnitude because of their high energy/power densities [21] (up to two or three orders of magnitude for Shape Memory Alloys vs. electromagnetic actuators). Unlike conventional actuators, smart materials are inherently distributed as they undergo deformation throughout their entire volume. While smart materials show promise to creating distributed actuation in a small package they still struggle to create simultaneous large strains and large forces. Unfortunately, smart materials that have large strains (greater than 100%), such as electroactive polymers and piezopolymers, have very low forces (in the milliNewton range) [22]-[25]. Alternatively, materials capable of modest force generation typically suffer small strains: 0.1-0.2% for piezoceramics, 1-2% for single crystals, 4-8% for shape memory alloys (SMA), and 3-5% for ferromagnetic SMAs [26]-[31]. Additionally, smart materials on their own are not capable of creating complex three dimensional motions.

1.2.3. Smart Material Actuator Architectures

While bulk smart materials cannot meet the growing actuation needs, they can be exploited in smart material actuator architectures to produce actuators capable of concurrent radical forces and strokes in the form of complex multi-dimensional actuation motions distributed throughout a structure. A smart material actuator architecture is the configuration of a raw form of a smart material into an actuator form that amplifies the force, displacement, and/or the type of motion produced by the base smart material. There are four types of smart material actuator architectures that have been employed to improve kinetic or kinematic actuation performance – frequency leveraged actuators, combinatorial actuators, externally leveraged actuators, and internally

leveraged actuators. Each of these actuator architectures enhance the capabilities of the base smart material by improving kinetic performance (either through enhanced force or displacement) and/or providing complex three dimensional motions.

1.2.3.1. Frequency Leveraged Actuation Architectures

Frequency leveraged actuators are smart material actuation architectures that accumulate a sequence of small deformations to produce larger actuation displacements. Numerous frequency leveraged architectures have been developed to enhance the displacements provided by the base smart material. For example, SMA ratchets combine a series of small ratchet steps to produce large linear actuation displacements, enabling applications such as implantable medical devices [17]. Piezoelectric inchworms use multiple individual actuators to clamp and progress a shaft through the actuator architecture [32], the individual steps enables the actuator to produce large precise motions such as those need for optics alignment and precision machining. A final example are piezoelectric ultrasonic actuators, which actuate the piezoelectric actuator at one of its resonant frequencies to create an acoustic wave that propagates the moving part along a smooth, low friction contact surface [33]. While ultrasonic actuators can be used for numerous large displacement high precision applications, their true strength is their enhanced energy density when compared to electromagnetic motors [34]. Frequency leveraged actuation architectures provide simultaneous large forces and displacements by enhancing actuator displacement but they are limited because they do not produce complex distributed motions.

1.2.3.2. Combinatorial (Building Block) Actuation Architectures

Combinatorial actuation architectures are building block actuators that enhance the force and/or displacement of smart material actuation architectures by combining individual actuators in series and/or parallel. The series and parallel assembly of leveraged architectures produce actuators with enhanced kinetic (force-displacement) performance by using the individual elements as building blocks or unit cells. For example, piezoelectric [35] and dielectric elastomer stacks [36] use individual pieces of material in series to produce enhanced displacements under the same applied load. Alternatively, bundles of SMA wires (parallel SMA wires) [37] have been used to enhance force output. Additionally, some leveraged actuation architectures (such as the piezoelectric Recurve [38] or C-block [39] can be used as building blocks to improve force and displacement output over that of individual actuators. Combinatorial actuators are the most

simplistic actuators that follow scaling rules for kinetic performance. While combinatorial actuators are a great, streamlined way to enhance the distributed force and displacement of actuators, they are limited in their ability to create three-dimensional complex motions.

1.2.3.3. Externally Leveraged Actuation Architectures

Externally leveraged actuation architectures connect the base smart material to external leveraging structures or mechanisms that transform the material output to produce a tailored performance to meet application needs. There are numerous types of externally leveraged actuators. Many externally leveraged architectures enhance the stroke provided by large force actuators (such as piezoelectric or magnetostrictive), or enhance the force output of large strain smart material actuators (such as EAPs). Other externally leveraged actuators are used as transducers that transfer lateral material displacements into actuator displacements in the normal direction. For example, piezoelectric Moonies [40], Cymbals [41], and X-frames [42], dielectric elastomer spiders [43], and smart material levers all provide actuation motions normal to the material actuation direction. Frequently, the material leveraging that improves the actuation motion is done so at the cost of actuator force output. Externally leveraged architectures can also be used to create shaped, distributed planar actuation. Dielectric elastomer bowties [43] and flexible frames [43] employ an external frame to pre-stress the base smart material and create uniquely shaped actuators; however, they provide small actuation loads. To create even more complex motions, smart material actuated compliant mechanisms [44]-[47] have been employed. While compliant mechanisms have been used to change the shape of a wing [44]-[47], the output motion created by compliant mechanisms is distributed across a surface rather than throughout a structure. All of these externally leveraged actuation architectures use a smart material to supply the actuation motion while external structure or mechanism produces the desired shape change. This increases the amount of non-actuating material in the structure and increases the overall size of the actuator, therefore reducing the energy density of the actuator. While externally leveraged actuation architectures are approaching complex motion, they are not able to provide simultaneous large forces and displacements, and if they do, the motions are not complex.

1.2.3.4. Internally Leveraged Actuation Architectures

Internally leveraged actuators use the internal stress in the structure to leverage the base smart material to provide enhanced actuation motions in an energy dense package. There are numerous

types of internally leveraged architectures that vary in complexity. The most simplistic are the internally leveraged geometries (such as SMA coil springs [48], SMA leaf springs [49], SMA torsion tubes [50], and EAP spring rolls [51]) that use the base smart material in a more complex state of stress (bending, torsion) to deliver a small set of basic actuation motions such as extension, bending, and torsion that are distributed throughout the actuator, but they do so with a sacrifice to the force of the actuator. A subclass of internally leveraged actuation architectures are induced strain actuators, which are composite actuators with multiple active elements or active elements mixed with passive elements that leverage the internal stresses of the smart material to create bending and torsional actuation motions. Various smart materials have been used to create active composites in the form of laminates [52][53], fibers [54]-[56], and particulates [57]. The motion output of the composite depends on the construction of the composite and the stress field of the material and can produce extension, bending, torsion, and combined motions. While active composites can generate mildly complex bending and twisting motions, the motions are not of the order desired for new applications and many composites suffer from debonding [54]. More sophisticated smart material composites, such as functionally graded piezoceramics [58], have led to the development more reliable composite structures and have the potential to create complex distributed motions, although not yet realized in applications.

Another type of internally leveraged actuation architectures is cellular actuators that use one (or more) unit cells of an internally leveraged smart material architecture by combining the unit cells in series and parallel to create two or three-dimensional structures; however research on cellular architectures has been limited. Smart material foams, such as shape memory polymer foam [59], have particulate inclusions or voids and are promising for self-healing structures, but the material distribution has not been optimized to achieve desired mechanical properties or obtain a predetermined shape upon actuation. Another promising cellular architecture is SMA honeycombs. Superelastic SMA honeycombs [60] have been experimentally tested with hexagonal and corrugated architectures that are capable of undergoing large, recoverable displacements under compressive loadings. Internally leveraged cellular architectures are extremely promising because through combinations of unit cells, the kinematic and kinetic performance of the actuator can be controlled. Cellular architectures could provide the ability to tailor the performance; the individual unit cells can be used as building blocks to amplify the kinetic performance and adjacent unit cells can be manipulated in non-uniform distributions so

that complex actuation motions can be designed and achieved. Cellular actuation architectures are an extremely promising approach that may have the ability to advance the capabilities of actuators and progress applications.

1.3. ACTIVE KNITS

Active knits are a novel type of internally leveraged cellular architecture that shows great promise. The internally leveraged network of unit cells that compose the active knit architecture enables complex distributed actuation motions with scalable radical kinetic performance. Active knits are capable of generating large strains beyond the base material because of their unique architecture and operation.

1.3.1. Active Knits Architecture

Active Knits are a smart material fiber based actuation architecture that provides complex three-dimensional distributed actuation motions with enhanced kinetic performance through a hierarchically organized cellular network of interlacing adjacent loops of a single strand or fiber. Knitted textiles (traditional and active) have a hierarchical architecture that is based on a knitting grid of unit cells combined in orthogonal rows (courses) and columns (wales). The knit architecture is differentiated from other textile architectures (weaving, braiding, stitching, etc) by its unique unit cells – the knit and purl loops (Figure 1a). The unit cells are composed of a 180° bulb-shaped loop extending into two legs that interlock with a ridge formed by the previous row. The loops are distinguished by the position of the ridge (rear ridge for knit loop, forward ridge for purl loop). The knitted loops are geometrically defined by their course height (C), wale width (W), loop length (L), and fiber diameter (d). The course height (C) is the vertical distance between identical reference points of adjacent rows. The wale width (W) is the horizontal distance between identical reference points on adjacent loops within a course. The loop length (L) is the length along the centerline of the fiber of a single knit loop. The fiber diameter (d) is the diameter of the foundational wire.

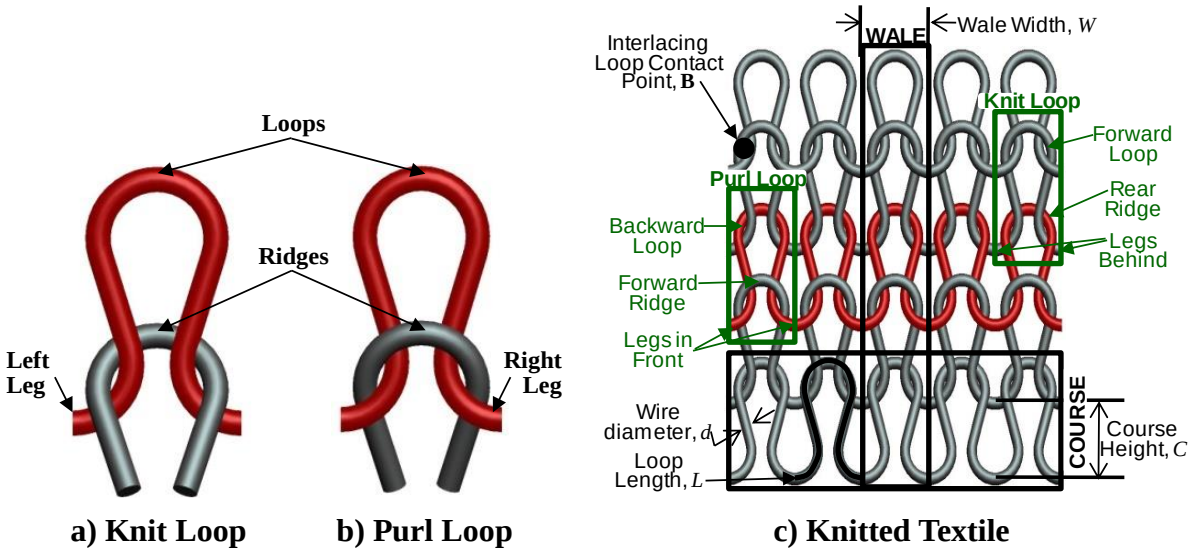

Figure 1. Active Knit Architecture.
An active knit is composed of unit cells: either a) knit loops or b) purl loops, patterns of which form c) knitted textiles.

The knitted loop unit cells can be combined to provide a wide variety of knit pattern textiles, which are defined by the arrangement of knit and purl loops. The most basic knit pattern, garter, has a symmetric arrangement of alternating rows of knit and purl loops (Figure 1c). A course is a row of knitted loops, shown in red in Figure 1c, which is composed of a single strand of alternating (up and down) curved loops. A wale is a column of knitted loops, the legs of each loop interlock with the top of the next loop down the wale (i.e. in the next course). In a course of knit loops, the legs of the upper loop in a wale overlap the top of the lower loop in the same wale and interlace behind the sides of the loop. Whereas, in a course of purl loops, the top of the lower loop overlaps the legs of the upper loop, which interlace behind the sides of the lower loop. The garter knit pattern, shown in Figure 1c, which is composed of alternating courses of all knit and all purl loops, forms a planar textile symmetric about the front and back. Numerous knit patterns can be created by changing the distribution of the knit and purl loops across the wales and courses of the textile. Regardless of the knit pattern, the loops within the architecture provide large curvatures and rotations through which loops interlace with the adjacent loop making contact at the *interlacing contact point*, **B**. The interlacing contact point is not a static point – it may change position as adjacent loops slip relative to each other during actuation.

1.3.2. Active Knits Operation

The operation of active knits is an important component of creating the large complex actuation motions provided by the knit architecture. Active knits go through operational transitions from one state to another resulting in a change in length, shape, and stiffness of the textile. In the case of SMA active knits the operational transitions are initiated by either a change in thermal loading, inducing a material transition from flexible Martensite to stiff Austenite (called the Shape Memory Effect), or by changes in mechanical loading. Typically, upon actuation the smart material fiber tries to return to its original, stress-free straight shape by recovering the strain induced in the smart material fiber during loop formation. The resulting actuation motion depends on the architecture of the active knit textile.

For symmetric garter knit pattern active knits, the straightening of the fiber causes the height of the individual loops to decrease (while slightly expanding the width) and the loops may slip relative to each other in the plane in which they lie. The change in loop geometry reduces the total length of the active knit textile which results in textiles with net strains that are orders of magnitude higher than the local strains within the material itself. The general actuation motion is harnessed in a four step (Figure 2) actuation process:

1. **Austenite Free State.** A typical garter knit pattern actuation cycle is initiated with the SMA textile in a heated state (Austenite) with no external loads (Free). The increased temperature causes the material to transition from the soft martensite phase to the stiff austenite phase. When heated the loops attempt to return to their naturally straight configuration resulting in a relatively wide wale width, W, and a relatively short course height, C. Even though many internal stresses and strains exist, the garter knit textile in the Austenite Free State (Figure 2a) is set as the zero deflection reference point for actuation.
2. **Austenite Extended State.** When a tensile load is applied to the textile in this heated state, the knit loops elongate, increasing the course height C, and lengthening the entire textile into the Austenite Extended State (Figure 2b).
3. **Martensite Extended State.** When the textile is allowed to cool under load to a temperature below its martensite finish transition temperature, the textile makes a material transition into the martensite phase and becomes less stiff. As a result, the course height of the loops elongates further into the Martensite Extended State (Figure 2c). The

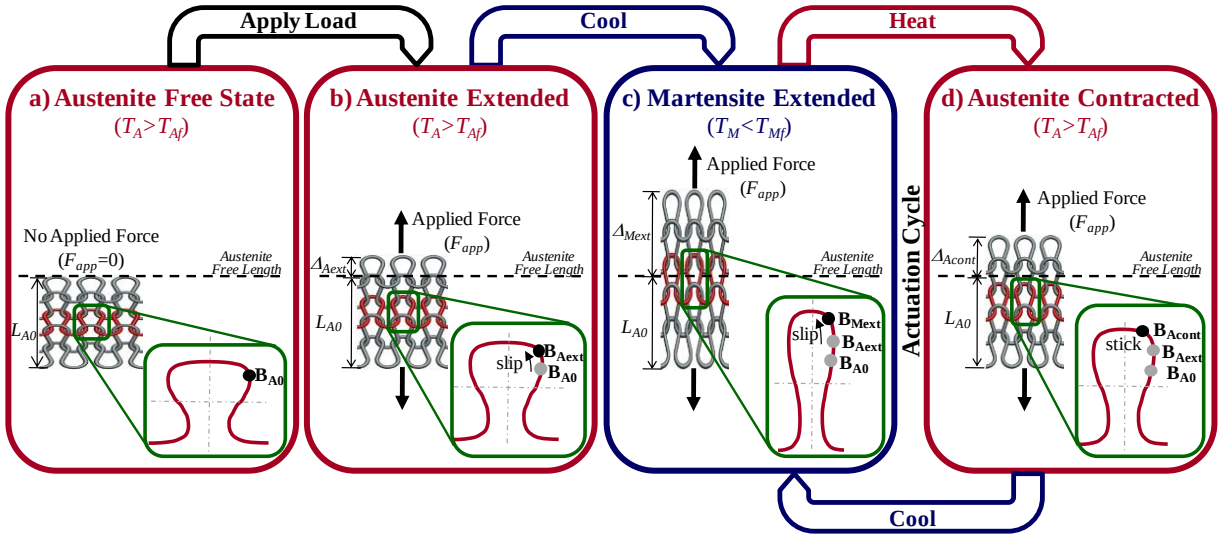

Figure 2. Active Knit Operation.
Active knits have four operational states: a) Austenite Free State, b) Austenite Extended State, c) Martensite Extended State, and d) Austenite Contracted State reached through thermal or mechanical operational transitions where a typical actuation cycle is alternates between the Martensite Extended and Austenite Contracted States.

Martensite Extended State is the first of two states in the cyclic portion of the typical actuation cycle.

4. **Austenite Contracted State.** The next state of the actuation cycle is entered when the material is heated under load to above its austenite finish transition temperature to the austenite phase. The resulting stiffening of the material causes the fibers within each loop to attempt to straighten to their natural straight shape, reducing the course height, and inducing contraction of the textile into the Austenite Contracted State (Figure 2d).

The hierarchical knit architecture transforms the contractile actuation strains of SMA fiber into very large three dimensional motions because individual loops change shape (height, width, and curvature) and propagate this amplification through the textile. The hierarchical architecture of Active Knits leverages the bulk material behavior to provide complex three-dimensional actuation motions distributed across a surface or throughout a structure.

1.3.3. Research Issues

Active knits show tremendous potential as an actuator technology, but they are in their infancy and no science base has been established to design, synthesize, and analyze this architecture. To realize and evaluate the potential of this new architectural framework five research areas need to be developed: active knit hierarchical architecture classification, active knit modeling, experimental validation, and case studies.

1.3.3.1. Hierarchical Architecture Classification

To effectively use the active knit technology in applications a formal language that describes the active knitted architecture needs to be constructed. Additionally, a hierarchical architecture classification structure is essential to identifying the actuation mechanism and determining the impact of architecture on kinematic actuator performance. For the active knit hierarchy to reveal the breadth of kinematic actuation motions produced by active knits, the knitted hierarchy must describe four component levels: 1) multiple types of unit cells, 2) homogeneous distribution of unit cells across the knitting grid of the textile, 3) heterogeneous distribution of unit cells across the knitting grid of the textile, and 4) non-planar orthogonal knitting grids. A complete understanding of the active knit hierarchy and a common language for discussion is needed to derive models and demonstrate feasibility to realize applications.

1.3.3.2. Active Knit Modeling

Models of the active knit structures must be developed to enable performance prediction and design synthesis. Different types of models are needed at different points in the design process. Further along in the design process, high fidelity models are needed to accurately predict the kinematic and kinetic performance. Early in the design process, simple, tractable models that can predict general kinematic and kinetic performance are useful for identifying an appropriate knit architecture and narrowing the set of geometric parameters that can produce the desired kinetic performance. Because active knits are complicated hierarchical structures the modeling process should be simplified by identifying the smallest repetitive element – the unit cell. Because of the variety of knitted structures, the knitted unit cell must be defined independently for each knit structure. All active knit models must incorporate the dual state nature of the foundational wire. Tractable models may use simple mechanical models to represent a simplified architecture; whereas, high fidelity models must capture the large rotations of the wire in the formed knitted loop and account for friction between interlacing adjacent loops to ensure accuracy. While executing the model it must transition between a set of defined states that account for the thermal and mechanical operational transitions that influence the load path and the internal and external friction that match the experimental conditions. The model must be built up to represent the entire knit structure by combining the unit cell model in series and parallel. It is necessary to develop models to provide design and analysis capabilities through model implementation.

1.3.3.3. Experimental Validation

A model must be experimentally validated to ensure the accuracy of its predictive capabilities. Because each of the active knit architectures display radically different kinematic actuation behaviors a different experimental setup and procedure is needed for each knit architecture. When designing the experiments it is necessary to ensure that each active knit architecture is tested for a particular motion and loading profile that is related to a potential application because a single type of experiment cannot capture and characterize the behavior of all active knits. New experimental setups, procedures, and techniques are needed to validate the active knits models and identify any limitations to the model including sensitivity to different design parameters.

1.3.3.4. Case Study

A case study is needed to demonstrate the ability of active knits to meet the kinematic and kinetic actuation specifications of new applications. To conduct a case study it is first necessary to identify types of potential applications, and then the kinematic motion and kinetic performance specifications of the application need to be identified and developed. An active knit architecture should be chosen for its ability to create the desired kinematic motion. Meeting the kinetic specifications of the application requires design insight to determine the geometric parameters and architectural configurations necessary to meet the simultaneous force and displacement requirements. The feasibility demonstration study should show that active knit pattern textiles have the potential to be used in applications by exploiting their unique performances to produce the simultaneous force and displacement required of some new applications.

1.4. RESEARCH GOALS AND OBJECTIVES

The goal of this research is to develop the fundamental scientific understanding of the active knit actuation architecture to enable the design, analysis, and synthesis of simultaneous large force and strain actuators that produce complex three-dimensionally distributed actuation motions in a compact package. Four research objectives are crucial to meeting this goal.

1. **Hierarchical Knit Architecture Classification.** Establish a formal language and a hierarchical classification structure that will identify the actuation mechanism and link the kinematic actuation motion to the hierarchical level, enabling exploration of the full breadth of possible actuator motions and providing a foundation for the modeling effort and insight into feasibility for applications.

2. **Fundamental Knitted Loop Modeling.** Develop predictive capabilities for the fundamental knitted loops (knit and purl) that will capture the kinematic and kinetic performance of the knitted loop and two-dimensional knit patterns by accounting for the dual state nature of active knits and friction between interlacing adjacent loops, providing an accurate tool for prediction, design, and tailoring of planar contractile active knits.
3. **Knit Pattern Modeling.** Formulate and experimentally validate a modeling approach that produces simple mechanical models at a level of fidelity useful for design that provide a tractable tool to predict the kinematic and kinetic performance associated with the complex motion generation of basic knit patterns that display three-dimensional actuation motions.
4. **Application Feasibility Demonstration.** Evaluate the applicability of active knits through a design case study that investigates the ability of active knits to create the desired kinematic actuation motions under application-level kinetic specifications.

It is necessary to address all these objectives to realize active knits as an enabler to numerous applications that require distributed complex three-dimensional actuation motions.

1.5. RESEARCH APPROACH

To fulfil the goals of this research and establish the science base for Active Knit Actuation Architectures the research objectives are addressed through four primary tasks: establishing an Active Knit Hierarchy, deriving an analytical model of the planar knitted loop and garter knit pattern architecture, developing a segment superposition modeling approach using the rib knit pattern as an example, and feasibility design study related to an Air Force flow control application.

1.5.1. Active Knit Hierarchy

Active knits are an exciting new actuation technology; however there is not an existing science base by which they can be evaluated. Before predictive models can be derived or application feasibility can be demonstrated, a formal language that describes the active knit architecture must be developed and the breadth of the hierarchy determined. Most research on traditional and engineering textiles use a two-level hierarchy to describe the mechanical response of the textile. The first level of the hierarchy is the knitted loop, which is combined in series and parallel to form the second level, the knit pattern. While this cellular hierarchical approach has proved useful for traditional engineering knits, it lacks the sophistication and hierarchical levels needed to capture

architectural variations that produce the large, complex, three-dimensionally distributed actuation motions that lend particular promise to active knits. To capture to breath of kinematic actuation motions produced by active knits, the knitted hierarchy must be expanded to four levels that capture 1) multiple types of unit cells, 2) homogeneous distribution of unit cells across the knitting grid of the textile, 3) heterogeneous distribution of unit cells across the knitting grid of the textile, and 4) non planar orthogonal knitting grids. To capture these complexities, a four level active knit hierarchy (knitted loop, knit pattern, grid pattern, and restructured grid) was is developed. Each level of the hierarchy is defined and various architectural examples of each level of the hierarchy were experimentally tested for their kinematic performance.

1. **Knitted Loop:** The knitted loop is the first level of the hierarchy, which, as the fundamental unit that makes up a single cell in the knitted grid, leverages bending and torsion in the smart material to create larger actuation motions. There are two knitted loops in the knit architecture – knit and purl loops. The knitted loops do not exist independently and must be constrained within a knit pattern, grid pattern, or restructured grid to display the large strain actuation behavior.
2. **Knit Patterns:** The second level, the knit pattern, is defined by the homogeneous arrangement of the interlacing knit and purl loops within the knitting grid of orthogonal rows and columns. The most basic knit pattern architecture is a knitting grid composed of a single type of loop (either all knit or all purl) called stockinette, which transforms from planar to scrolling upon actuation. Many other knit patterns are formed by combining both types of loops in striped patterns in the knitting grid: vertical stripes form rib knit patterns that create accordion-like motion upon actuation, horizontal stripes form garter knit patterns that provide planar contraction, and diagonal combinations form the seed knit pattern that generates arches. Combining knitted loops across the knitting grid in different knit patterns transforms the individual motions of the knitted loops into distributed actuation behaviors.
3. **Grid Patterns:** The third level of the knit hierarchy, grid patterns, is composed of regions of knit patterns that are arranged spatially across the knitting grid to form more complicated, heterogeneous patterns. By varying the knit patterns used across the knitting grid, different motions can be produced over different regions of the textile. The most basic grid pattern is formed by synthesizing two knit loop patterns across a single textile.

Combining knit loop patterns in a knit loop pattern distribution is a powerful tool that produces textiles that create controllable complex three-dimensional motions distributed heterogeneously over an entire surface forming variable surface actuators.

4. **Restructured Grids:** The fourth level, restructured grids, modifies the orthogonal knitting grid to provide textiles with restructured grids that transform and expand the type of motions produced at the lower levels of the hierarchy. Four ways of restructuring the grid – Post-Knitting Connections, Course-Wise Restructuring, Grid Cell Merging, and Re-Ordered Grids – were investigated. Post-knitting connections provide a structure that can further leverage the underlying behavior of the knit pattern or grid pattern used in the construction of the textile. Course-wise restructured grids produce three-dimensional textiles that are constrained by the helically connected knitted loops, and produce novel out-of-plane motions a result of the skewed, asymmetric knitted loops of the restructured grid. Grid cell merging controls the boundary conditions though manipulation of the shape of the actuator, achieving new complex three dimensional motions and realizing alternative complex actuator shapes. Reordered grids create a restructured grid that produces tailorable motions that are not available from the basic knit loop patterns alone.

This classification and illustration of representative active knits provides a useful catalog of a variety of complex motion capabilities and delivers insight that aids in the understanding, modeling, and design of this new actuation paradigm to meet growing actuation needs. The complete details of the active knit hierarchy are provided in Chapter 2 of this document.

1.5.2. Two-Dimensional Analytical Knitted Loop Model

To advance active knit technology and establish the science base to implement the technology in applications, a model that captures the kinetic performance of active knitted textiles is needed. Active knits are complicated hierarchical structures; therefore, the first step in creating a predictive model was to model the kinetic behavior of the first level of the active knit hierarchy – the knitted loop. Knitted loops are assembled according to the knitting grid to create knit patterns; therefore, the kinetic performance of the individual loops is scaled in series and parallel to predict the performance of knit pattern active knit textiles. While existing passive knit models serve as a foundation for the kinetic modeling of active knits, no existing models are capable of predicting the actuation performance of active knits. However, existing models can be modified and combined to capture the actuation behavior of active knits by including the thermal and mechanical

operational transitions that occur during active knit actuation and the influence of the load path and the interlacing loop friction. An analytical state-based actuation model of the planar knitted loop in the garter knit pattern fabricated from variable stiffness smart material wire which accounts for the loading path and the friction between interlacing adjacent loops was is developed. The states of operation are defined based on the mechanical loading of the textile, the transition between different material stiffness, and the paths followed to arrive at each state. Operational transitions between these states induce frictional forces (stick or slip) depending upon the state and path, which affect the actuation response. A load-extension model was derived for each state of a typical actuation cycle with respect to the unit cell of a single loop of the textile based on the stress-strain behavior of the active material with assumptions made to allow analytical tractability. Elastica Theory and Euler-Bernoulli beam bending were used to capture the large deformations within a loop of wire. The resulting kinematic and kinetic relations for a single cell scaled the load-extension behavior of the entire knit textile for each state, and provided analytical algebraic transcendental expressions for the net actuation motion as a function of the applied tensile load on the textile. The model was validated experimentally for an SMA garter knit textile over a range of applied forces with good correlation (4.1% - 6.1% average relative displacement error for each extended state, 2.8% average relative displacement error for the contracted state, and 2.0 mm absolute displacement error for the actuation). The two dimensional analytical active knit loop model provides the ability to predict actuation motions for the large stroke, large force garter knit pattern actuation architecture, enabling the design of planar contractile active knitted architectures for a wide range of applications and providing the foundation for models of more complex knitted architectures that produce three-dimensional actuation motions. The development and validation of the two-dimensional analytical model of the knitted loop and garter knit pattern are provided in detail in Chapter 3 of this document.

1.5.3. Three-Dimensional Analytical Reduced Order Knit Pattern Model

To capture more advanced knit patterns that have out-of-plane motions, a segment superposition modeling approach was developed. The modeling approach provides a modular, tractable, and scalable approach to predicting the kinematic and kinetic performance of three-dimensional actuation architectures to provide insight during early stages of the design process. The approach reduces the complexity of three-dimensional knit architectures by establishing a clear procedure and representing the architecture with a system of simple mechanical models. To

demonstrate the segment superposition modeling approach, the approach was followed to develop a segmented model of the 2x2 rib knit actuator architecture. The unit cell of a 2x2 rib knit pattern is identified as a single loop, which is segmented into five straight segments. It was determined that the primary actuation mechanism in the architecture is torsion along two segments of the unit cell. A simple torsion-based model was developed that predicts the force-displacement performance of actuator. The model identifies geometric relationships between the height and width of the knitted actuator and measurable geometric parameters including wire diameter, loop dimensions, and the angles through which torsion segments are rotated. The torque in the twisted segment of the unit cell is related to the wire diameter, torsional rigidity of the wire, the torsion length, and the angle through which the segment is rotated. The segmented 2x2 rib knit model was experimentally validated for a range of applied loads with good correlation. The development and validation of the segment superposition modeling approach is provided in detail in Chapter 4 of this document.

1.5.4. Feasibility Demonstration Study

Active knits are a promising actuation architecture that produces unique actuation motions which are unattainable with current technologies, however, the feasibility of using active knits in applications has yet to be demonstrated. A feasibility demonstration study was conducted using rib knit pattern active knits to meet the simultaneous force and deflection specifications required for flow control of an aircraft. Flow control has been of significant interest to the aerospace community because actively manipulating flow characteristics around the wing can enhance high-lift capability and reduce drag; thereby, increasing fuel economy and improving maneuverability and operation over diverse flight conditions which enables longer, more varied missions. Changing the shape of the wing to employ distributed actuators across the surface of the wing through the use of contour bumps is a theoretically promising way to control air flow over the wing; however, no actuators currently exist to achieve this task. Rib knit pattern active knits actuate normal to the surface, producing span-wise discrete periodic arrays that can withstand aerodynamic forces while supplying the necessary displacement for flow control. The technical specifications for the contour bump applications were developed from existing theoretical research. The orientation and configuration of rib knit pattern textiles are described such that the active knit actuator can with stand aerodynamic pressures while supplying the necessary displacement for flow control. Two rib knit pattern active knit prototypes were created and tested using a specially

designed experimental rig (producing 6.3 and 6.4 mm actuation displacement under 2.5 and 1.4 kPa). Series and parallel combinations of identical rib knit pattern prototypes were experimentally explored to meet the technical specification required by the contour bump application. The measured knit performance was on the scale of the necessary aerodynamic pressures and displacements (with three sets of two nestled prototypes simultaneously actuating 20.8 mm under a 11.1 kPa load); thus, the rib knit pattern active knit is potential technical solution for distributed actuation of local surface profiles in flow control, although numerous implementation issues still exist. This feasibility demonstration study shows that active knit pattern textiles can be used in applications by exploiting their unique performances to meet the kinematic and kinetic specifications new applications. The flow control case study is described in Chapter 5.

1.6. OUTCOMES AND CONTRIBUTIONS

Active knits are a new cellular architectural paradigm with the potential to revolutionize actuators by producing simultaneous radical forces and displacements, in the form of complex three-dimensional actuation motions distributed throughout a structure, all in a small package size. The ability to create complex shape change will enable applications across diverse fields including aerospace, biomedical, and consumer devices. While a significant amount of research has been conducted on smart materials based actuation architectures, existing architectures lack the sophistication to produce truly complex actuation motions. The active knitted actuation architecture has been identified as a promising approach to creating shape change, however, several research issues have to be addressed to enable the implementation of the active knit architecture in devices. This research establishes the scientific basis for active knitted actuators.

Active knit actuation architectures produce unprecedented actuation through a hierarchically arranged structure. A hierarchical classification scheme is established to explore the breadth of actuation motions and a language is developed to describe the knitted architectures and their corresponding kinematic actuation behaviors. The classification scheme produces a catalog of different active knit motions and provides an understanding of the relationship between hierarchical level and kinematic actuation behavior. Insight from the hierarchy aids in the identification of the actuation mechanism and provides a starting point for the derivation of models that predict kinematic and kinetic performance.

Predictive capabilities are provided by analytical models of two- and three-dimensional active knit architectures. The design process can be informed through different modeling approaches. High fidelity models can provide enhanced accuracy to meet application specifications whereas simple segmented models can identify the impact of different parameters on performance. Two different modeling approaches – a high fidelity model of two-dimensional active knits and a low fidelity model of three-dimensional active knits – address the need for diverse predictive capabilities. The two-dimensional analytical model considers the large rotation bending of the wire and incorporates the dual state nature of the active material and the friction between interlacing loops to predict the cyclic actuation performance of planar actuating active knits. The segment superposition modeling approach provides a modular, tractable, and scalable modeling approach to predict complex out-of-plane actuation motions and provide insight during the design process. A modeling procedure is outlined for each approach. Regardless of the fidelity of the model, the initial modeling steps are to identify the smallest repetitive element, establish geometric relationships, and develop force equilibrium interactions. The models predict the unique performance of the various active knit architectures while highlighting important design points including maximum displacement, strain, and work. The modeling approaches set the foundation for design of actuators and enable performance tailoring to meet application specifications.

A feasibility demonstration study shows effective ways to use the unique actuation motions of active knits to enable applications. The procedure used in the feasibility demonstration study – identifying potential application, defining technical specifications, choosing active knit architecture to produce desired kinematic motion, and experimentally testing for quasi-static kinetic performance – can be followed to realize other applications. Additionally, the feasibility demonstration study shows that even more architectural configurations can be developed to further leverage the hierarchical nature of the active knit architecture. The active knit architecture can be used as a building block architecture to leverage performance in series and parallel combinations to meet application specifications. The feasibility demonstration study shows that this new actuation architecture can be used as an enabling technology to realize a variety of applications.

The contribution of this research extends beyond active knitted actuators. The expanded knit hierarchy can be used to design complex architectures for traditional and engineering textile applications and the models can be used to enhance predictive capabilities. The improved handling of friction in the two-dimensional model could be used to predict hysteretic friction behavior, a

capability not currently available. Additionally, the modeling approach could be expanded to work with other active/passive material combinations and activation stimuli that may provide different performance characteristics (force, speed, frequency). This primary research on active knits provides the foundation for further development and use in structural applications.

This research provides the fundamental knowledge needed to develop active knits to meet the demand for advanced actuators. The radical forces and strains and complex, distributed, three-dimensional behaviors of these architectures go well beyond anything currently accessible through traditional actuation or conventional smart material actuation architectures. This novel technology will enable advancements in current applications (shape morphing, flow control, deployable structures, safety mechanisms, medical devices, etc.), as well as open the door to applications yet imagined.

Chapter 2. ACTIVE KNIT HIERARCHICAL ARCHITECTURE

Active knits are a new actuation paradigm, therefore there is not an existing science base by which they can be evaluated. Before predictive models can be derived, or application feasibility can be demonstrated, a formal language that describes the active knit architecture must be developed. While traditional and engineering textiles do not undergo actuation, the mechanical force-deflection behavior of these textiles has been investigated [61]-[86]. The existing models can provide some guidance for establishing the scientific foundation to investigate the mechanism and motion of active knit actuator architectures. Most research on both traditional and engineering textiles use a cellular approach to determine the behavior of textiles [82]-[86]. In these existing cellular methods, the textile is divided into a grid of unit cells that represent the smallest repeating element in a textile. The predicted performance of a single unit cell is extrapolated to represent the behavior of the entire textile. This two level hierarchical approach has been useful for identifying the extensional performance of plain knitted materials, which are those with the simplest knitted architectures. While this cellular hierarchical approach has proved useful for traditional engineering knits, it lacks the sophistication and hierarchical levels needed to capture architectural variations that produce the large, complex, three-dimensionally distributed actuation motions that lend particular promise to active knits. To capture the breath of kinematic actuation motions produced by active knits, the knitted hierarchy must be expanded to four levels that capture 1) multiple types of unit cells, 2) homogeneous distribution of unit cells across the knitting grid of the textile, 3) heterogeneous distribution of unit cells across the knitting grid of the textile, and 4) non planar orthogonal knitting grids.

This chapter defines a hierarchical architectural classification for active knit actuators. This classification establishes language for clear communication of the variety of architectures. Additionally, the expanded classification structure unveils important behavioral trends of each hierarchical level and exposes lessons of how each level can be utilized to design knit actuators tailored to applications that need large, complex, three-dimensionally distributed motions. This

classification provides a foundation for the modeling effort, an understanding for design, and insight into feasibility for applications.

Leveraging the cellular approach, the hierarchical classification of active knitted architectures (Figure 3) is based on a knitting grid with orthogonal rows (courses) and columns (wales). The architectural hierarchical classification extends the simple two-level hierarchy of traditional and engineering textiles to four levels

1. The first level of the hierarchy is the ***knitted loop*** which, as the fundamental unit within a single cell in the knitted grid, leverages bending in the smart material to create larger actuation motions.
2. The second level is composed of ***knit patterns*** in which the loops combine across the knitting grid in different ways, transforming the individual motions of the knitted loops into distributed actuation behaviors.
3. The third level, ***grid patterns***, combines different regions of knit patterns over the knitting grid to produce complex, potentially non-homogeneous motions.
4. The fourth level, ***restructured grids***, modifies the orthogonal knitting grid to provide textiles with restructured grids that modify and expand the type of motions produced at the lower levels of the hierarchy.

In this chapter, each level of the hierarchy is defined and various architectural examples of each level of the hierarchy are provided. The active knit actuation mechanism is identified and the link between active knit kinematic behavior and hierarchical architecture level is described and experimentally examined. This classification and illustration of representative active knits provides a useful catalog of a variety of complex motion capabilities and delivers insight that aids

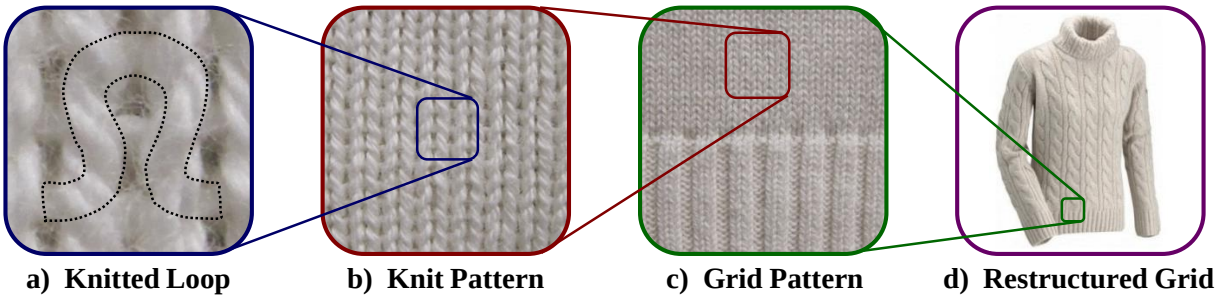

Figure 3. Hierarchical Knit Architecture.
All knit materials are hierarchical structures where the behavior is influenced by each of the hierarchical levels: a) Knitted Loops, b) Knit Patterns, c) Grid Patterns, and d) Restructured Grids.

in the understanding, modeling, and design of this new actuation paradigm to meet growing actuation needs.

2.1. MATERIALS AND METHODS

While any flexible, smart material fiber that changes in shape or stiffness could be used to create active knitted actuators, each of the active knits described in this paper were made from shape memory alloy (SMA) wire. SMAs utilize the shape memory effect to create temperature induced solid state actuators. The shape memory effect exploits the reorientation of internal lattice structure to return a plastically deformed material back to its initial shape when it is heated above its transition temperature [68]. During the typical shape memory process, the material starts in the low temperature, twinned martensite phase. A mechanical load is applied and the material is deformed as the lattice structure reorients to the de-twinned martensite phase. The load is removed and the material is heated above the transition temperature, causing the material to return to its original shape as the lattice structure enters the highly aligned, stiff austenite phase. Upon cooling, the material remains the same shape as the lattice structure shifts into the twinned martensite phase. The material phase change creates useful strains, on the order of 3-8%, during the thermo-mechanical actuation process [68].

The experimental characterization technique used for active knitted actuators must account for the two components of the shape memory effect of SMA material: the mechanical loading and the temperature dependent actuation. The mechanical loading and resulting deformation of the foundational wire are addressed through the active knit manufacturing process. All active knits in this paper were hand knit using traditional knitting techniques with 8 to 15 mil diameter Dynalloy Flexinol® SMA wire. During the knitting process, the initially straight SMA wire (in the martensite twinned phase) is knit directly off the spool by wrapping the wire around a knitting needle (3 to 10 mm in diameter) to form an interlacing network of adjacent loop-based unit cells. The wrapping process bends the wire to the point of plastic deformation, forcing the material into the de-twinned martensite phase. The material remains in the knitted configuration because of the plastic deformations of the wire and the interconnections of adjacent loops, which prohibit unraveling. Actuation of the active knit occurs when the textile is heated above the transition temperature of the SMA wire using a heat gun. As the bent wires straighten, recovering some of the plastic deformation induced during the knitting process, the active textile transforms into its

three dimensional configuration, which is governed by the hierarchical architecture of the active knit. The experimental characterization technique was established with the material properties in mind to characterize a variety of active knits to determine the breadth of actuator behaviors possible with the active knit architecture.

2.2. LEVEL 1: KNITTED LOOPS

The first level of the hierarchical architecture is composed of two basic *knitted loops* – knit and purl (Figure 4) –which are the unit cells of the knit architecture. Both the knit and purl loops are unit cells made up of a loop, two legs, and a ridge (Figure 4b, c). The loop is curved slightly more than 180°, creating a tear-drop shape that forms the upper portion of the knit unit cell. The loop extends into the legs, where adjacent unit cells attach to one another. The ridge is the uppermost portion of the loop from the previous course (row); the intersecting ridge divides the loop from the legs. The feature that distinguishes between the loops is the location of the loop and legs with respect to the ridge. The knit loop (Figure 4b) is created by passing through the loop in the previous course from the back to the front and is characterized by a forward loop and a rear ridge. The legs of the knit loop interlock with the ridge, and then extend behind the ridge. Since the ridge is in the rear for knit loops only the base of the loop is visible; the base of the knit loop appears as a "V" like shape on the textile and is represented in the symbolic grid with a "V" (a standard notation in traditional knitting – shown in Figure 4b). The purl loop is the opposite of

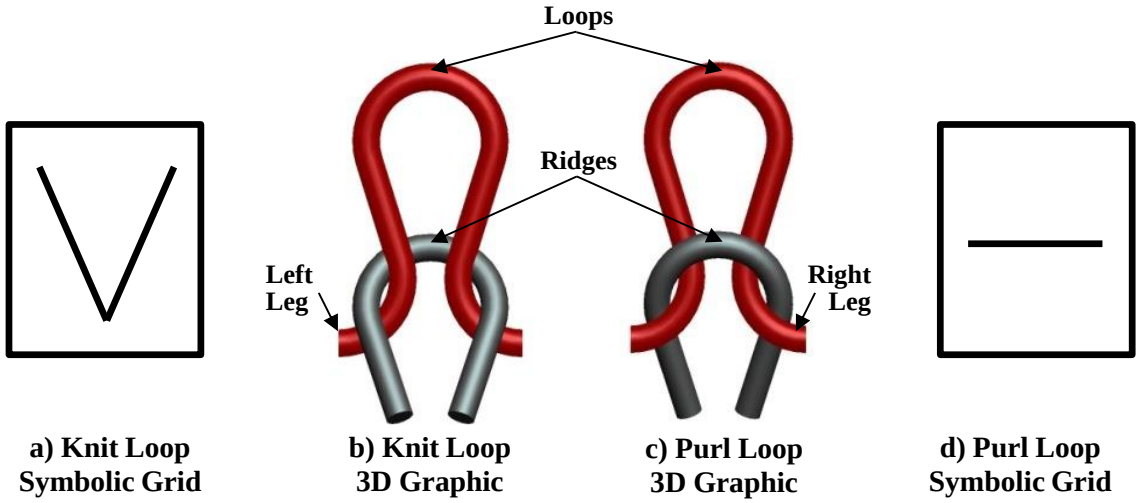

Figure 4. Knitted Loops.
Two types of knitted loops make up the first level of the hierarchical knit architecture: A knit loop. a) represented by a V in the symbolic grid, having b) a forward loop, rear ridge, and legs extending to the rear, and a purl loop, d) represented by a horizontal dash in the symbolic grid, having c) a rear loop, forward ridge, and legs extending forward.

the knit loop. The purl loop (Figure 4c) is created by passing through the loop in the previous course from the front to the back and is characterized by a backward loop and a forward ridge. The legs of the purl loop interlock with the ridge, and then extend in front of the ridge. Because the ridge is in the front for purl loops it is visible; the ridge of the purl loop appears as a "-" like shape on the textile and is represented in the symbolic grid with a "-" (a standard notation in traditional knitting – shown in Figure 4d). A purl loop on one side of the textile appears as a knit loop on the other side.

All knitted textiles (traditional and active) demonstrate extreme elasticity. This elasticity is a result of the curved loops, which allow bi-directional stretching as the loop is pulled height-wise or width-wise. In the case of SMA wire, the wire, which is nominally straight, is bent into the loop shape when in the cold, relatively soft martensite state. When heated to the relatively stiff austenite state, the wire attempts to straighten, opening the loop, resulting in a reduced loop height and a slightly increased loop width. When allowed to cool, the wire returns to the martensite state and the loop relaxes. The bending and straightening of the base fiber occurs in both knit and purl loops within knitted textiles, however, the knitted loop alone does not exist on its own and must be constrained in a knit pattern, grid pattern, or restructured grid to display this behavior. The unique loop structure of the knit architecture leverages the strain of the SMA wire, enabling the large distributed actuation strains of the active knit textile.

2.3. LEVEL 2: KNIT PATTERNS

The second level of the architectural hierarchy, the knit pattern, is defined by the homogeneous arrangement of the interlacing knit and purl loops within the knitting grid of orthogonal rows and columns. Knit patterns are nearly planar (i.e., they have a minimal out of plane thickness) textile swatches composed of multiple knitted (knit and/or purl) loops. The most basic knit pattern architecture is a knitting grid composed of a single type of loop (either all knit or all purl) called stockinette. Many other knit patterns are formed by combining both types of loops in striped patterns in the knitting grid: either vertical, horizontal, or diagonal combinations of knit and purl loops. The architecture of the knit pattern is composed of a homogeneous repeatable pattern and is defined by the type of knitted loops and location of adjacent knitted loops to one another within the knitting grid. To link the kinematic actuation motion to the knit pattern

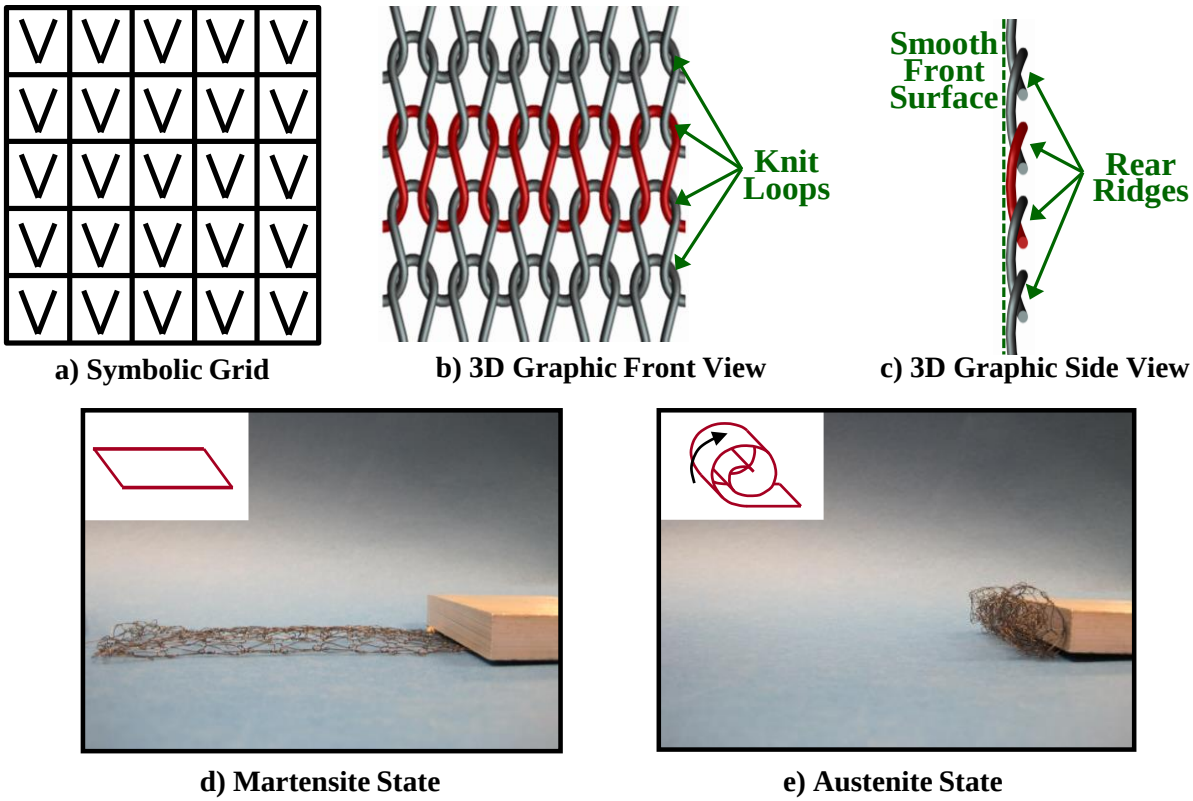

Figure 5. Solid Knit Pattern – Stockinette.
The rolling actuation motion of stockinette is driven by the asymmetric architecture. Shown are the a) symbolic grid composed of all knit loops represented by V's, b) the front view 3D graphic of all knit loops, and c) the side view 3D graphic of the slight out-of-plane of curvatures that result in a smooth front surface and rear ridges. The pictures demonstrate the d) elongated prototype in cold martensite state and the e) rolled actuated prototype in the hot austenite state.

level of the active knit hierarchy prototypes of some basic knit patterns (stockinette, garter, welt, rib, and seed) were fabricated and their actuation behavior was experimentally observed.

2.3.1. Solid Knit Pattern – Stockinette

The solid knit pattern is created with a single type of knitted loop (Figure 5), either all knit loops (represented by "V" in the symbolic grid – shown in Figure 5a) or all purls loops (represented by a "–" in the symbolic grid – not shown) appear in the knitting grid. There is only one type of solid knit pattern, stockinette, because a purl loop is the other side of a knit loop, and a solid pattern of purl loops is simply a solid pattern of knit loops on the reverse side. Therefore, either type of loop can be repeated to create the same knit loop pattern. The architecture of the stockinette knit pattern forms an asymmetric topology about the front and back of the textile; the front side of the textile is smooth and resembles columns of "V"s from the knit loops (Figure 5a, b), whereas the back side has rows of ridges from the purl loops. The asymmetric topology results from pulling

each course of knitted loops from the back of the previous course to the front, causing the loops to arch out of the plane because each course lies on an offset cylindrical surface (Figure 5c).

The architecture of the solid knit pattern produces asymmetrical actuation motions of solid knit pattern active knits. During actuation, each course of loops attempts to straighten, forcing the shape of the loop to change because loops are constrained by adjacent courses of loops. The height of the loop is reduced which forces the ridges toward one another, causing the loops to bend even further out-of-plane. This out-of-plane bending propagates through the textile resulting in a slight rotation between each course of knitted loops ending in a tube-like structure. To demonstrate the out-of-plane bending provided by the solid knit pattern a stockinette knit pattern prototype was constructed on 5.5 mm needles, using 10 mil wire and 10 loops to create a prototype 12.5 cm long. Upon thermal actuation (heating above the material's phase transition temperature) the prototype, which is initially flat (Figure 5d), rolls into a tight scroll with an outer diameter of 2 cm (Figure 5e), reducing the length of the textile by 84%. The solid knit pattern of stockinette creates a bending moment that creates a unique rolling motion which could enable applications such as complex deployable structures.

2.3.2. Horizontally Striped Patterns – Garter and Welt

Horizontally striped patterns are created when courses of knit loops are alternated with courses of purl loops in the knitting grid. When a single course of knit loops is alternated with a single course of purl loops the horizontally striped knit loop pattern is called garter (Figure 6). The architecture of the garter knit pattern results in a symmetric textile topology with consistent courses of horizontal ridges on each side of the textile (Figure 6a, b). The alternating courses of knit and purl loops lie on angled planes (the loops are not arched out of plane as is the case for stockinette – as shown in Figure 6c). Garter knit pattern textiles are very elastic along the length of the textile as a result of the bent loops and angled planes.

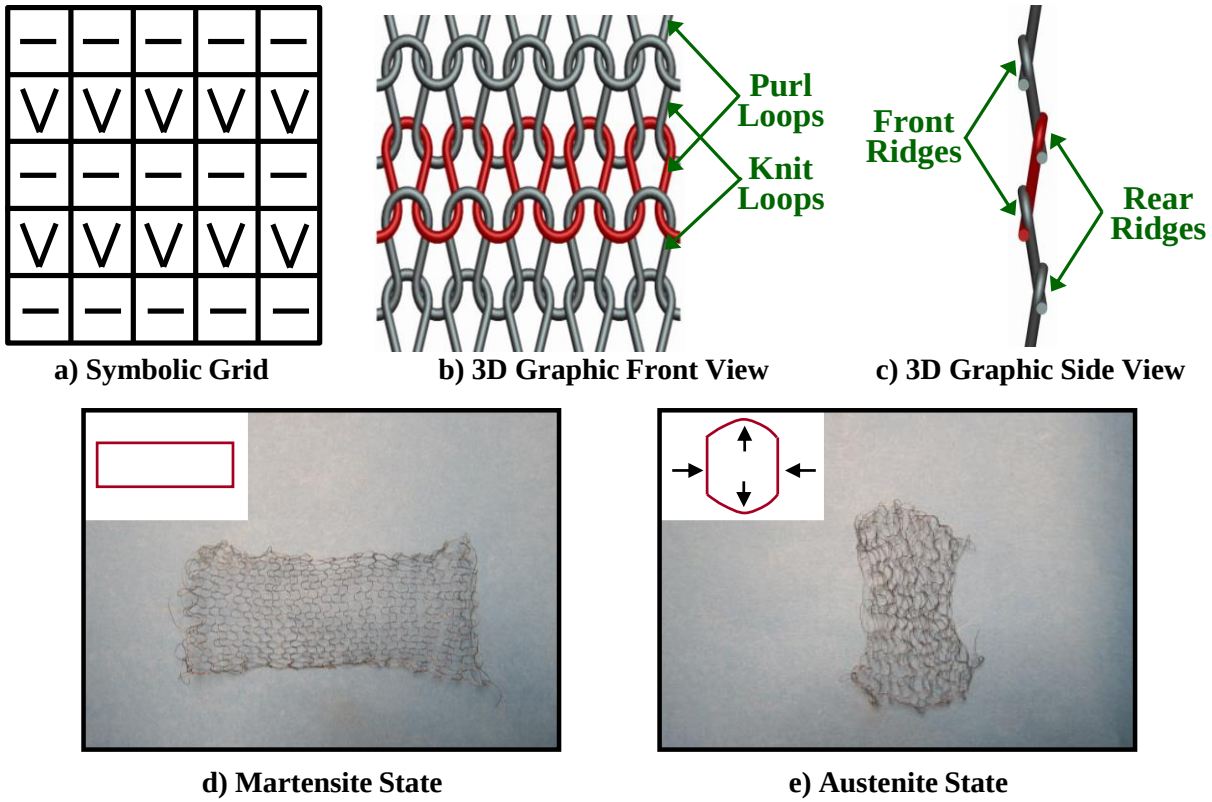

Figure 6. Horizontally Striped Knit Pattern – Garter.
The distributed contraction of garter is driven by the symmetric architecture. Shown are the a) symbolic grid composed of alternating courses of knit (V) and purl (–) loops, b) the front view 3D graphic of alternating courses of knit and purl loops and c) the side view of alternating front and rear ridges. The pictures demonstrate d) the flat elongated prototype in the cold martensite state and e) the contracted prototype in the hot austenite state.

The architecture of the garter knit pattern produces nearly planar symmetrical actuation motions of garter knit pattern active knits. During actuation, the curved SMA fiber in each loop attempts to return to its original straight shape; causing the loops in each course to straighten and slip relative to each other in the plane in which they lie, reducing the total length of the textile. To demonstrate the contractile behavior, a rectangular garter prototype was created with 8 mil wire on 5.5 mm diameter needles yielding a prototype with 10 loops in each course, for a total length of 14 cm. Upon thermal actuation, the prototype contracted in length by 70% while expanding laterally 80% (Figure 6c and d). The symmetric garter knit loop pattern leverages the motion produced by knitted loops, providing considerable strain amplification, an order of magnitude over material strain alone, and could be used as a distributed planar contractile surface actuator for applications requiring large motions with compact packaging such as morphing structures.

Another horizontally striped knit pattern – welt – is created by alternating more than one course of knit loops with the same number of courses of purl loops (Figure 7) in the knitting grid.

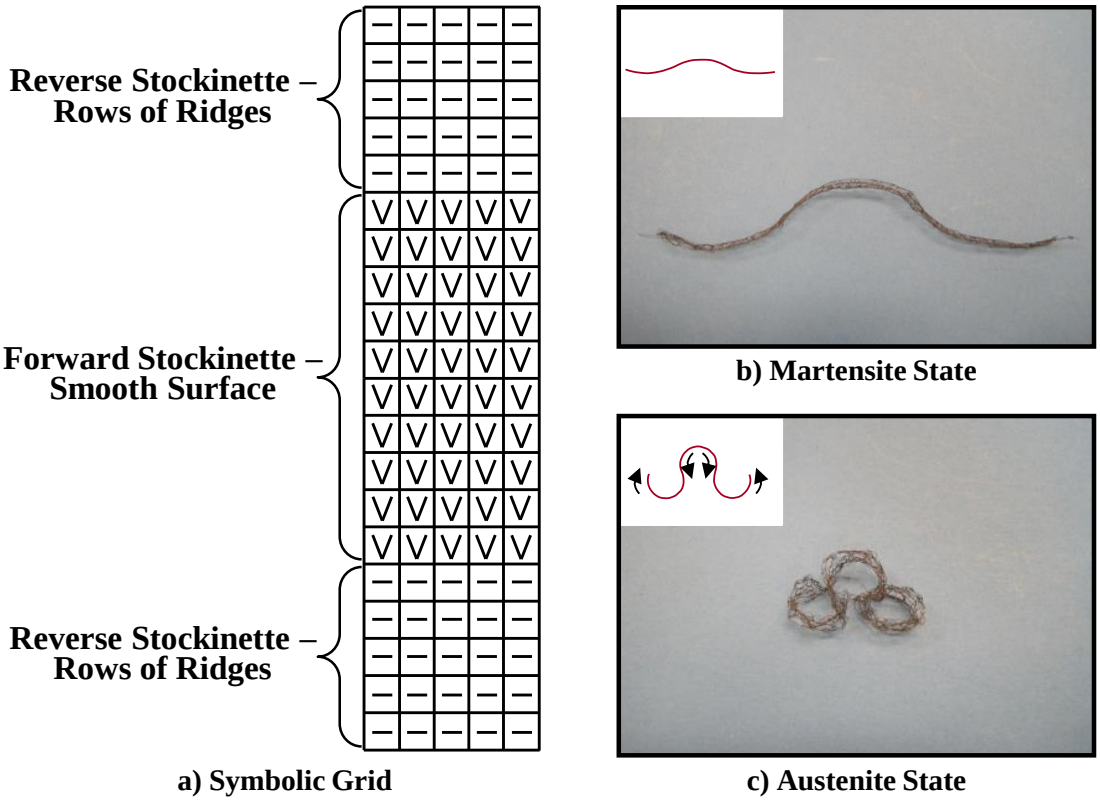

Figure 7. Horizontally Striped Knit Pattern – Welt.
More complicated motions can be obtained by welt patterns, *n* courses of knit loops alternating with *n* courses of purl loops. Textiles knit following the a) 10x10 welt symbolic grid produces out-of-plane motion when the welt actuates from b) a flat elongated textile in the cold martensite state into c) a curled and contracted textile in the hot austenite state.

This produces a *mxm* welt textile (Figure 7a) with alternating rows of smooth surfaces ("V"s) and rows of ridges ("–"s). The welt architecture is much like alternating a number of rows of stockinette front with stockinette back. The loops within the welt knit pattern arch slightly out-of-plane where the direction of the arching is determined by the type of loop (knit or purl) used in that segment of the welt.

The architecture of welt knit pattern produces symmetric actuation motions with some out-of-plane bending of welt knit pattern active knits. The textile, which initially lies flat, actuates into a corrugated shape of alternating arched rows, increasing the thickness of the textile while decreasing the total length of the textile. To demonstrate the corrugation actuation behavior, a 10x10 welt prototype (ten courses of knit alternating with ten courses of purl) was created using 8 mil wire, 5.5 mm knitting needles and 5 loops. Upon thermal actuation the welt provided enhanced contractions (67%) over the garter knit pattern as the loop contractions were coupled with the out-of-plane arching (Figure 7b, c). Welt knit pattern active knit textiles provide out-of-plane surface

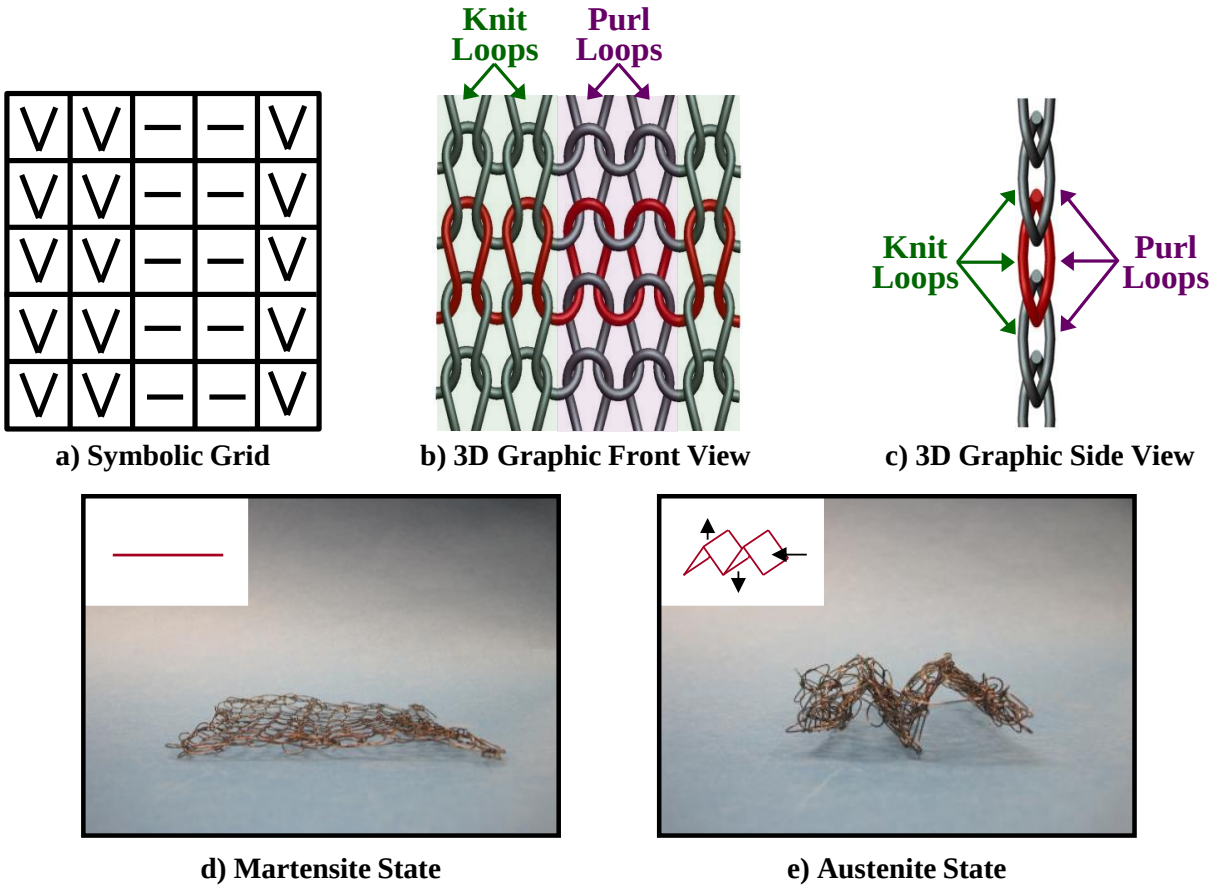

Figure 8. Vertically Striped Knit Pattern – Rib.
The accordion-like actuation motion of rib is driven by the constrained asymmetric architecture. A 2x2 rib is shown with a) symbolic grid, b) a front view 3D graphic of alternating columns of knit and purl loops and c) a side view 3D graphic of columns with slight out-of-plane curvatures that alternate in different directions. The pictures demonstrate d) the flat prototype in the cold martensite state and e) the expanded accordion ridges of the prototype in the hot austenite state.

displacements that can be used as surface texturizing actuators in addition to providing extremely large contractile motions.

2.3.3. Vertically Striped Patterns – Rib

Vertically striped patterns, or rib knit patterns, are created by alternating columns of knit loops with columns of purl loops in the knitting grid (Figure 8). This produces a textile with symmetric columns (Figure 8a, b), alternating between smooth columns of the front of stockinette (knit loops) and columns of ridges of the back of stockinette (purl loops). The knit loops and purl loops of the rib knit pattern arch out of the plane of the textile in different directions (Figure 8c). A 1x1 rib alternates a single column of knit loops with a single column of purl loops, whereas an *nxp* rib knit pattern alternates *n* columns of knit loops with *p* columns of purl loops.

The architecture of the striped rib knit pattern produces a series of connected planes in an accordion-like shape for active rib knit textiles. Initially, the columns of the textile lay flat in a nearly planar textile; however, the columns rotate relative to one another because the change in the leg position relative to the ridge creates angular movement, resulting in the accordion-like surface that has an increased thickness and decreased width. To demonstrate the accordion-like actuation behavior provided by active rib knit pattern textiles a 2x2 rib prototype was created using 15 mil wire, 5.5 mm needles and 10 loops for a prototype that measured 6.5 cm long. The prototype transforms from planar (Figure 8d) to a series of connected planes 45^{o} to one another (Figure 8e), reaching a height of 2 cm while reducing the width by 40% without change to the prototype length. The vertically striped knit pattern of rib creates a large distributed accordion-like motion that can provide controllable three-dimensional textures or act as an embeddable planar lift.

2.3.4. Diagonally Striped Patterns – Seed

Diagonally striped knit patterns are created with alternating diagonals of knit and purl loops in the knitting grid. One diagonally striped knit pattern is seed (Figure 9). The seed knit pattern is created by alternating single knit and purl loops in the first course and in the adjacent course single purl loops are alternated with single knit loops (Figure 9a,b, c). This creates an alternating pattern that results in a textile with checkerboard-like surface of smooth forward loops and rear ridges.

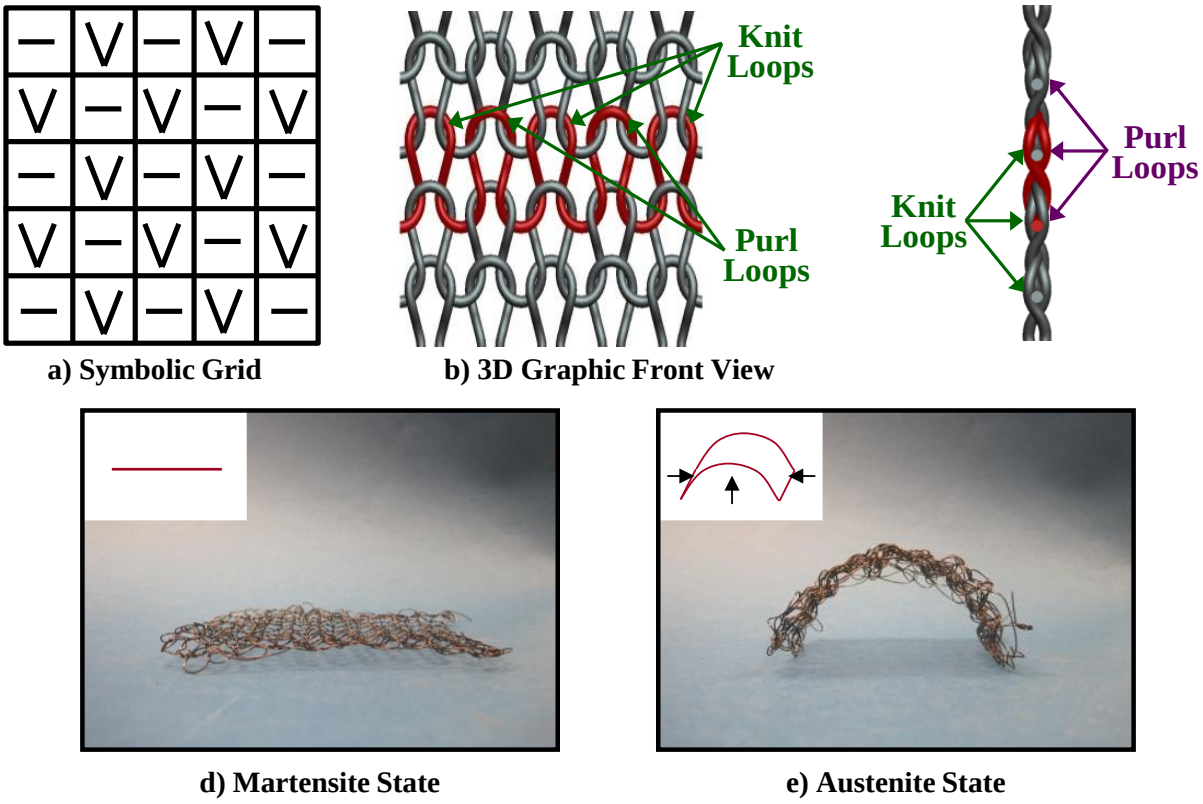

Figure 9. Diagonally Striped Knit Pattern – Seed.
The synclastic arching of seed is driven by the checkerboard-like architecture that causes bending through the rows and columns. Shown are the a) symbolic grid, the b) front view 3D graphic of the checkerboard knit and purl loop pattern and the c) side view 3D graphic. The pictures demonstrate the d) flat prototype in the cold martensite state and e) synclastic arches of the prototype in the hot austenite state.

The architecture of the diagonally striped knit pattern produces synclastically arching shape in active diagonal striped knit textiles. The arching is a result of each loop contracting horizontally and vertically while being constrained by the edges of the textile, causing the horizontally and vertically symmetric knit pattern to arch along the horizontal and vertical axes. To demonstrate the synclastically arching of diagonally striped active knits a seed prototype was produced with 5.5 mm needles using 15 mil wire with 10 loops for a total length of 7.5 cm. When heated the length and width of the prototype did not change but curved, creating a nearly 180° arch (Figure 9d, e). The diagonally striped knit loop pattern creates a dome-shaped actuator that could be used to actively texture a surface or to produce gross three-dimensional reshaping of a surface.

2.4. Level 3: Grid Patterns

The third level of the knit hierarchy, *grid patterns*, is composed of regions of knit patterns that are arranged spatially across the knitting grid to form more complicated, heterogeneous patterns. By varying the knit patterns used across the knitting grid, different motions can be produced over

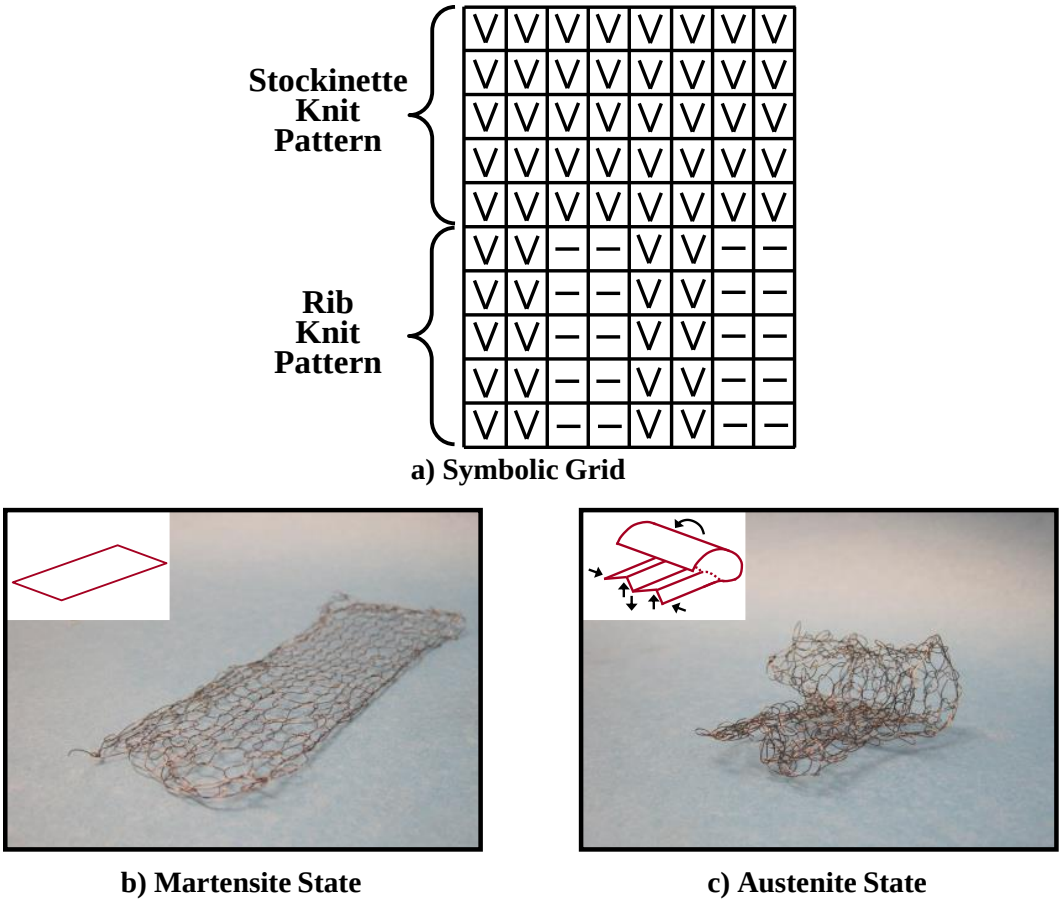

Figure 10. Grid Pattern.
Multiple patterns can be combined to form a heterogeneous grid pattern. a) This symbolic grid shows a grid pattern composed of rib and stockinette knit patterns. In the cold martensite phase the textile is relatively flat (b); upon actuation half of the textile accordions and the other half flips over to cover the accordion portion (c). Combining knit patterns into a grid pattern creates distributed controllable three-dimensional motions.

different regions of the textile. The more complicated architectures of the grid patterns provide enhanced complexity and increased variety of available three-dimensional shape changing behaviors as compared to a homogeneous knit pattern. A grid pattern is formed by connecting multiple regions of knit patterns (by connecting the edge loops of adjacent knit loop patterns) to form a larger and more complex textile with regionally varied surface topologies. Combining different knit loop patterns into grid patterns constructs knit textiles that are capable of generating complex motions by producing different behaviors in different actuation areas. The most basic combination knit loop pattern distribution is formed by synthesizing two knit patterns across a single textile.

To demonstrate the grid pattern level of the active knit hierarchy, a prototype made using 12 mil wire and 6.5 mm needles with 8 loops was constructed of stockinette for 6 cm and rib for

6 cm (Figure 10a). The unique combination of the rib and stockinette knit loop pattern causes one side of the prototype to accordion while the other side flips over to cover the accordioned portion (Figure 10b, c). Combining knit loop patterns in a knit loop pattern distribution is a powerful tool that produces textiles that create controllable complex three-dimensional motions distributed heterogeneously over an entire surface forming variable surface actuators.

2.5. LEVEL 4: RESTRUCTURED GRIDS

The fourth level of the hierarchical architecture, *restructured grids*, refers to how loops in the textile are connected in modified knitting grids. Knit patterns and grid patterns, which are created row-wise in a back-and-forth manner to form a grid of rows and columns of loops, are planar and rectangular. However, other textile shapes can be produced by connecting loops in non-orthogonal restructured knitting grids. Using restructured grids creates knitted structures with varied internal connections or modified boundary conditions and results in textiles that can be used to shape and leverage the mechanical behavior of the underlying knits, producing new behaviors and enhancing the kinematic performance. This section describes four ways of restructuring the grid – Post-Knitting Connections, Course-Wise Restructuring, Grid Cell Merging, and Re-Ordered Grids.

2.5.1. Post-Knitting Connection

Post-knitting connections are operations done on one or more knit textiles after the knitting process has been completed. Typically, post-knitting connections involve connecting two edges to one another, thus creating a three dimensional structure (much in the way a knitted garment is created from flat knit pieces). The act of connecting the edges bends the textile, which forms a restructured grid that it is no longer composed of planar orthogonal rows and columns. The result of the restructured grid is a textile that has a three-dimensional structure that can further leverage the underlying behavior of the knit pattern or grid pattern used in the construction of the textile. While any edge of a textile could be connected to another edge of the same textile (top to bottom, left to right, bottom to left, etc.), both of the examples given in this section use a top to bottom connection, which forms a belt.

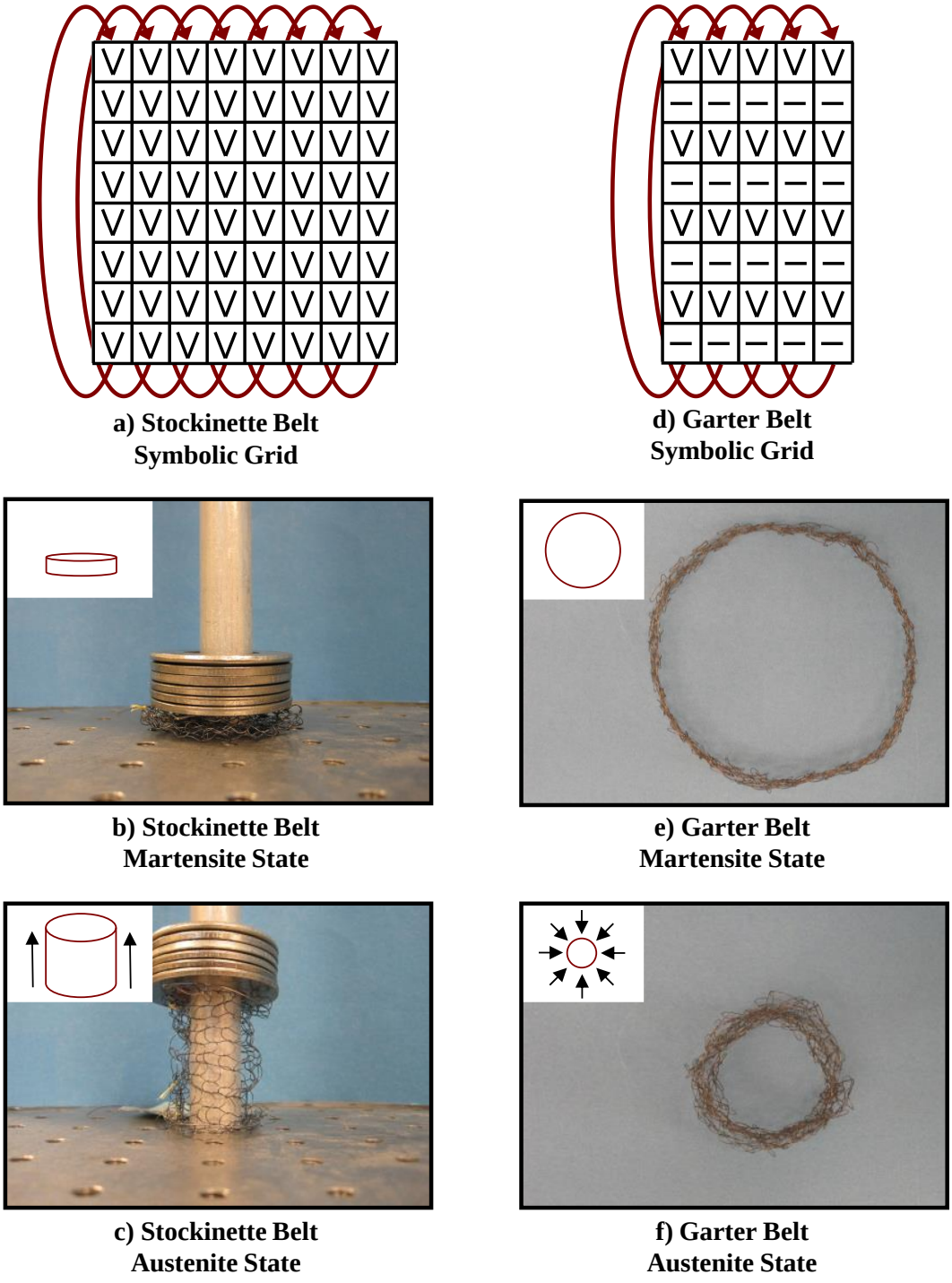

Figure 11. Restructured Grid – Post-Knitting Connection.
Post-knitting connections can be used to create Active Knit belts. a) A stockinette grid pattern is connected along the top and bottom of the prototype to form a stockinette belt which b) actuates from the initially compressed martensite state to c) lift the applied load in the expanded austenite state. d) A garter grid pattern is connected along the top and bottom of the prototype to form a garter belt which e) actuates from the initially expanded cylinder in the martensite state to f) a contracted cylinder in the austenite state. The post-knitting connection restructures the knitting grid to form a structure that further leverages the kinematic behavior of the foundation knit pattern.

One example of a post-knitting connection is a stockinette belt (Figure 11a, b, c) which is created by joining the first and last course of a stockinette textile, forming a three-dimensional tube. The post-knitting connection of the stockinette belt bends the knitted loops, increasing the out-of-plane curvature to approach that of the actuated state of the stockinette knit pattern. During actuation, the wire in the knitted loops tries to straighten, and, because the loops are already bent, the straightening of the wire results in a change in width of the belt with negligible changes to the diameter of the belt. To demonstrate this post-knitting connection, a stockinette belt prototype (12 mil wire on 8 mm needles over 8 loops for 12 cm) was created by seaming the top and bottom of the planar textile to create a tube. Upon thermal actuation the stockinette belt is able to lift 1.8 N in the wale-wise direction while expanding to four times its length with little change to the belt diameter (Figure 11b, c). This connection is another set of boundary conditions that allows relatively little material to do a huge amount of work in a small package size. The post-connected stockinette belt amplifies the intrinsic material strain by two orders of magnitude while preserving its ability to produce useful forces, producing a tubular structure that provides support to the otherwise flexible sheet that could be used to create deployable space structures.

Another example of post-knitting connection is a garter belt (Figure 11d), which is created by joining the first and last course of a garter knit pattern textile. Connecting the ends transforms the textile from planar to tubular, inducing slight curvature along the length of the loops. Because the base knit pattern is garter, the primary motion of the belt is contraction. Joining the top and bottom edges of the contractile textile forms a belt that contracts in diameter during actuation. To demonstrate this, a garter knit pattern belt prototype was created from a textile made with 8 mil wire on 6.5 mm knitting needles over 5 loops until it was 45 cm long by connecting the first and last course of the textile. The knit acted as a contractile belt reducing the diameter from 7 cm to 3.3 cm, reducing the cross sectional area of the belt by 78%, and slightly expanding the belt width (Figure 11e, f). The connected garter structure could be used as a smart mechanical transmission belt or could be used as a parallel actuator to increase the load supported by the actuator.

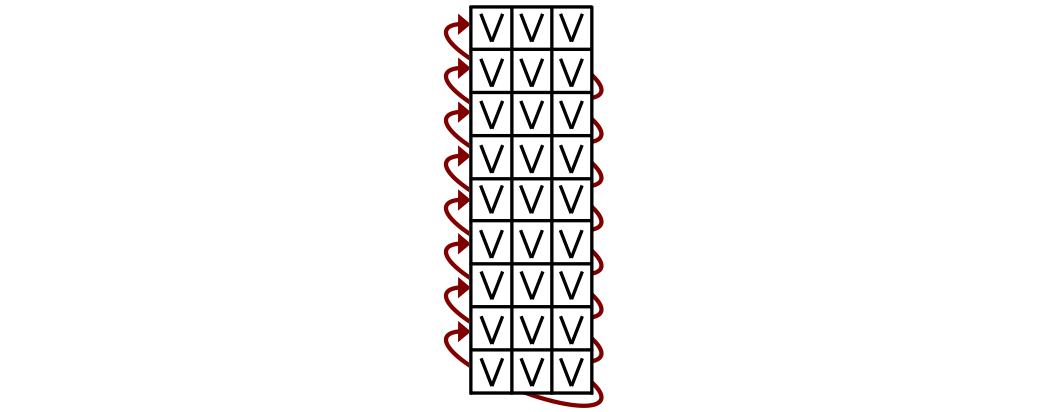

a) Symbolic Grid

b) Martensite State **c) Austenite State**

Figure 12. Restructured Grid – Course-Wise Restructuring.
Course-wise restructuring can be used to create I-cord textiles. a) Courses of a stockinette grid pattern are restructured by helically knitting across the textile to form knitted tubes which actuate from b) long thin tubes in the martensite state to c) a helically coiled structure in the austenite state. Course-wise restructuring forms restructured grids that produce novel out-of-plane actuation behaviors.

2.5.2. Course-Wise Restructuring

Course-wise restructuring is an alternative knitting order that uses a restructured grid to connect the side edge loops across the textile during the knitting process (rather than after knitting as is the case for post-knitting connections) to form a three-dimensional structure. Course-wise restructuring is accomplished using circular knitting, a method in which each course of knit loops are knit over the previous course creating a helical pattern of interlacing adjacent loops. The knit loops in course-wise restructured textiles are skewed (asymmetric) because a single course is helically connected as opposed to the orthogonal rows and columns of loops formed using simple orthogonal knitting grids. Active knits created using course-wise restructured grids produce three-dimensional textiles that are constrained by the helically connected knitted loops, and produce novel out-of-plane actuation motions a result of the skewed, asymmetric knitted loops of the restructured grid.

An I-cord is a type of textile that can be created using a course-wise restructured grid (Figure 12a). Active I-cords are created by circularly knitting with a single SMA fiber to create a long thin seamless three dimensional tube that provide simultaneous contraction and rotation upon actuation. Traditionally, I-cord textiles have a base knit pattern of stockinette. Stockinette I-cords are asymmetric about the inside and outside of the cylinder: The outside of the tube is smooth because of the forward loops (similar to the front of a stockinette knit pattern), while the inside of the cylinder has a continuous spiraling ridge (similar to the back of a stockinette knit pattern). For thinner I-cords, where each pass of the helix consists of a small number of loops, the straight knit tube spirals into a tight helix when actuated, increasing the diameter of the textile while reducing the length. As the individual loops are heated they shrink in height and increase in width. The width increase propagates through the textile altering the angle between knitted loops which creates the helical shape. To demonstrate the helical actuation behavior of course-wise restructured grids an I-cord prototype was made by helically knitting 3 loops of 8 mil wire on 3 mm diameter needles using stockinette knit pattern until the prototype was 25 cm long. The 0.2 cm diameter seamless tube at room temperature (Figure 12b) spiraled to a maximum coil diameter of 0.8 cm while reducing in length by 70% when exposed to heat above the transition temperature (Figure 12c). By restructuring the grid at the course-wise level, I-cord textiles provide extreme contraction at a point and act as a unique type of torque generator that can produce huge rotations (360° rotation per inch of actuator length) in a very thin package.

2.5.3. Grid Cell Merging

Merging grid cells decreases the number of loops in a course, forming a restructured grid that results in textiles with complex, non-rectangular shapes. Decreasing the number of knitted loops in a course through grid cell merging is a technique often used in complex patterns to create three-dimensional draping textiles, as in the shoulder of a sweater. Active knits created using grid cell merging not only produce textiles with non-rectangular shapes, they provide unique actuation motions unattainable by knit patterns or grid patterns alone. For example, a triangular textile is one possible textile shape that can be created using grid cell merging. Triangular textiles are created by decreasing the number of loops in each course by one. These decreases occur along the edges of the textile, modifying the boundary conditions. The added boundary condition modifies the behavior of the base knit pattern active knits by constraining the edges to curl as two loops are twisted to occupy the same cell in the knitting grid.

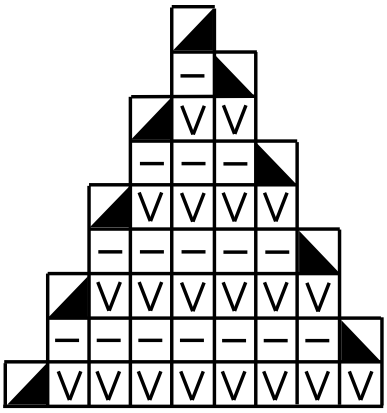

a) Symbolic Grid

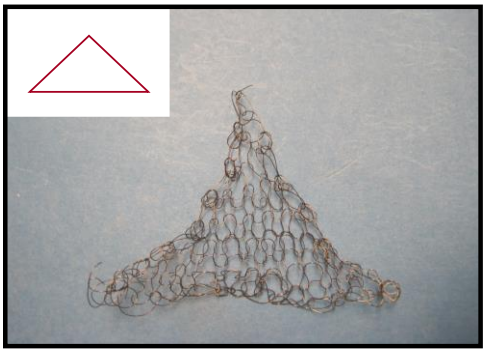

b) Martensite State

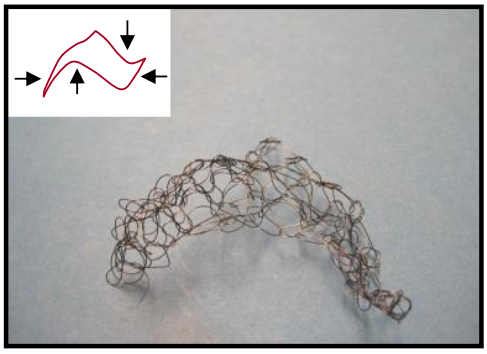

c) Austenite State

Figure 13. Restructured Grid – Grid Cell Merging.
Grid cell merging can be used to create triangular actuators. a) Courses of a garter grid pattern are manipulated by merging adjacent grid cells in alternating courses to form a triangularly shaped actuator. The triangular actuator actuates from b) the flat triangular shape in the martensite state to c) a contracted triangle with ends that curl in opposite directions due to the asymmetric boundary conditions in the austenite state. Grid cell merging restructures the grid to provide complex actuator shapes.

To demonstrate the kinematic behavior of grid cell merged active knits, a triangular textile was created (Figure 13a) using 10 mil wire and 6 mm needles with 14 loops. The textile was knit using the garter knit pattern and at the beginning of each course, two loops were knit together, decreasing the number of loops by one at the start of each course, creating a triangle with a height of 6 cm (Figure 13b). Upon actuation, the height of the triangle decreases (characteristic of the garter knit pattern) and the two base corners curl, one upward and one downward (Figure 13c). The legs bend in different directions because of the alternating boundary conditions, a result of knitting loops together in each course on alternating sides of the prototype. By controlling the boundary conditions though manipulation of the shape of the actuator, new complex three dimensional motions can be achieved and alternative complex actuator shapes are realized, neither of which have been possible through other actuation strategies.

2.5.4. Re-Ordered Grids

Re-ordered grids change the local connectivity of knitted loops within a knit textile. In knit patterns and grid patterns the row and column adjacency of the knitted loops is maintained. A re-ordered grid forms a restructured grid, modifying the connectivity of the rows and/or columns and resulting in loops that are crossed into different columns or loops that are stretched into different rows. One example of this is cabling, which is a method of attaching adjacent regions of knit pattern together by overlapping the edge loops of each adjacent pattern such that the order of two sets of columns in the earlier rows is reversed. The overlapping of the loops creates a torque within the textile causing it to twist about the vertical axis. This twisting occurs because the crossing of the loops pulls opposite corners of the textile toward one another, generating rotation about the length of the textile.

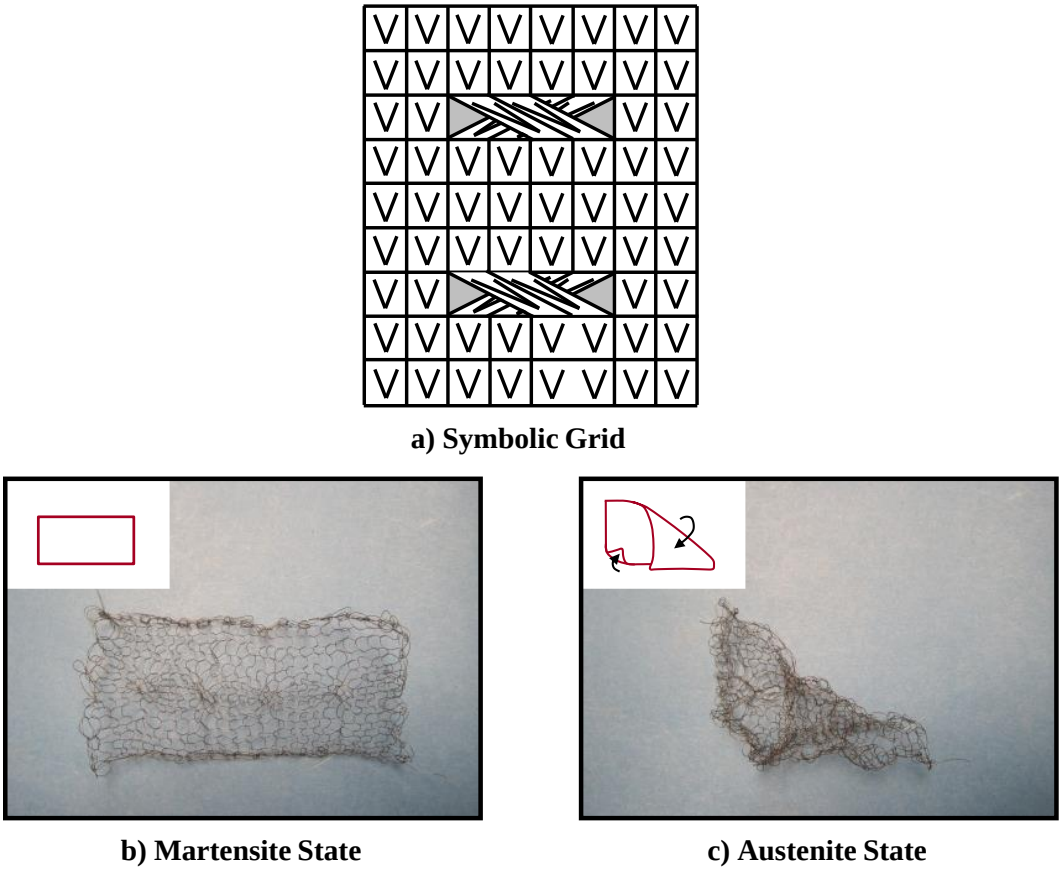

a) Symbolic Grid

b) Martensite State **c) Austenite State**

Figure 14. Restructured Grid – Re-Ordered Grids.
Re-ordered grids can be used to make cables in a knitted textile. a) The four innermost knit cells are overlapped (the two cells on the left are bent and stretched to the right and the two cells on the right are bent and stretched to the left). The cable actuator actuates from b) a flat rectangle in the martensite to c) a rectangle that is torqued along its length in the austenite state. Re-ordering the grid creates new motions unavailable with knit patterns alone.

To demonstrate the actuation behavior of a re-ordered grid active knit a cable was created by overlapping the four centermost loops in every 6th course of a textile made with a stockinette knit loop pattern (Figure 14a). This cable prototype was made using 8 mil wire, 5.5 mm needles, and 12 loops for a total of 13 cm. The top of the rectangular prototype (Figure 14b) remains in position while the bottom edge bends upward by 90° and rotates 90° about the vertical axis (Figure 14c), providing a combined bending and torsion. Reordering the cells within the knitting grid creates a restructured grid that produces tailorable motions that are not available from the basic knit loop patterns alone.

2.6. ACTIVE KNIT HIERARCHY CONCLUSIONS

This chapter leveraged the cellular hierarchical approach of traditional and engineering textiles to develop a more sophisticated classification of active knits that accounts for 1) multiple types of unit cells, 2) homogeneous distribution of unit cells across the knitting grid of the textile, 3) heterogeneous distribution of unit cells across the knitting grid of the textile, and 4) non planar orthogonal knitting grids. A four level hierarchy was introduced and experimental examples were provided (Table 1) to demonstrate the advancing complexity of actuation behaviors (Table 2): knitted loops, knit patterns, grid patterns, and restructured grids. The first level of the hierarchical architecture, ***knitted loops***, acts as the unit cell of the knitting grid and produces large strains as the bent loops leverage the strain of the foundational wire. The second level of the hierarchy, ***knit patterns***, forms homogeneous patterns of adjacent knit and purl loops across the knitting grid that interact to provide three-dimensional actuation motions such as rolling, contraction, accordion, and arching. The third level, ***grid patterns***, combines multiple knit patterns to form heterogeneous patterns across the knitting grid which affords complex and controlled three dimensional actuation motions across different areas of the textile such as arching in one area and accordioning in another. The fourth level, ***restructured grids***, restructures the knitting grid by forming both uniquely shaped and three dimensionally structured textiles that leverage the behavior of knit patterns and grid patterns to provide new three-dimensional actuation motions distributed across a surface and throughout a structure such as deployable tubes, contractile belts, coiling tubes, triangular actuators, and twisting surfaces.

Table 1. Summary of Prototypes and Experimental Results.
Representative prototypes of each hierarchical level were manufactured according to design parameters (wire diameter, needle diameter, number of loops, and prototype length) and experimentally tested, resulting in a wide variety of large, complex three-dimensionally distributed actuation motions.

Level	Architectural Configuration	Textile Name	Wire Diameter (mil)	Needle Diameter (mm)	Number of Loops	Length (cm)	Number of Rows	Actuation Motion	
Level 2: Knit Pattern	Solid	Stockinette	10	5.5	10	12.5	20	Scrolls	2 cm outer diameter
									84% length reduction
	Horizontally Striped	Garter	8	5.5	10	14	30	Contracts	70% length reduction
		10x10 Welt	8	5.5	5	17	30	Contracts and Arches	67% length reduction
	Vertically Striped	2x2 Rib	15	5.5	10	6.5	16	Accordions	2.0 cm height
									40% width reduction
									45° planes
	Diagonally Striped	Seed	15	5.5	10	7.5	20	Arches	<180° arch
Level 3: Grid Pattern	Spatially Arranged Knit Patterns	Stockinette and Rib	12	6.5	8	12	24	Accordions and Arches	45° degree planes covered by 180° arch
Level 4: Reconstructed Grids	Post Knitting Connection	Stockinette Belt	12	8	8	12	20	Expands	435% height increase under 1.8 N
		Garter Belt	8	6.5	5	45	55	Contracts Radially	78% reduction in cross sectional area
	Course-Wise Restructuring	I-cord	8	3	3	25	40	Spirals	0.8 cm coil diameter
									70% length reduction
	Grid Cell Merging	Garter Triangle	10	6	14	6	14	Contracts and Bends	35% height reduction
									Legs bend in opposite directions
	Re-Ordered Grids	Cable	8	5.5	12	13	30	Twists and Bends	90° bending and 90°axial rotation

Table 2. Impact of Hierarchical Level on Actuation Behavior.
The enhanced physical complexity of each level of the active knit hierarchy produces increasingly complex impacts on the actuation behavior.

Level	Description	Impact
Level 1: Knitted Loops	>180° curved loops that form the unit cell of the knitting grid	Leverages bending of foundational smart material wire to produce large displacements
Level 2: Knit Pattern	Homogeneous patterns of adjacent knit and purl loops across the knitting grid	Provides three-dimensional actuation motions
Level 3: Grid Pattern	Heterogeneous patterns of adjacent knit and purl loops or multiple knit patterns across the knitting grid	Affords complex and controlled three dimensional actuation motions across different areas of the textile
Level 4: Reconstructed Grids	Manipulated knitting grids that form uniquely shaped and three dimensionally structured textiles	Expands upon the behavior of knit patterns and grid patterns to create new three-dimensional actuation motions distributed across a surface and throughout a structure

The experimental survey of the actuation behavior of a variety of key active knit architectures at different hierarchal levels opens the door for a broader understanding of the actuation mechanism and gives a glimpse into the potential of this new architecture scheme. The language developed around the hierarchy provides a consistent basis through which a variety of architectures and their actuation behavior, application potential and impact, can be explored and discussed. For example, the hierarchy identified the basic unit as the knitted loop, and demonstrated the assembly of more complex levels of textiles. Development of the hierarchical classification establishes a starting point for the derivation of models that provide a quantitative basis for the kinematic and kinetic performance of the knitted loop, and then an approach to build up textile models to capture the ever-increasing complex motion afforded by each level of the hierarchy. This kinematic active knit hierarchy study has shown that the basic architectural element, the knitted loop, has the potential to be transformed innumerable ways and may provide more novel complex distributed motions through the discovery of additional architectural manipulations. This classification and illustration of representative active knits provides a useful catalog of a variety of complex motion capabilities and delivers insight that aids in the understanding and design of this new actuation paradigm to meet growing actuation needs.

Chapter 3. TWO-DIMENSIONAL ANALYTICAL MODEL OF PLANAR ACTIVE KNITTED LOOPS

To advance active knit technology and establish the science base to implement the technology in applications, a model that captures the kinetic performance of active knitted textiles is needed. Active knits are complicated hierarchical structures; therefore, the first step in creating a predictive model is to model the kinetic behavior of the first level of the active knit hierarchy – the knitted loop. Knitted loops are assembled according to the knitting grid to create knit patterns; therefore, the kinetic performance of the individual loops is scaled in series and parallel to predict the performance of knit pattern active knit textiles. This chapter presents a model of the active knitted loop that predicts the kinetic actuation performance of a planar knitted loop and planar actuating garter knit pattern active textiles.

Most existing knit models take a hierarchical modeling approach, which extrapolates the performance of a unit cell to predict the load-extension behavior of an entire textile. Even though several models exist for knitted loops, none of them includes active materials or the large deformation states created through activation. Geometric models of knitted loops were combined to represent plain knit pattern apparel fabrics in their relaxed state have existed for most of the last century [61]-[67]. Other small-deformation models characterize the geometry of the knitted loop using the stitch density [68]-[69] and have been expanded to include the initial tension of the curved knitted loop [70]-[73]. More recently, materials knitted from glass, steel, and carbon fiber materials have been investigated for use within composites for their potential for improving energy absorption, bearing and notched strengths and fracture toughness [74]-[78]. Models that are more sophisticated [79]-[81] have been developed recently that take into account larger deformations of the knitted loop from engineering materials, represent expanded architectures, accept different stress profiles and look at the knit from a micromechanics point of view such as the bridging model, but they still use only traditional engineering materials and apply to only a few knit pattern architectures.

While existing passive knit models serve as a foundation for the kinetic modeling of active knits no existing models are capable of predicting the actuation performance of active knits. However, existing models can be modified and combined in order to capture the actuation behavior of active knits by including the thermal and mechanical operational transitions that occur during active knit actuation and including the influence of the load path and the interlacing loop friction. The first and most important modification is to incorporate the dual state nature of the active knits, which no existing knit models capture. The actuation motion produced by active knits is a result of the material transformation between stiff austenite phase and the flexible, less stiff martensite phase. An active knit model must incorporate the dual stiffness material behavior of the active material. Because active knits cycle between states, incorporating friction between interlacing adjacent loops is essential. Most existing models neglect friction between adjacent loops and the few models that include friction only predict the extension of the knitted loop under load. Adjacent loops of active knits stick or slip past one another as they cycle between extended and contracted states depending on the motion direction and loading history. The varying states of friction are not covered in any existing models and must be included in an active knit model to accurately predict the hysteresis due to friction. By modifying and combining existing passive knit models, particularly those developed by Hong [74] and Shanahan [73], a quasi-static analytical model is developed that predicts the actuation of the active knit based on the state it is in, the state it came from, and the inter-loop friction experienced during the operational transition into the state.

This chapter presents an analytical state-based actuation model of the planar knitted loop in the garter knit pattern fabricated from variable stiffness smart material wire which accounts for the loading path and the friction between interlacing adjacent loops. The states of operation are defined based on the mechanical loading of the textile, the transition between different material stiffness, and the paths followed to arrive at each state. Operational transitions between these states induce frictional forces (stick or slip) depending upon the state and path, which affect the actuation response. A load-extension model is derived for each state of a typical actuation cycle with respect to the unit cell of a single loop of the textile based on the stress-strain behavior of the active material with assumptions made to allow analytical tractability. Elastica Theory and Euler-Bernoulli beam bending are used to capture the large deformations within a loop of wire. The resulting kinematic and kinetic relations for a single cell scale the load-extension behavior of the entire knit textile for each state, and provide analytical algebraic transcendental expressions for

the net actuation motion as a function of the applied tensile load on the textile. The model is validated experimentally for a thermally actuated SMA garter knit prototype over a range of applied forces with good correlation. The two dimensional analytical active knit loop model provides the ability to predict actuation motions for the radical stroke and force garter knit pattern actuation architecture, enabling the design of active knitted architectures for a wide range of applications.

3.1. TWO-DIMENSIONAL PLANAR LOOP MODEL NOMENCLATURE

A	Inflection point at end of loop leg
B	Interlacing contact point
C	Point at top of loop
C	Course height
C_1, C_2, C_3, C_4	Functions of angles used to simplify notation
D	Center of the unit cell
D	Knitting needle diameter
d	Wire diameter
E	Elliptic integral of the second kind
E_A	Base material Austenite Young's modulus
E_M	Base material Martensite Young's modulus
$\hat{E}$	Difference between complete and incomplete Elliptic integrals of the second kind
F	Elliptic integral of the first kind
F_{app}	Externally applied force to knit textile
F_{loop}	Externally applied force to knit loop
F_{UC}	Externally applied force to unit cell
$\hat{F}$	Difference between complete and incomplete Elliptic integrals of the first kind
I	Second moment of inertia of wire cross-section
k_1, k_2	Geometric functions of angles used in elliptic integrals
L	Knit loop length
$L_{subscript}$	State dependent length of knit textile
M	Bending moment at top of loop
N_c	Number of courses in knit textile
N_W	Number of wales in knit textile
O	Unit cell origin
P	Reaction force at end of loop leg
R	Reaction force at interlacing contact point
s	Length along loop
T	Horizontal wire tension at top of loop
W	Wale width
X,Y	Global coordinate system
x,y	Local coordinate system for segment BC
x',y'	Local coordinate system for segment AB
α	Loop state angle of the connecting leg at **A**
β	Loop state angle of the reaction force between adjacent loops
Δ	Knit textile deflection
δ	Unit cell deflection

ε_1, ε_2, φ_{1B}, φ_{2B}	Geometric functions of angles used in elliptic integrals
γ	Loop state angle of force P at **A**
μ	Coefficient of friction between interlacing loops
θ, θ'	Deflection angle along loop
Subscripts	
A	Austenite phase
ACT	Actuator
cont	Contracted state
ext	Extended state
M	Martensite phase
0	Initial state with zero external load

3.2. GARTER KNIT PATTERN ARCHITECTURE AND OPERATION

Garter knit pattern textiles generate large distributed planar contractile actuation motions as a result of their symmetrical loop architecture. The symmetric knit pattern actuator undergoes a four state operational procedure that results in a constant load actuation cycle. The unique garter knit pattern architecture and multi-state operation are described in this section.

3.2.1. Garter Knit Pattern Architecture

The architecture of a knit pattern is defined by the arrangement of *knit* and *purl* connections between interlaced loops of adjacent courses (Figure 16). A course is a row of knit loops, shown in red in Figure 16, which is composed of a single strand of alternating (up and down) curved loops. A wale is a column of knit loops, the legs of each loop interlocking with the top of the next loop down the wale (i.e. in the next course). In a knit connection, the legs of the upper loop in a wale overlap the top of the lower loop in the same wale and interlace behind the sides of the loop, whereas in a purl connection the top of the lower loop overlap the legs of the upper loop which interlace behind the sides of the lower loop. The ordering of the knit and purl connections define the knit pattern architecture where the garter knit pattern, composed of alternating courses of all knit and all purl connections, forms a planar textile symmetric about the front and back. The loops within the garter knit pattern architecture provide large curvatures through which loops interlace with the adjacent loop making contact at the *interlacing contact point*, **B**. The interlacing contact point may change position as adjacent loops slip relative to each other against friction, depending on the relative magnitudes of the loading and contact forces and the coefficient of friction between the wires. The garter knit is geometrically defined by its course height (C), wale width (W), loop length (L), and fiber diameter (d). The course height (C) is the vertical distance between identical

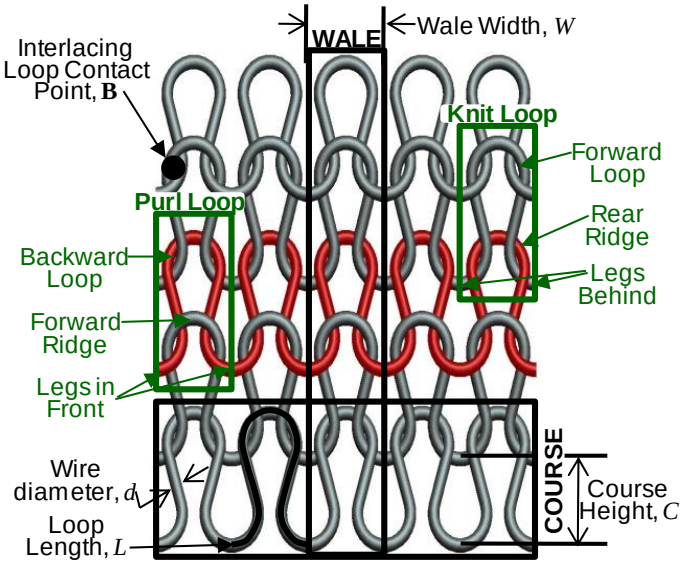

Figure 15. Basic Garter Knit Pattern Architecture.
In a garter knit, forward knit loops and backward purl loops make up courses (rows of loops) and wales (columns of loops), characterized by the course height (*C*), wale width (*W*), wire diameter (*d*), and loop length (*L*).

reference points of adjacent rows. The wale width (*W*) is the horizontal distance between identical reference points on adjacent loops within a course. The loop length (*L*) is the length along the centerline of the fiber of a single knit loop. The fiber diameter (*d*) is the diameter of the foundational wire.

3.2.2. Garter Knit Pattern Operation

SMA garter knit textiles go through *operational transitions* from one state to another resulting in a change in length and stiffness of the textile. The operational transitions are initiated by either a change in thermal loading, inducing a *material transition* from flexible Martensite to stiff Austenite, or by changes in mechanical loading. During these operational transitions, different friction conditions occur between loops of the knit (stick or slip) depending on the loading and the initial state. The state of the textile is defined by the thermal loading (Austenite or Martensite), the mechanical loading and the loading path by which the textile arrived into that *State* (*Free, Extended,* or *Contracted*). A typical actuation cycle (depicted in Figure 16) is initiated from the *Austenite Free State* with an operational transition into the *Austenite Extended State*, and then cycles between the *Martensite Extended State* and the *Austenite Contracted State*. The length of the textile in each state, and therefore the motion produced by each operational transition, depends on four factors: 1) the state it is in, 2) the state it came from, 3) the magnitude of the mechanical

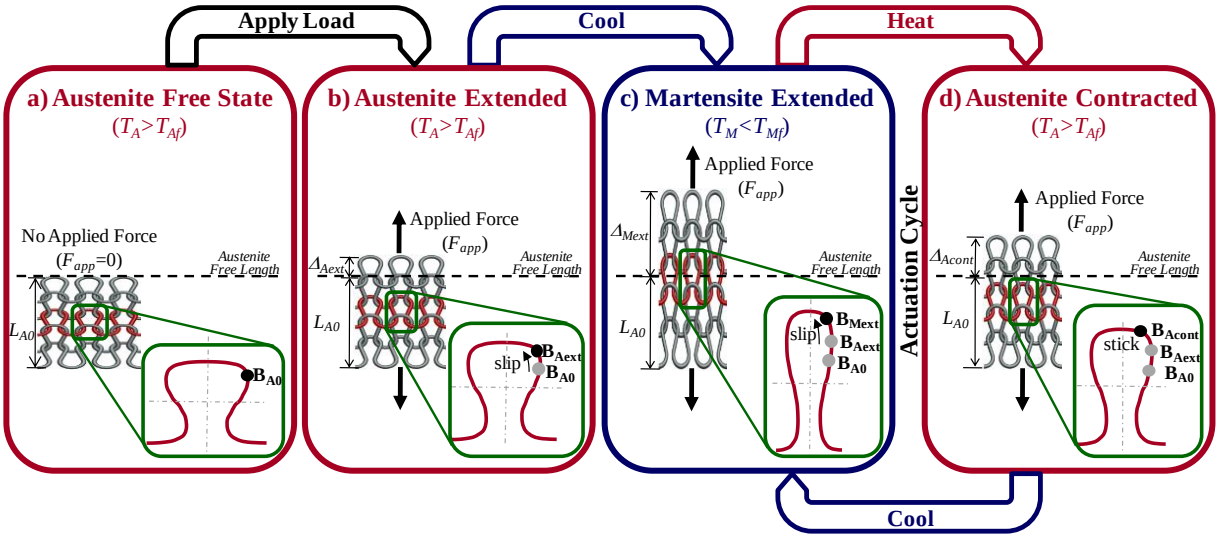

Figure 16. Active Garter Knit Pattern Operational States.
A garter knit has four operational states: a) *Austenite Free State*, b) *Austenite Extended State*, c) *Martensite Extended State*, and d) *Austenite Contracted State* reached through thermal or mechanical operational transitions where a typical actuation cycle is alternates between the *Martensite Extended* and *Austenite Contracted States*.

loading, and 4) the inter-loop friction conditions experienced during operational transition into its state.

3.2.2.1. Austenite Free State

A typical actuation cycle is initiated with the SMA garter knit textile in a heated state with no external loads. When the temperature of the SMA is raised above its Austenite Finish transition temperature, it makes a material transition from a soft Martensite phase to a stiff Austenite phase. In transitioning, deformations experienced in the Martensite state are recovered, producing the Shape Memory Effect of SMA. While the material phase of SMA is a function of both temperature and stress, for modeling purposes, it is assumed that a complete thermal transition occurs throughout the wire and that the bending stresses are low enough such that no areas of stress induced martensite are developed. Because the Martensite strains are recovered, the Austenite Free State provides a zero reference for computing material strains. In a knitted structure, however, the material is not actually in a zero-strain state since the wires, which come from the manufacturer trained to a straight shape, are bent in loops. When heated they attempt to return to their naturally straight configuration resulting in a relatively wide wale width, *W*, and a relatively short course height, *C*. Even though many internal stresses and strains exist, the garter knit textile length L_{A0} in the Austenite Free State (Figure 16a) is set as the zero deflection reference point for actuation.

3.2.2.2. Austenite Extended State

When a tensile load, F_{app}, is applied to the textile in this heated state, the knit loops elongate, increasing the course height C, and lengthening the entire textile by a deflection Δ_{Aext}, relative to the Austenite Free length, L_{A0}. During this operational transition into the Austenite Extended State (Figure 16b), the adjacent loops of wire generally slip past each other from an initial point of contact $\mathbf{B}_{A0}$ along the loop to a final interlacing contact point $\mathbf{B}_{Aext}$. The resulting friction resists the slip and therefore resists elongation of the textile, reducing the deflection Δ_{Aext} into this state.

3.2.2.3. Martensite Extended State

When the textile is allowed to cool under load to a temperature below its Martensite Finish transition temperature, the textile makes a material transition into the Martensite phase and becomes less stiff. It is assumed that the stiffness decreases as a result of a complete thermal transition as all the material cools below the Martensite finish temperature. As a result, the course height of the loops elongates further into the Martensite Extended State (Figure 16c) in which the textile is deflected by Δ_{Mext} relative to the Austenite Free length, where $\Delta_{Mext}>\Delta_{Aext}$. During this operational transition, adjacent loops slip further past each other from the Austenite Extended interlacing point of contact $\mathbf{B}_{Aext}$, to the Martensite Extended interlacing point of contact $\mathbf{B}_{Mext}$ such that friction again reduces the deflection experienced by the textile during this operational transition. The Martensite Extended State is the first of two states in the cyclic portion of the typical actuation cycle.

3.2.2.4. Austenite Contracted State

The next state of the actuation cycle is entered when the material is heated under load to above its Austenite Finish transition temperature to the Austenite phase. The resulting stiffening of the material causes the wires within each loop to attempt to straighten to their natural straight shape, reducing the course height, and inducing contraction of the textile to a length deflected from the Austenite Free length by a distance Δ_{Acont}, where $\Delta_{Mext}>\Delta_{Acont}>\Delta_{Aext}$. During this operational transition into the Austenite Contracted State (Figure 16d), friction between the loops opposes relative motion of the interlacing point of contact back downward toward the Austenite Extended interlacing point of contact $\mathbf{B}_{Aext}$. In most cases, the friction is observed to completely block slippage such that the Austenite Contracted interlacing point of contact $\mathbf{B}_{Acont}$ remains stuck at the Martensite Extended interlacing point of contact $\mathbf{B}_{Mext}$. Thus, even though the thermal and

mechanical loading are identical in the Austenite Extended State and the Austenite Contracted State, the length in the Austenite Contracted State is longer than that of the Austenite Extended State due to the change in direction and stick-slip nature of the friction conditions experienced in arriving at each state.

Actuation against an applied force F_{app} occurs cyclically between the *Austenite Contracted State* and the *Martensite Extended State*, where the net actuation deflection Δ_{ACT} is equal to the difference between the *Martensite Extended* deflection and the *Austenite Contracted* deflection ($\Delta_{ACT}=\Delta_{Mext}-\Delta_{Aext}$).

3.3. ANALYTICAL GARTER KNIT PATTERN MODEL

An analytical state-based actuation model is derived for the garter knit pattern architecture to predict the load-extension behavior of each state and net actuation motion as a function of the applied tensile load on the textile, thermal load and material phase, and path dependent friction. While several load-extension models exist for passive textile knits [61]-[81], they do not model the multi-state contractile actuation of active knits. Existing knit models are typically purely geometric and only capture small deformations, while engineering models that account for larger deformations only predict the load-extension behavior of a passive single-state knit. None of these existing models incorporate thermal and mechanical operational transitions from one state to another, and they all neglect the influence of the load path and the interlacing loop friction.

These passive knit models however, do provide a starting foundation for the modeling of the load-extension of individual states of an active knit. By modifying and combining existing passive knit models, particularly those developed by Hong [74] and Shanahan [73], a quasi-static analytical model can be developed that predicts the actuation of the active knit based on the state it is in, the state it came from, and the inter-loop friction experienced during the operational transition into the state. The required modifications include incorporating slipping and sticking between adjacent interlacing loops, enforcing compatibility of displacements and curvature at the interlacing contact point, and accounting for the change in stiffness between states.

The modeling approach uses a quarter of the knit loop as the unit cell of the garter knit pattern architecture. Geometric relations are established for the unit cell taking advantage of the high level of symmetry within the structure to describe the position of key points and inflections within the cell. The reference *Austenite Free State* is modeled to establish the base geometry and loop shape,

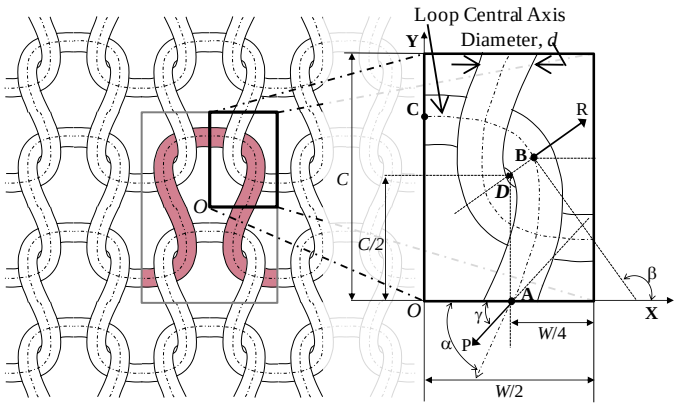

Figure 17. Planar Knit Unit Cell.
The knit unit cell is one quarter of a knit loop (shown in red) and is defined by geometric parameters (course height - *C*, wale width - *W*, loop length - *L*, wire diameter – *d*) and unknown characteristic angles (α, β, and γ) .

as well as the load-extension behavior of the *Austenite* and *Martensite Extended*, and the *Austenite Contracted States*. For each state, the shape of the loop is established using Elastica Theory and Euler-Bernoulli beam bending to capture the large bending rotations using a small-strain linear deflection approximation of the SMA wire in each phase. Equilibrium equations are developed for the loop including the stick or slip friction interaction between loops depending on the particular operational transition. The resulting governing differential equations are integrated along the loop using boundary conditions derived from geometry to provide a set of algebraic equations relating a set of three unknown loop state angles to the overall size of the cell. Kinetic relations for each state are formulated to relate the loading on each loop to its shape providing fully analytical transcendental equations from which the load-extension behavior of the unit cell is derived. The difference between the load-extension behavior of the *Martensite Extended* and *Austenite Contracted States* describes the actuation behavior of the unit cell. The unit cell properties are scaled by the numbers of courses and wales to provide the load-extension behavior and net actuation behavior of the entire knit textile.

3.3.1. Assumptions

To simplify the modeling approach and to enable analytical tractability, several assumptions about the fibrous active material and loop architecture are employed. The fiber is assumed to be a naturally straight, inextensible, incompressible, homogeneous, elastic rod that experiences the shape memory effect. The SMA wire is assumed to be trained to a straight shape that is recoverable upon heating at low load levels. While inextensibility is not traditionally associated with SMA wire because of its large axial extension and contraction capability, it is used in the knitted model

because at typical load levels the extension of the knit is assumed to be governed by the change of shape in the knit loop caused by bending. The inextensibility assumption implies a constant diameter for the SMA wire.

The effective modulus of elasticity is phase dependent (E_A, E_M), assuming the material fully transforms between states as discussed in the operation section, and is derived from small strain limiting cases of the nonlinear stress-strain relationships. In reality, the bending curvatures of the SMA material may not allow complete transformation into the austenite phase and a portion of the material may be in the stress induced martensite phase. Also, while linear elastic assumptions apply well to the full austenite state they only apply to the martensite state for small strains. However, these simplified material assumptions are made to enable tractability of the analytical model, and they do apply to situations with relatively large loop to wire diameter ratios, therefore to more loosely knit architectures.

In addition to assumptions about the fibrous material several loop architecture assumptions have been implemented. Every loop in the knitted textile is assumed to have the same planar geometry with no out of plane behavior during deformation. Interlacing loops from adjacent courses are assumed to always be in contact and the central axes of these loops are separated by one wire diameter (Figure 17). A simplified fiber reaction force, R, acting at a single point between the interlacing fibers perpendicular to the fiber axis is assumed while a frictional force, μR, acts at the same point along the fiber in the opposite direction of the sliding motion.

3.3.2. Geometric Relations

Geometry plays a crucial role in the development of an analytical model of active knitted material because it allows for the establishment of physical constraints between the known geometric parameters (course height-C, wale width-W, loop length-L, and wire diameter-d) and the unknown loop state angles (α, β, and γ). The three angles (the angle of the reaction force (R) between adjacent loops – β, the angle of the connecting leg at **A** – α, and the angle of force P at **A** – γ) describe the geometric loop shape under different loads. The undetermined loop state angles vary during loading to allow for the direction of internal forces to change and slipping of the interlacing contact point during extension. The geometric constraints are developed by analyzing a unit cell of the garter knit pattern architecture. The unit cell is one quarter of the knit loop and a quarter of the interlacing adjacent loop (Figure 17). A complete knit loop can be assembled using

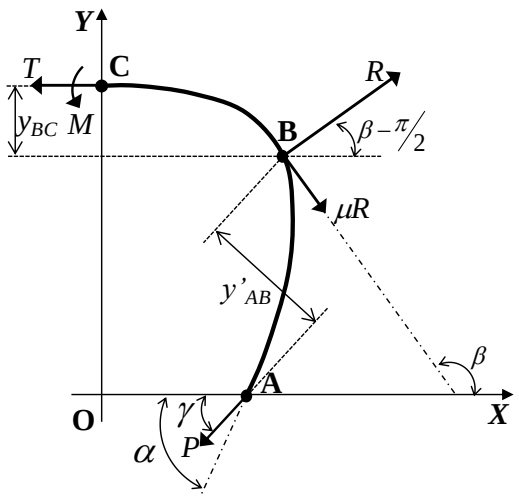

Figure 18. Garter Knit Unit Cell Free Body Diagram.
The free body diagram of the garter knit unit cell includes the internal forces and moments – *T*, *R*, μR, *P*, and *M* and the loop state angles (α, β, and γ)..

symmetry by rotating and reflecting the unit cell about the *X* and *Y*-axes defining the origin at this center of symmetry, **O**, and matching the connection points at the top (or bottom) of the loop at **C** and at the end of the connecting leg at **A**. Symmetry dictates the position and curvature at point **A**. To ensure compatibility of displacements along the length of the wire **A** must be located in the bottom center of the unit cell at (0,*W/4*). Continuity requires **A** to be an inflection point acting along the angle α, because the direction of the curvature of the wire in the knit loop changes therefore **A** cannot support a moment. From **A** the wire begins to curve upward until it reaches the interlacing contact point **B**, the point along the central axis of the knit loop through which the resultant force between adjacent loops acts. To maintain symmetry, the line of action of the resultant force, *R*, which acts perpendicular to the tangent line at **B,** must pass through the center of the unit cell, **D**, located at (*W/4*,*C/2*) and representing the point of interaction between adjacent loops, requiring **B** to lay a distance of *d/2* from **D** along an angle of β-$\pi/2$. From **B**, the foundational wire continues to curve toward the top of the knit loop, point **C**, located at an unknown height along the left-most edge of the unit cell.

Four different geometric relations can be derived from the unit geometry. The first geometric constraint,

$$\frac{W}{4} = X_B - \frac{d}{2}\cos\left(\beta - \frac{\pi}{2}\right), \tag{1}$$

relates $X_{B,}$ the *X*-coordinate of the interlacing contact point, **B**, to *W/4*, the *X* position of point **A**, using the assumption that the adjacent interlocking wires are in contact and incompressible, therefore separated by the wire diameter, *d*, along the line of action of *R*. Similarly, a second constraint,

$$X_B - X_A = \frac{d}{2}\cos\left(\beta - \frac{\pi}{2}\right), \tag{2}$$

couples the difference in the *X*-coordinates of the interlacing contact point and leg end, X_B and X_A, to the horizontal component of the distance between the loop interaction point, **D**, and half the wire diameter. Using the same assumptions as used for the development of wale width constraint (Equation 1), a third constraint,

$$\frac{C}{2} = Y_B - \frac{d}{2}\sin\left(\beta - \frac{\pi}{2}\right), \tag{3}$$

associates the *Y*-coordinate of point **B**, with the vertical location of the center of the unit cell, *C/2*, using the wire diameter, *d*, and angle, β. The final geometric constraint,

$$\frac{L}{4} = s_{AB} + s_{BC}, \tag{4}$$

is a compatibility equation relating the length of wire in the loop, *L*, to the combined length of segment **AB**, s_{AB}, and length of segment **BC**, s_{BC}, in this quarter knit loop established using the inextensibility assumption.

3.3.3. Austenite Free Reference State

The *Austenite Free State* acts as a reference state upon which all further calculations are made. The state is developed by analyzing the force equilibrium interactions and the governing differential equations for the segment of the loop above and below the interlacing contact point. The analysis allows for kinematic loop state equations to be derived in terms of measureable geometric parameters (course height – *C*, wale width – *W*, loop length – *L*, wire diameter – *d)* and unknown loop state angles (α, β, and γ) which can be solved to provide the loop state angles. Once the loop state angles are known, the corresponding kinetic information (internal forces) can be

calculated. The kinematic and kinetic values provide a reference state for the extension and contraction of the knitted structure.

3.3.3.1. Force Equilibrium Interactions

The free body diagram of the planar knit loop (Figure 18) is separated into two segments at the interlacing contact point (**B**) by the resultant force, *R*, transmitted by the adjacent interlocking loop. A friction force, μR, acts perpendicular to *R* at **B** in the positive *X* and negative *Y* direction to resist extension from the as-knit geometry which typically has more overlap and slack between courses. A single force *P* acts on point **A** at an angle of γ relative to the *X*-axis, which is an inflection point and cannot support a moment. At point **C,** a horizontal force, *T*, acts in the negative *X*-direction and a bending moment, *M*, acts counterclockwise (no shear can be supported due to symmetry).

Force-equilibrium analysis in the *X* and *Y* forces and moments provides kinetic loop relationships. Force equilibrium in the *X*-direction results in

$$T = R\left(\sin\left(\beta\right) - \mu\cos\left(\beta\right)\right) - P\cos\left(\gamma\right). \tag{5}$$

Equilibrium in the *Y*-direction produces

$$R = \frac{-P\sin\left(\gamma\right)}{\mu\sin\left(\beta\right) + \cos\left(\beta\right)}, \tag{6}$$

which can be combined with the tension in the top of the loop from the *X*-direction equilibrium (Equation 5) to eliminate *R* and give the relationship

$$T = -P\left(\sin\left(\gamma\right)\frac{\sin\left(\beta\right) - \mu\cos\left(\beta\right)}{\cos\left(\beta\right) + \mu\sin\left(\beta\right)} + \cos\left(\gamma\right)\right). \tag{7}$$

For future simplification the substitution

$$k_1 = \sin\left(\gamma\right)\frac{\sin\left(\beta\right) - \mu\cos\left(\beta\right)}{\cos\left(\beta\right) + \mu\sin\left(\beta\right)} + \cos\left(\gamma\right) \tag{8}$$

is made, where k_1 is a function of the geometric angles β and γ only.

The moment balance about **B** is

$$M = Py'_{AB} - Ty_{BC} \tag{9}$$

and can be simplified to

$$M = P\left(y'_{AB} + k_1 y_{BC}\right) \tag{10}$$

using the modified equation for the tension in the top of the loop (Equation 7), where y'_{AB} is the perpendicular distance between the line of action of P and **B** and y_{BC} is the vertical distance between **B** and the top of the loop, **C**.

3.3.3.2. Analysis of Governing Differential Equations

The governing differential equations describing the bending of the knit loop are developed using Elastica theory and Euler-Bernoulli beam bending. Elastica Theory is a theory of solid mechanics that accounts for large elastic rotations of structures during bending or buckling [76]. The use of Elastica Theory requires manipulation of the governing differential equations using the relations $dx/ds=cos(\theta)$ and $dy/ds=sin(\theta)$ to obtain closed form solutions involving complex elliptic functions. Bending of the knit unit cell is analyzed in two sections, segments **AB** and **BC**, while imposing continuity of displacements and slopes at **B**.

3.3.3.2.1. Lower Loop Segment AB

Segment AB is treated as an elastic rod pinned at A with an applied end load, P, and analyzed using a transformed coordinate system (x',y') centered at A where x' is along but opposite the line of action of P (Figure 19a). The differential equation describing this portion of the loop is simply

$$\frac{d\theta'}{ds} = \frac{Py'}{E_A I} \tag{11}$$

as determined from Euler-Bernoulli beam bending where θ' is the angle with the x'-axis, s' is the length along the loop, E_A is the phase dependent effective elastic modulus of the wire in the austenite phase, and I is the second moment of inertia of the wire cross section.

The governing differential equation for segment **AB** (Equation 11) is differentiated and the Elastica relation $dy/ds=sin(\theta)$ is used to obtain

$$\frac{d^2\theta'}{ds^2} = \frac{P}{E_A I}\frac{dy'}{ds} = \frac{P}{E_A I}\sin\left(\theta'\right) \tag{12}$$

.

This equation is multiplied by $d\theta/ds$ and rearranged, giving

$$\frac{d}{ds}\left[\frac{1}{2}\left(\frac{d\theta'}{ds}\right)^2+\frac{P}{E_A I}\cos(\theta')\right]=0 \quad , \tag{13}$$

which can be integrated to determine the length of the wire, $s_{AB,}$ using the boundary conditions derived from geometry and the fact that point **A** is an inflection point

$$\theta'|_{s=0}=\alpha-\gamma \quad , \tag{14}$$

$$\frac{d\theta'}{ds}|_{s=0}=0 \quad \text{, and} \tag{15}$$

$$\theta'|_{s=s_{AB}}=\beta-\gamma \quad . \tag{16}$$

Two substitutions,

$$u=\cos\left(\frac{\theta'}{2}\right) \quad \text{and} \tag{17}$$

$$z=\arcsin\left(\frac{u}{\cos\left(\frac{\alpha-\gamma}{2}\right)}\right) \quad , \tag{18}$$

are useful to manipulate the integral into a closed for elliptic integral describing the length of segment **AB**,

$$s_{AB}=\sqrt{\frac{E_A I}{P}}\hat{F}\left(\varepsilon_1,\varphi_{1B}\right) \quad , \tag{19}$$

where

$$\varepsilon_1=\cos\left(\frac{\alpha-\gamma}{2}\right) \quad , \tag{20}$$

$$\varphi_{1B}=\arcsin\left(\cos\left(\frac{\beta-\gamma}{2}\right)\Big/\cos\left(\frac{\alpha-\gamma}{2}\right)\right) \quad \text{, and} \tag{21}$$

$$\hat{F}\left(\varepsilon_1,\varphi_{1B}\right)=F\left(\varepsilon_1,\pi/2\right)-F\left(\varepsilon_1,\varphi_{1B}\right) \tag{22}$$

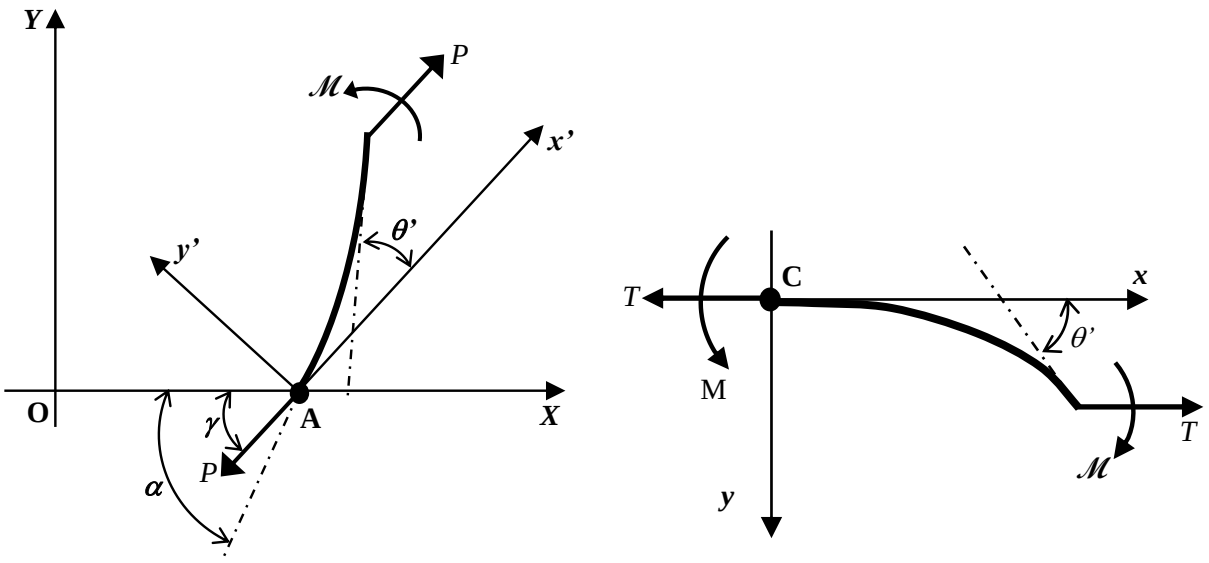

a) Free Body Diagram for Segment AB **b) Free Body Diagram for Segment BC**

Figure 19. Loop Segment Free Body Diagrams.
Free body diagrams are shown for analysis of the governing differential equations of the two segments in the garter knit pattern unit cell: a) Segment AB and b) Segment BC.

given $F(\varepsilon_1,\pi/2)$ is a complete elliptic integral of the first kind and $F(\varepsilon 1,\phi_{1B})$ is an incomplete elliptic integral of the first kind. The curvature, $d\theta/ds$, at any point along the length of segment **AB** is found by differentiating the length along the loop (the general form of Equation 19) with respect to θ to obtain the equation

$$\frac{d\theta}{ds}\Big|_{s=s_{BC}} = 2\varepsilon_1\sqrt{\frac{E_A I}{P}}\cos\left(\varphi_{1B}\right). \tag{23}$$

Integrating the combination of the Elastica assumptions and the curvature relationship (Equation 23) the x' and y' coordinates for loop segment **AB** are determined to be

$$x'_{AB} = \sqrt{\frac{E_A I}{P}}\left\{\hat{F}\left(\varepsilon_1,\varphi_{1B}\right) - 2\hat{E}\left(\varepsilon_1,\varphi_{1B}\right)\right\} \text{ and} \tag{24}$$

$$y'_{AB} = 2\sqrt{\frac{E_A I}{P}}\varepsilon_1\cos\left(\varphi_{1B}\right), \tag{25}$$

where

$$\hat{E}\left(\varepsilon_1,\varphi_{1B}\right) = E\left(\varepsilon_1,\pi/2\right) - E\left(\varepsilon_1,\varphi_{1B}\right), \tag{26}$$

and $E(\varepsilon_1,\pi/2)$ is a complete elliptic integral of the second kind and $E(\varepsilon_1,\phi_{1B})$ is an incomplete elliptic integral of the second kind. Transforming the coordinate system from the local x',y' to the global X,Y through the angle γ results in

$$X = \frac{W}{4} + x'\cos(\gamma) - y'\sin(\gamma) \quad \text{and} \tag{27}$$

$$Y = x'\sin(\gamma) + y'\cos(\gamma) \quad . \tag{28}$$

The analysis of the lower loop segment **AB** provides half the fundamental equations used in determining the loop state angles.

3.3.3.2.2. Upper Loop Segment BC

Segment BC is treated as an elastic rod clamped at **C** with a horizontal load, T, and an applied moment, M, while **B** is free to move (Figure **19**b) but must satisfy continuity conditions with **AB**. Segment **BC** is analyzed using the transformed coordinate system (x,y) where x is shifted vertically from X, **C** acts as the origin, and y acts in the negative Y direction. The differential governing equation for segment **BC** is given by

$$\frac{d\theta}{ds} = \frac{Ty + M}{E_A I} \quad , \tag{29}$$

where θ is the angle between the x-axis and the tangent line to the loop. The modified equation for the tension in the top of the loop (Equation 7) and the moment at the top of the loop (Equation 10) are substituted into the governing differential equation for segment **BC** (Equation 29), which is differentiated and the Elastica relation is employed resulting in the manipulated equation

$$\frac{d}{ds}\left[\frac{1}{2}\left(\frac{d\theta}{ds}\right)^2 + \frac{T}{E_{A,M} I}\cos(\theta)\right] = 0 \quad . \tag{30}$$

The differentiated governing differential equation (Equation 30) can be integrated to determine the length of the wire, s_{BC}, in segment **BC** using the geometric boundary conditions

$$\theta|_{s=0} = 0 \quad , \tag{31}$$

$$\theta|_{s=s_{BC}} = \pi - \beta \quad , \text{ and} \tag{32}$$

$$\frac{d\theta}{ds}\Big|_{s=s_{BC}} = 2\varepsilon_1\sqrt{\frac{E_A I}{P}}\cos\left(\varphi_{1B}\right), \tag{33}$$

where the boundary condition for the curvature at the interlacing contact point **B** (Equation 33) enforces continuity of wire curvature at **B**. Employing the substitutions

$$u = \cos\left(\frac{\theta}{2}\right) \text{ and} \tag{34}$$

$$z = \arccos\left(u\right), \tag{35}$$

this integration results in an equation describing the length of segment **BC**,

$$s_{BC} = \sqrt{\frac{E_A I}{P}}\sqrt{\frac{2}{k_1 + k_2}}F\left(\varepsilon_2, \varphi_{2B}\right), \tag{36}$$

where

$$\varphi_{2B} = \frac{\pi - \beta}{2}, \tag{37}$$

$$\varepsilon_2 = \sqrt{\frac{2k_1}{k_1 + k_2}}, \text{ and} \tag{38}$$

$$k_2 = 2\varepsilon_1^2\cos^2\left(\varphi_{1B}\right) + k_1\cos\left(\beta\right), \tag{39}$$

and $F(\varepsilon_2, \phi_{2B})$ is an incomplete elliptic integral of the first kind. The *x* and *y* coordinates of **B** can be determined to be

$$x_{BC} = \sqrt{\frac{E_A I}{P}}\sqrt{\frac{2}{k_1 + k_2}}\left(\frac{2}{\varepsilon_2^2}E\left(\varepsilon_2, \varphi_{2B}\right) + \left(1 - \frac{2}{\varepsilon_2^2}\right)F\left(\varepsilon_2, \varphi_{2B}\right)\right) \tag{40}$$

and

$$y_{BC} = \sqrt{\frac{E_A I}{P}}\sqrt{\frac{2}{k_1 + k_2}}\left(\frac{-2}{\varepsilon_2^2}\left(\sqrt{1 - \varepsilon_2^2 \cdot \sin^2\left(\varphi_{2B}\right)} - 1\right)\right) \tag{41}$$

using the Elastica criteria. No coordinate transformation is needed for the *x*-coordinate but the equation

$$Y = Y_{AB} + \left(y_{BC} - y\right) \tag{42}$$

transforms any local coordinate y into a global coordinate *Y*.

3.3.3.3. Kinematic Relations

The kinematic equations developed during the analysis of the knit unit cell provides a set of nonlinear algebraic loop state equations that relate the initially measurable geometric parameters: wale width (*W*), course height (*C*), wire diameter (*d*), and loop length (*L*), to the unknown loop state angles. During the *Austenite Free State*, when no external load is applied to the knit unit cell, the loop state equations can be solved to obtain the loop state angles and the internal forces can be calculated.

The geometric constraints (Equations 1-4) can be modified with the new definitions of the coordinates and loop length segments (Equations 19, 27, 28, 36, and 40) in terms of the unknown loop state angles (α, β, and γ) and manipulated to eliminate the unknown force *P* to obtain the three loop state equations:

$$\frac{L}{W} = \frac{C_4}{C_1 - C_3}, \tag{43}$$

$$\frac{L}{C} = \frac{2C_4}{C_2 + C_3 \cot\left(\beta\right)}, \text{ and} \tag{44}$$

$$\frac{L}{d} = \frac{2C_4 \sin\left(\beta\right)}{C_3}, \tag{45}$$

which relate the geometric parameters (*W, C, L,* and *d),* which can be measured from any loop in the *Austenite Free State* of the knit textile, to the unknown loop state angles. The three algebraic loop state equations provide a set of simultaneous nonlinear equations where the C_i's are only functions of α, β, and γ and are given by

$$C_1 = \sqrt{\frac{2}{k_1 + k_2}}\left[\frac{2}{\varepsilon_2^2}E\left(\varepsilon_2, \varphi_{2B}\right) + \left\{1 - \frac{2}{\varepsilon_2^2}\right\}F\left(\varepsilon_2, \varphi_{2B}\right)\right], \tag{46}$$

$$C_2 = \sin(\gamma)\left\{ f(\varepsilon_1, \varphi_{1B}) - 2e(\varepsilon_1, \varphi_{1B}) \right\} + 2\varepsilon_1 \cos(\gamma)\cos(\varphi_{1B}), \tag{47}$$

$$C_3 = \cos(\gamma)\left\{ f(\varepsilon_1, \varphi_{1B}) - 2e(\varepsilon_1, \varphi_{1B}) \right\} - 2\varepsilon_1 \sin(\gamma)\cos(\varphi_{1B}), \text{ and} \tag{48}$$

$$C_4 = f(\varepsilon_1, \varphi_{1B}) + \sqrt{\frac{2}{k_1 + k_2}} F(\varepsilon_2, \varphi_{2B}). \tag{49}$$

By making the initial material assumptions, the set of nonlinear differential equations was reduced to a set of three simultaneous transcendental algebraic equations. Using the measured geometric parameters, the system of loop state equations (Equations 43-45) can be solved numerically to determine the unknown loop state angles (α, β, and γ) that describe the unloaded loop. The kinematic analysis of the loop state equations provides the unknown geometric angles describing the loop in the *Austenite Free State*.

3.3.3.4. Kinetic Relations

Once the loop state angles are known the load at **A** can be determined using the geometric length constraint and the definition of C_4 (Equations 4 and 49) to be

$$P_A = \frac{16 E_A I C_4^2}{L^2} \tag{50}$$

acting at an angle γ to the X axis. The load, P_A, is the internal force at point **A** that maintains the loop shape. The initial tension in the top of the loop, T_0, can be determined using the equation of the tension in the top of the loop (Equation 7) and the initial Y component of the force P_A, P_{y0}, can be calculated using the relationship, $P_{y0} = P_A \sin(\gamma)$. While there are no external forces acting on the knit loop, internal tensions exist within the loop.

3.3.4. Austenite and Martensite Extended States

The development of the equations representing the *Austenite* and *Martensite Extended States* parallels that of the *Austenite Free State*. The force-equilibrium interactions are identical with friction still opposing extension. The governing differential equations for the *Austenite Extended State* are equivalent to those of the *Austenite Free State*, while the governing differential equations for the *Martensite Extended State* are the same except E_A (the Austenite elastic modulus) is replaced by E_M (the representative Martensite elastic modulus). However, with the kinematic

relations an additional loop state equation is developed because the relationship between the wale width and course height must be determined as the textile is extended. The kinetic relations differ with the inclusion of an external load in the expression of the load *P* at the leg of the unit cell and the development of a load-deflection relation for both the unit cell and the entire textile. The kinetic and kinematic relations for the *Austenite* and *Martensite Extended States* are developed for Austenite as an illustration, where the Martensite relations differ only by the material modulus of elasticity E_M.

3.3.4.1. Kinematic Relations

The characteristic loop state angles must be calculated for the *Extended State* under applied loads as the textile extends, requiring an additional constraint because the wale width, W, narrows from the *Austenite Free State* as the course height, C, lengthens. The loop length, *L*, and the diameter, *d*, remain constant during extension therefore the wire diameter/loop length loop state equation (Equation 45) can still be used. The wale width/loop length loop state equation (Equation 43) establishes a relationship to the load dependent loop state angles (α, β, and γ). A third equation is necessary to solve for these unknown angles. This is derived from the assumption that the tension in the top of the loop, *T*, remains constant from the *Austenite Free State* as increases in the horizontal component of *R* are taken up through *P* due to symmetry thus there can be no change in horizontal loading [74] of the unit cell. Constant horizontal loop tension produces the relationship

$$T_A = \frac{-16E_A I C_4^2 k_1}{L^2}, \tag{51}$$

as derived from the equation for the tension in the top of the loop (Equation 7) and the equation for the load, *P*, applied at **A** (Equation 50). In the constraint for the tension at the top of the loop (Equation 51) the tension, T_A, is known from the *Austenite Free State*, and the loop length (*L*), the moment of inertia (*I*), and the Elastic Modulus E_A are known values based on the phase of the material and the measured geometric properties, while C_4 and k_1 are geometric functions of the unknown loop state angles. The set of three simultaneous transcendental algebraic equations for the extended state loop state (Equations 43, 45, and 51) can be solved to obtain the set of loop state angles that describe the loop shape for that extended state.

3.3.4.2. Kinetic Relations

The loops state angles are used to calculate the applied force and the corresponding deflection of the knit unit cell from the *Austenite Free State*. The kinetic behavior of the textile is calculated by scaling the force on the knit loop by the number of wales in the textile while the deflection is scaled by the number of courses.

The applied force distributed on each unit cell, F_{UC}, is the difference between the initial internal force component acting in the *Y*-direction, P_{y0}, and the *Y*-component of *P*, P_y, in the extended state and is calculated as

$$F_{UC} = P_y - P_{y0} \tag{52}$$

after using the kinetic equation (Equation 50) to determine the force, *P*, acting at **A** for the extended loop. The associated deflection is calculated using the geometric constraint between the course height and the wire diameter, the global *Y*-coordinate transformation, and the definition of C_2 (Equations 3, 28, and 47) as

$$\delta_{A,ext} = 2\left(\sqrt{\frac{E_A I}{P_A}}C_2 - \sqrt{\frac{E_A I}{P_A}}C_{20}\right) + d\left(\cos(\beta) - \cos(\beta_0)\right), \tag{53}$$

which represents the difference between the initial course height and the extended course height under known applied load. The force-deflection relationship is comprised of transcendental expressions for the applied loop force (F_{UC}) and the corresponding deflection ($\delta_{A,ext}$) which are parameterized by the wale width *W*. The set of loop state angles (α, β, and γ) obtained following the kinematic analysis are used in Equations 52 and 53 to compute the force and deflection relationship as the width of the wale decreases.

The model of the knitted textile is developed by scaling the force-deflection model of the planar knit unit cell. It was assumed during the development of the knit model that a knit loop was made up of four identical unit cells rotated and reflected about the *X* and *Y* axes and a knitted textile was made of a matrix of knit loops. The total force in a knitted loop, F_{loop}, is twice that of the unit cell, $F_{loop}=2F_{UC}$, because there are two knit legs supporting the same force in each knit loop. The total force in a knitted textile is the addition of the force through all of the loops in the row or wale, N_W, and can be expressed as $F_{app}=N_W F_{loop}$. The extension of the unit cell is the same

as the extension of a knitted loop therefore the extension of the textile is total extension through each course, N_C, and can be calculated using the relationship $\Delta = N_C \delta_{Aect}$. The load-extension of the knit unit cell is thus scaled to predict the load-extension of the entire knitted textile.

3.3.5. Austenite Contracted State

The development of the equations for the *Austenite Contracted State* parallels that of the *Austenite Free State*. The force-equilibrium interactions are similar but sticking at the interlacing contact point (**B**) is assumed. The governing differential equations for the *Austenite Contracted State* are exactly the same as the equations for the *Austenite Free State*. However, the kinematic relations require knowledge of the *Martensite Extended State* to enforce the assumption that no slipping occurs during actuation under a constant load, leading to two new loop state equations involving the applied load and constant segment length. The kinetic relations for the unit cell and the entire textile produce the load-extension relationship for the *Austenite Contracted State* while actuator displacement is provided by subtracting the *Austenite Contracted State* from the *Martensite Extended State.*

3.3.5.1. Kinematic Relations

During actuation the knit loops widen as the Martensite bending strain in the loop segments is recovered because the material stiffens during the transition into austenite. The interlacing contact point acts as a pin joint due to sticking between adjacent loops. The applied load in the *Y*-direction remains constant for the *Austenite* and *Martensite Extended* and the *Austenite Contracted States* since the actuation cycle occurs against a constant applied load,

$$F_{UC} = P_{yUC,Aext} = P_{yUC,Mext} = P_{yUC,Acont}, \tag{54}$$

where $P_{yUC,Aext}$ is the load applied to extend the unit cell in the austenite phase, $P_{yUC,Mext}$ is the load applied to extend the unit cell in the martensite phase, and $P_{yUC,Acont}$ is the load under which the unit cell is actuated to the *Austenite Contracted State* from the *Martensite Extended State*. The actuation force, $P_{yUC,Acont}$, can be broken into two components,

$$P_{yUC,Acont} = P_{y,Acont} - P_{y0,Acont} = P_{Acont} \sin\gamma_{Acont} - P_{Acont\,0} \sin\gamma_{Acont\,0}. \tag{55}$$

Combining and rearranging the above equations in terms of known forces and angles gives

$$P_{Acont} \sin\gamma_{Acont} = P_{yUC,Mext} + P_{y0,Acont}, \tag{56}$$

where the applied load for the *Martensite Extended State*, $P_{yUC,Mext}$, and the *Y*-component of the *Austenite Contracted State*, $P_{y0,Acont}$, are known. The internal force acting on the knit unit cell at point **A**, P_{Acont}, can be calculated using Equation 50, resulting in

$$\frac{16E_A IC_4^2}{L^2}\sin\gamma_{Acont} = P_{yapp,Mext} + P_{y0,Acont}, \tag{57}$$

which is a loop state equation for the new contracted loop geometry.

The geometric constraint that the segment lengths must add to a quarter of the measured loop length (Equation 4) is given by the same loop state equation as was used for the *Extended States*, (Equation 45), which is the second loop state equation for the *Austenite Contracted State*.

The third loop state equation is developed using the sticking assumption, which requires the lengths of segment **AB** and **BC** to remain constant during contraction. Since the previous constraint requires lengths to add to a quarter of the measured loop length only one segment (s_{AB} or s_{BC}) can be held constant without over-defining the system. Segment **AB** is held constant between the *Martensite Extended* and *Austenite Contracted* giving the relationship

$$\frac{s_{AB}}{L} = \frac{\hat{F}_{AB}}{4C_4}. \tag{58}$$

Equations 45, 57, and 58 are the loop state equations for the *Austenite Contracted State* and are expressed in terms of measured geometric parameters previously determined from the *Martensite Extended* and *Austenite Free State*, and the unknown loop state angles. The set of three simultaneous algebraic transcendental equations can be solved numerically to determine the shape of the knit loop in the austenite contracted state.

3.3.5.2. Kinetic Relations

The actuation force is the same as the force applied to the unit cell, $P_{yUC,Acont}$ and is given by F_{UC}. The corresponding deflection from the *Austenite Free State* is provided by

$$\delta_{A,cont} = 2\left(\sqrt{\frac{E_A I}{P_A}}C_2 - \sqrt{\frac{E_A I}{P_A}}C_{20}\right) + d\left(\cos(\beta) - \cos(\beta_0)\right), \tag{59}$$

the same equation used for the *Austenite* and *Martensite Extended States*. The actuation displacement of the knit unit cell is the difference between the *Martensite Extended* and the *Austenite Contracted* deflections,

$$\delta_{act} = \delta_{M,ext} - \delta_{A,cont} \quad (60)$$

3.3.6. Textile Actuation Prediction

Prediction of the overall knit textile actuation from the unit cell model is done by scaling the force and actuation displacement of the unit cell in the *Austenite* and *Martensite Extended States* by the number of courses (rows) and wales (columns) in the textile. The total applied force under which the knit textile is actuating is $F_{app}=2N_W F_{UC}$, while the total actuator displacement of the knitted textile is $\Delta_{act}=N_C\delta_{act}$. The modeling procedure presented in this section produces an analytical model that captures the kinematic and kinetic behavior of each state experienced by this complex actuation architecture.

3.4. GARTER KNIT PATTERN EXPERIMENTAL VALIDATION

Experiments were conducted to understand the behavior of this new architectural actuation approach and assess the model's ability to predict the load-extension of each state and the net actuation. The model predictions were calculated in MATLAB using the measured initial geometric parameters of the knit prototype from the *Austenite Free State* (course height-*C*, wale width-*W*, wire diameter-*d*, and loop length-*L*) and material properties (E_A and E_M). The model prediction was compared to the experimental results for the load-extension curves in the *Austenite* and *Martensite Extended States*, the *Austenite Contracted State*, and also for net actuation between the *Martensite Extended State* and the *Austenite Contracted State*.

3.4.1. SMA Material Properties

The material properties of the Flexinol® wire were experimentally determined before validation of the analytical model. The Austenite force-deflection curve for straight Flexinol® 70°C wire was generated by electrically heating the straight wire above the material's Austenite finish temperature then measuring the load on the wire during axial elongation. Upon mechanical unloading, the wire returned to the Austenite free length and wire was cooled to 20°C (below the Martensite finish temperature). The Martensite force-deflection curve was generated by measuring the load on the wire during wire extension at this lower temperature. This process produced two stress-strain curves (Figure 20): a nearly linear austenite curve and a less stiff Martensite curve with a nearly constant stress plateau. Linear elastic approximations of the stress-strain curves in the two phases were used, because the model assumes small strains during bending of the loops. The Austenite elastic modulus was found to be E_A=73 GPa while the representative Martensite modulus, taken from the initial low-strain slope, was E_M=19.8 GPa. These values are within the ranges of published elastic modulus values which vary from 70 to 75 GPa for Austenite and 18 to 28 GPa for Martensite [87]-[88].

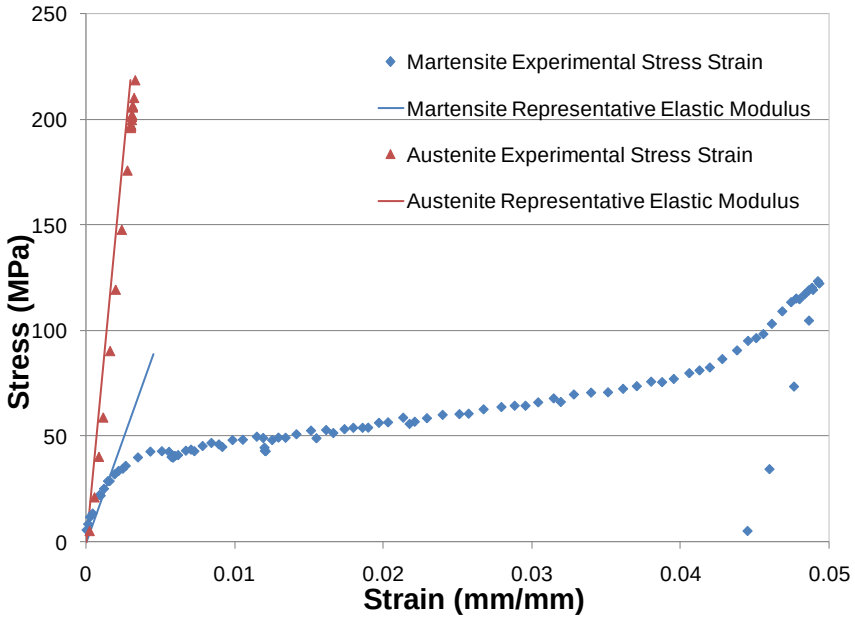

Figure 20. Experimental Material Properties of SMA Wire.
The experimentally obtained material properties of Dynalloy Flexinol® 70°C SMA wire are represented with linear elastic Austenite (73 GPa) and Martensite (19.8 GPa) Moduli.

3.4.2. Active Knit Prototype

A knit prototype was fabricated by hand knitting with 8 mil diameter, *d*, Dynalloy Flexinol® 70°C shape memory alloy wire for 15 courses and 10 wales using 5.5 mm diameter knitting needles, D (Table 3, Figure 21). The reference length and width of the prototype in the *Austenite Free State* were measured to be L_{A0}=22.6 mm and $W_{totalA0}$=85.0 mm. The average course height, *C* was determined by dividing the total prototype length by the total number of courses (N_C=15) resulting in a course height of 1.5 mm. Similarly, the wale width, *W*, was calculated by dividing the prototype width by the number of wales, (N_W=10), for a wale width of 8.5 mm. The total wire length in the knit prototype was determined post knitting by comparing the prototype weight to the weight of a single wire of known length with the same diameter, then the loop length, *L*, of a single knit loop was calculated by dividing the total length by the total number of loops in the prototype (N_C*N_W), resulting in a knit loop length of 20.2 mm.

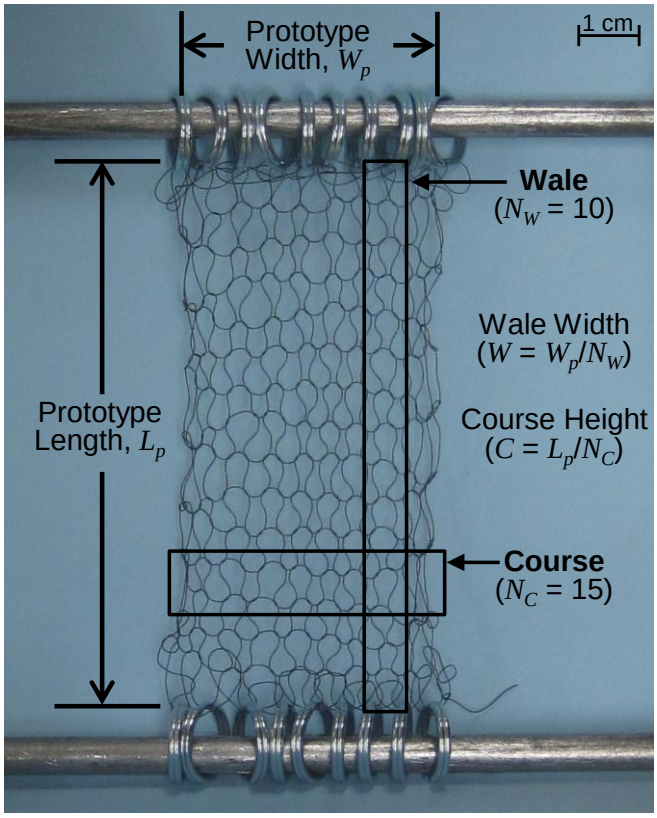

Figure 21. Garter Knit Pattern Active Knit Prototype.
The garter knit pattern active knit prototype in the *Martensite Extended State* under a 1 N applied load is labeled with prototype geometric parameters.

Table 3. Garter Knit Pattern Prototype Geometric Parameters.
Geometric parameters (d, D, N_C, N_W) used to create garter knit pattern knit and the measured Austenite Free State textile and unit cell geometries (L_{A0}, $W_{totalA0}$, C_0, W_0, and L).

d (mil)	D (mm)	N_C	N_W	L_{A0} (mm)	$W_{totalA0}$ (mm)	C_0 (mm)	W_0 (mm)	L (mm)
8.0	5.5	15	10	22.6	85.0	1.5	8.5	20.2

3.4.3. Experimental Method

The experimental set up depicted in Figure 22 was utilized for all the garter experiments. The prototype was mounted to the experimental setup in its *Martensite Free State* to parallel horizontal smooth rails at the top and bottom of the prototype which moved orthogonally on linear bearings along parallel guide rails that spanned the length of the prototype. Free lateral (wale-wise) contraction during longitudinal (course-wise) prototype extension was permitted by a series of steel rings attaching the knit actuator to the smooth rails. Free lateral motion is critical to maintain free boundary conditions and uniform deformations of all the loops within the prototype as assumed by the model.

The prototype was run through a thermo-mechanical cycle (Figure 16) in an Envirotronics EnviroFLX300 environmental chamber matching the same set of operational states and transitions upon which the model was based. The prototype was heated to until it no longer deformed under increased applied load (100°C) and the length of the prototype in the *Austenite Free State* L_{A0} (Figure 16a) was measured between the steel ring attachments using a US Digital linear encoder strip with 250 divisions per inch. The width of the entire prototype $W_{totalA0}$ was measured using digital calipers. A weight was attached to the prototype around a pulley, resulting in extension of the Austenitic prototype into the *Austenite Extended State* (Figure 16b) and the length L_{Aext} was recorded. The environmental chamber and the prototype were cooled to 20°C, the prototype continued to extend into the *Martensite Extended State* (Figure 16c), and length L_{Mext} was recorded. Heating the environmental chamber and prototype to 100°C caused the prototype to contract under load into the *Austenite Contracted State* (Figure 16d), with a measured length of L_{Acont}. The weight was removed and the prototype returned to the *Austenite Free State* at which time a larger load was applied to the prototype and the testing process was repeated. This sequence ensures that the friction is acting against the elongation of the knit during extension and against contraction during actuation.

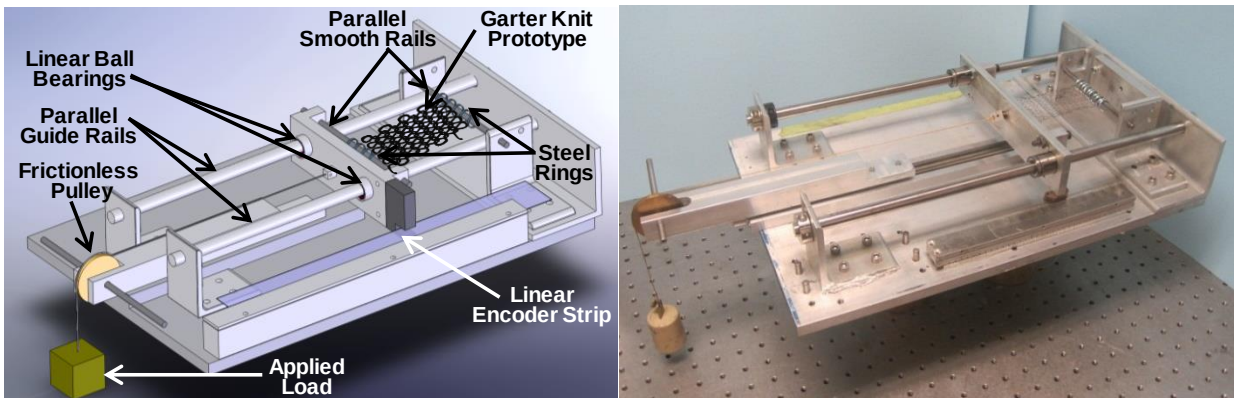

Figure 22. Garter Knit Pattern Experimental Setup.
Experimental setup (schematic on left, experimental on right) used to determine the load-extension behavior of the Garter Knit Pattern States and the resulting actuation behavior.

3.4.4. Austenite and Martensite Extended States

The experimental and theoretical results are shown in Figure 23 for *Austenite Extended States* and Figure 24 for the *Martensite Extended States*. Both the theory and experimental results of the *Austenite* and *Martensite Extended States* displayed "J" shaped load-extension curves similar to the load-extension curves of passive knits [73]-[74]. For each experimentally applied load (F_{app}) the knit prototype underwent a deflection from the *Austenite Free State*, $\Delta_{Aext}=L_{Aext}-L_{A0}$ for the *Austenite Extended State* deflection and $\Delta_{Mext}=L_{Mext}-L_{A0}$ for the *Martensite Extended State* deflection. During lower relative force loadings the knit underwent extreme stretching, up to approximately 200% strain for a 6 N applied load for the *Austenite Extended State* and 250% strain for a 3 N applied load for the *Martensite Extended State*. As the applied load was further increased the knit stiffened, the loops continued to stretch (up to 300% strain for the *Austenite Extended State* and 330% strain for the *Martensite Extended State* under an applied load of 15 N), but at a decreased rate because the loops experienced less change in curvature and more longitudinal alignment of the legs of the loop.

Using a friction value of μ=0.13, both the Austenite and Martensite theoretical load-extension curves provided excellent correlation with the experimental data with an average relative displacement error of 6.1% and an average absolute displacement error of 1.9 mm over the experimental range of applied loads (0 to 20 N) for the *Austenite Extended State* and 4.1% average relative displacement error and 1.8 mm average absolute displacement error over the experimental range of applied loads (0 to 12 N) for the *Martensite Extended State*. The coefficient of friction (μ=0.13) was found independently for both the *Austenite Extended State* and the *Martensite*

Extended State using a least squares analysis best fit over a range of coefficients between μ=0.1 and μ=0.15. The bounding coefficients of friction were chosen based on published values for the friction of smooth stainless steel materials [89]-[90]. A range of friction values were investigated because it is difficult to accurately measure the coefficient of friction between two wires. A coefficient of friction of μ=0.13 was independently found to be the best representation of the friction in each of the Austenite and Martensite Extended states, supporting the physical correctness of this parameter as opposed to a pure fit parameter. The theoretical load-extension results for the two friction cases bounded the majority of the experimental data points in both the Austenite and Martensite Extended States. The smaller friction value, μ=0.1, resulted in an average relative displacement errors of 10.4% for Austenite and 8.6% for Martensite over the range of applied loads for each state, while the larger friction value, μ=0.15, resulted in average relative displacement errors of 18.6% for Austenite and 7.5% for Martensite. All theoretical calculations involving friction provided vast improvements over the frictionless theory which was considerably less stiff than the experiments with an average relative displacement error of 22.3% for the Austenite Extended State and 22.5% for the Martensite Extended State over the range of applied loads for each state. While previous research has shown strong correlations between experimental and theoretical frictionless results (within 10% average displacement error) [74], the inclusion of friction in the modeling of the load deflection of active knits vastly improved the average displacement error, reducing the error by 3.7 times for the Austenite Extended State and 5.5 times for the Martensite Extended case. Slippage between loops was observed during the operational transitions into the Austenite and Martensite Extended States, validating the friction assumptions used in the model.

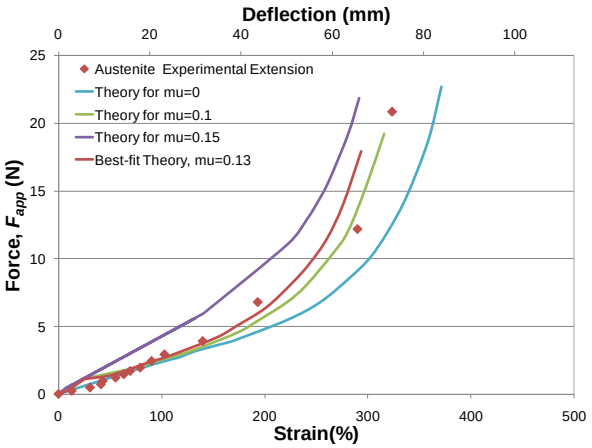

Figure 23. Austenite Extended State.
Theoretical and experimental results agree with an average relative displacement error of 6.1% with coefficient of friction μ=0.13.

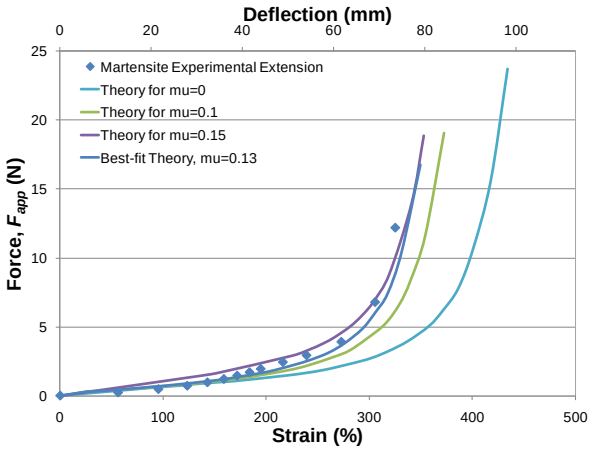

Figure 24. Martensite Extended State.
Theoretical and experimental results agree with an average relative displacement error of 4.1% with coefficient of friction μ=0.13.

3.4.5. Austenite Contracted State

The operational transition into the *Austenite Contracted State* from the *Martensite Extended State* included sticking of the interlacing contact point. The sticking of adjacent loops prohibited loops from sliding past one another, thus the actuation motion was solely a result of the loops straightening. The theoretical *Austenite Contracted States* were assembled to produce a load-extension relationship where the load is the applied force the knit actuates against (F_{app}) and the deflection ($\Delta_{Acont}=L_{Acont}-L_{A0}$) is the difference between the recovered length and the length of the *Austenite Free State*. This theoretical load-extension relationship produces another "J" shaped curve which matches the experimental results in form and magnitude (Figure 25). Both the theoretical and experimental *Austenite Contracted* results are stiffer than that of the *Martensite Extended* load-extension curve, but less stiff than the *Austenite Extended* curve: the *Austenite Contracted* knit stretched under low force loadings to 220% strain for a 3 N applied load before becoming stiffer as the knit stretched to 320% strain under a 15 N applied load. The loops were observed to stick during the operational transition into the *Austenite Contracted State*, validating the friction assumptions used in the model for this state. The theoretical *Austenite Contracted* curve quantitatively matches the experimental extremely closely with an average relative displacement error of 2.8% with an average absolute displacement error of 1.8 mm over the range of applied forces actuated against, 0 to 12 N.

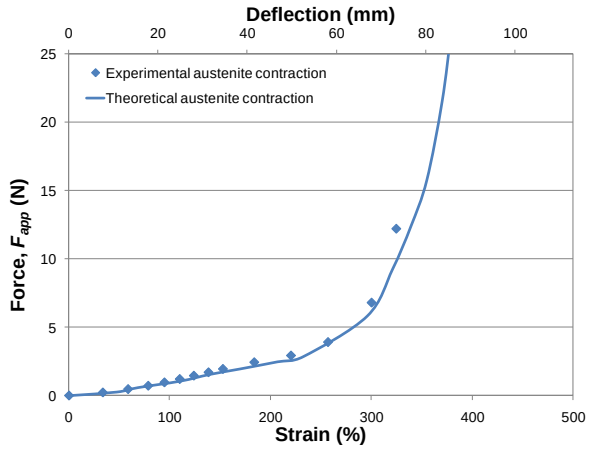

Figure 25. Austenite Contracted State.
Theoretical and experimental results agree with an average relative displacement error of 2.8%.

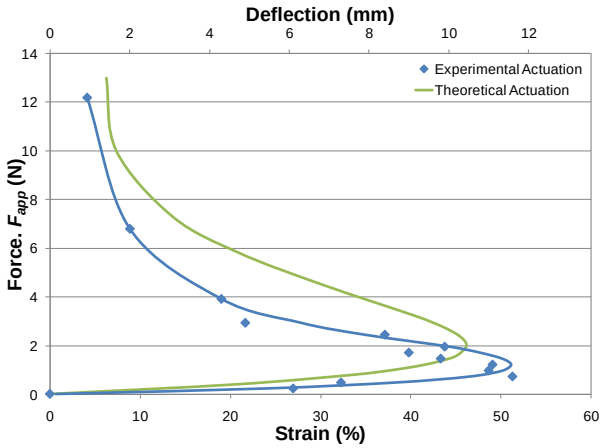

Figure 26. Garter Knit Actuation Results.
Knit Prototype transitions between Martensite Extended and Austenite Contracted states to create theoretical actuation curve with same form as experimental results with an average absolute displacement error of 2.0 mm.

3.4.6. Net Actuation

The net actuation performance ($\Delta_{ACT} = \Delta_{Mext} - \Delta_{Acont}$) is obtained by subtracting the displacement of the *Austenite Contracted State* from the *Martensite Extended State* at each applied load, as this is the motion obtained when actuating under a constant load. The theoretical and experimental actuation curves show the same distinctive qualitative performance (Figure 26). As the load increased the net actuation strain increased to a maximum peak actuator strain then decreased under increased applied loads as the prototype was not able to recover as much of the martensite strain. The shape of the actuation curves is unique: for small deflections, where the loops do not change shape much, net displacement increases as load increases since the performance is dominated primarily by the difference in stiffness between the two material phases. Whereas for larger deflections, where the loops are narrow and elongated, larger loads produce smaller net deflections since the austenite phase loses its ability to recover motion through the reduced leverage of the elongated loops. This implies that there is an optimal deflection point for designing such actuators to provide the maximum possible deflection (and a similar, but differently located configuration for maximum work) for which the predictive model can aid in designing the ideal active garter knit for a given application.

The theoretical and experimental actuation curves are also an excellent quantitative match given the complex behavioral form and assumptions made during the development of the analytical model. The peak actuator strain, 51.2%, was observed under a 1.22 N applied load while, theoretically, a 46.2% peak actuator strain was predicted under a 2 N applied load. The model

accurately predicts the peak actuator motion within 5% strain at a higher applied force than experimentally witnessed. The experimental and theoretical actuation curves correlate with an average absolute displacement error of 2.0 mm over the 12 N range of applied actuation forces which is slightly larger compared to 1.8 mm over each of the *Martensite Extended* and *Austenite Contracted States*. The differences between the theoretical and experimental actuation results stem from compounding the displacement errors for both the *Martensite Extended* and *Austenite Contracted States* through subtraction during the calculation of the actuation behavior and also result from the assumptions made during modeling, particularly, state dependent stick-slip friction, full material transition into each state, and linear elastic material behavior. The friction assumption of constant sliding during extension gives larger strains than experimentally witnessed while the constant sticking assumption allows more force to be transferred under restricted motions consistent with the validation shown in Figure 26. The validity of the small strain assumption (and therefore the homogenous phase and linear elastic assumptions) can be estimated from the loop curvature by examining the ratio of the wire diameter, *d*, to the loop diameter as approximated by the knitting needle diameter, D. For the validation prototype, this ratio is 0.037, indicating that the largest strains, along the outer surface of the bent wire, violate the small strain assumption However, in the *Austenite Extended State* the loops straighten significantly, reducing the maximum strain, and most of the material, even in the *Martensite Extended State*, will experience lower strains. Even with these assumptions the prediction was quite good, capturing the kinematic loop shape change and the kinetic performance of the contractile active knit.

Large actuation motions with unprecedented strains were observed during all the experiments. The garter knit pattern architecture significantly amplified the strain of a bulk individual fiber (in the case of SMA 8% recoverable and 3-4% actuation), to as much as 250% recoverable strain allowed for moderate forces of tens of Newtons and 51% actuation strain (Figure 26) under a 1.2 N applied load. The knitted actuator also provides enhanced force performance, axially contracting SMA wires 8 mil in diameter operate at a maximum strain of 4% under a 5.8 N applied load while the active knit prototype generated 4.1% strain under a large applied load of 12.2 N. The active knit actuator enhanced the strain by an order of magnitude and the force by two times that of the same diameter straight SMA wires, affording enhanced actuation capabilities to a variety of application domains and enable new technologies.

3.5. TWO-DIMENSIONAL ANALYTICAL MODEL CONCLUSIONS

This chapter expanded upon existing knit models to capture the cyclic actuation behavior of planar active knits by incorporating the dual states of the material and the various friction states between interlacing adjacent loops. The active knit predictive model was developed defining the operational states, identifying and geometrically defining the smallest repetitive unit cell, developing predictive capabilities of the active knit loop and garter knit pattern active textiles, and experimentally validating the model.

The first step in developing the active knitted loop model was to outline the typical actuation cycle of garter knit pattern textiles: *Austenite Free, Austenite Extended, Martensite Extended,* and *Martensite Contracted States* while considering the mechanical and thermal operational transitions the textile undergoes during deformation. While the first level of the hierarchy is the knitted loop, the smallest repetitive element, or unit cell, is a quarter of a knit loop. Geometric constraints are developed and force equilibrium analysis of the unit cell is completed while assuming different friction conditions (stick or slip) during the operational transition depending on the loading and the initial state of the textile. Elastica Theory and Euler Bernoulli beam bending are used in addition to the knit geometry and the force equilibrium to develop governing differential equations that can be solved to determine the deflection from the *Austenite Free State* of the textile and thus the relative displacement between the *Martensite Extended* and *Austenite Contracted States* for constant load actuation. A set of fully analytical transcendental algebraic equations (as opposed to a set of coupled differential equations) describe the deflections experienced within a unit cell for each operational state, and are scaled to produce the load-extension properties of the entire garter knit pattern textile for each state as well as the net actuation performance.

The analytical model of the knit loop and garter knit pattern was experimentally validated for its ability to predict the load-extension behavior of each of the states and the constant load actuation performance. A garter knit pattern prototype was fabricated from 70°C Flexinol® wire with a diameter of 8 mil using 5.5 mm knitting needles for 10 loops and 15 rows. The prototype was cycled through the modeled sequence of operational states under a variety of external loads from 0 to 12 N in order to validate the model. The model predicts the load-extension behavior of the textile in each of the states in addition to predicting the load-extension actuation performance, providing an excellent match to the experimental results particularly considering the modeling assumptions: dual stiffness, linear-elastic material with prescribed friction states. The *Martensite*

and *Austenite Extended States* were predicted with an average relative displacement error of 4.1% and 6.1% using a coefficient of friction μ=0.13 as found independently via a best fit analysis for each the *Martensite* and *Austenite Extended States*. The theoretical *Austenite Contracted State* agreed with the experimental results with a 2.8% average relative displacement error. The results validate the observed friction requirements – sliding for *Extended States* and sticking for *Contracted States*. The theoretical actuation, the difference between the *Martensite Extended* and *Austenite Contracted States*, was found to match the form and magnitude of the experimental results with an average absolute displacement error of 2.0 mm. The model accurately predicts the qualitative and quantitative performance of planar contractile garter knit pattern active knits.

The unique shape of the actuation curve with increasing net displacement versus force at low load, a maximum displacement peak, and decreasing displacement at further increasing loads provides the opportunity for tailoring of architectural parameters such as loop size, wire diameter, and the number of courses and wales within the textile to optimally match the specific needs of a particular application. This highly leveraged garter knit pattern architecture allows for large strains (51%) at moderate forces (1.22 N) and usable strains (4.1%) at enhanced forces (12 N) over the material alone (4% strain at 5.8 N). This new actuation capability goes beyond what is possible with conventional actuation technology and the current state of the art in smart materials actuators, meeting increasing needs for large contractile actuation surfaces.

The development of the two-dimensional analytical active knitted loop model provides the capability to predict the large strain, moderate force kinetic performance of planar active knits, which is a capability that did not previously exist. The incorporation of friction between interlacing adjacent knitted loops in the active knitted loop model greatly improved the average displacement error by reducing the error by 3.7 times for the Austenite Extended State and 5.5 times for the Martensite Extended case. Additionally, the inclusion of the dual state, multi-stiffness material enabled the model to capture the cyclic actuation behavior. The inclusion of friction and the dual state material was required to capture the hysteretic behavior of active knitted structures, producing an analytical model that provides a tractable tool for the prediction, design, and tailoring of active garter knit pattern actuators. In addition, the model provides an improved ability to predict the kinetic performance of all knitted loops (active and passive) with higher fidelity than previously possible and an analytical form that is better suited for design. Both active

and passive knits experience friction between adjacent loops, therefore the inclusion of friction in a knit loop model can increase the accuracy provided by the model to better represent the kinetic performance of all knit loops. The inclusion of friction also enables the analysis of passive knits that undergo multiple operating states including cyclic loading and thermal loading during manufacturing. The developed model is useful for predicting the kinetic actuation performance of planar knits and provides a framework for developing a three dimensional model that can capture the out of plane behavior of more complicated knit patterns.

Chapter 4. THREE-DIMENSIONAL SEGMENT SUPERPOSITION ANALYTICAL MODELING APPROACH

The active knit architecture has the unique ability to provide complex three-dimensional actuation motions. The complex actuation motions are a result of the hierarchical architecture, which combines basic knitted loops (the first level of the hierarchy) into increasingly complex patterns that leverage the foundational smart material through extension, contraction, bending, torsion, and/or buckling. To fully advance this actuation technology, predictive capabilities of complex knitted patterns are required. Chapter 3 presented a two-dimensional analytical model that accurately captures the large rotation in-plane bending of the foundational dual-stiffness smart material wire in the planar garter knit actuator architecture. While the two-dimensional model predicts the force-deflection and actuation behavior of planar knitted loops, it does not account for the other material deformation modes such as tension, extension, torsion, buckling, or out-of-plane bending. To provide predictive capabilities for complex three-dimensional knit actuators, a new modeling approach is required to simultaneously capture different deformation modes within the knit architecture.

The kinematic and kinetic performance of complex knit architectures that actuate out-of-plane are difficult to predict due to the multiple deformation modes, complex geometry, and nonlinear dual-state material properties. To accurately capture all the complexities of three-dimensional active knit actuators, finite element models need to be developed. However, a simplified, less accurate modeling approach would be useful to provide insight early in the design process through the exploration of new architectures to produce desired kinematic motions and the identification of the impact of geometric parameters on kinetic performance. To address the need for modular, tractable, and scalable models for use in design, a segment superposition modeling approach is developed. The segment superposition modeling approach reduces the complexity of modeling complex knit actuators by establishing a clear procedure and representing the architecture with a system of simple mechanical effects models. The segment superposition modeling approach establishes a framework to predict the kinetic performance using a five step process. The first step

is to identify the unit cell by analyzing symmetry in the architecture. The second step is to segment the unit cell by replacing the curvilinear geometry with a system of linear segments. The third step is to enumerate the individual simple effects models for different possible deformation modes such as tension, extension, torsion, bending, and buckling. The fourth step is to predict the force-deflection performance in response to a single deformation mode using simple mechanical equations. The fifth step is to superimpose the force-deflection or the various individual models to predict the performance of the actuator.

This chapter presents a new modeling approach – the segment superposition modeling approach – that establishes a framework to predict the kinetic performance of complex three-dimensional active knit architectures. The general five step modeling approach (identifying the unit cell, segmenting the unit cell, enumerating simple individual segment models, predicting the force-deflection of the individual segment models, and superimposing the force-deflection of multiple segment models to predict performance of the unit cell and actuator) is outlined. The segment superposition modeling approach is demonstrated using the 2x2 rib knit pattern architecture. The first four steps of the segment modeling approach are followed. The unit cell is identified as a single loop and segmented into five linear segments. A torsional simple effects model is developed using simple torsion equations and knowledge of the geometry, physical constrains, and material behavior. The modeling approach is experimentally validated for the ability of the model to predict the force-height relations ship for each of the states and the constant load actuation displacement. The segment model of the 2x2 rib knit actuation architecture accurately predicts the qualitative and quantitative performance of the accordion-like actuation behavior of 2x2 rib knit actuators. The segment superposition modeling approach provides the ability to predict the three-dimensional actuation behavior of complex knit architectures and establishes the framework to aid in the design of complex active knit architectures to meet the need for advanced actuators in applications.

4.1. SEGMENT SUPERPOSITION MODELING APPROACH

The segment superposition modeling approach is a new approach to modeling complex knit architectures. The approach can be used to model active or passive knit architectures by reducing the complexity of the knit architecture by representing the architecture with a system of simple models that provide a modular, tractable, and scalable approach to predicting the performance.

The segment superposition modeling approach consists of five steps: identifying the unit cell, segmenting the unit cell, enumerating simple mechanical effects models of one or more segments, generating force-deflection for each mechanical effect, and superimposing individual mechanical effects to obtain bulk performance of the knit actuator.

4.1.1. Identify Unit Cell

The first step to the segment supposition modeling approach is to identify the unit cell of the desired textile based actuator architecture. The unit cell is the smallest repetitive element that can be translated and/or rotated to represent the architecture of the actuator. The fundamental element of the knit architecture has been identified as the knitted loop (Section 2.2), as a result of the manufacturing process of all knitted textiles, which requires complete loops to interlock together to form knitted textiles. While the fundamental element is a knitted loop, the smallest repetitive element, or unit cell, of each knitted architecture is governed by the architecture and operation of the active knit. Relating points of symmetry within the architecture to specific kinematic actuation behaviors can help identify the bounds of the unit cell. For example, the unit cell for planar knitted loops, the first level of the hierarchy, was identified as a quarter of a knit loop (Section 3.3); Symmetry about the wale direction (column) reduced the size of the unit cell to half a knitted loop, whereas an inflection point reduced the unit cell to a quarter of a knit loop. The quarter knit loop was successfully scaled to represent the entire planar actuating garter knit textile.

The size and complexity of the unit cell increases for higher levels of the hierarchy. Higher levels of the hierarchy produce more complex three-dimensional actuation behaviors as a result of their more complex architecture and operation. Knit patterns, architectures represented by the second level of the hierarchy, produce homogeneous actuation motions. The three-dimensional homogeneous actuation motions can be represented by a single unit cell that includes a quarter to multiple knitted loops. The symmetry of the more complex knit pattern unit cells must be investigated about all three axes to fully capture the behavior. Just as in the case of the planar knitted loop, the performance of the unit cell can be can be further scaled to represent the entire textile. Grid patterns, the third level of the active knit hierarchy, consist of heterogeneous patterns that provide different actuation motions over different areas of the textile. These more advanced textile architectures require multiple local unit cells to predict the performance in each discrete area of the grid pattern. Each individual unit cell must be scaled to predict the performance of each

area of the textile, paying special attention to connecting regions, which may need an intermediary unit cell. The segment superposition method will be particularly handy for the last level of the hierarchy, restructured grids. Restructured grid are uniquely shaped and structured architectures with complex localized architectures. Unit cells of lower levels of the hierarchy can be spatially arranged with specialized unit cells that capture the connection, merging, re-ordering, and non-planar orientation of complex architectural elements.

4.1.2. Segment Unit Cell

The second step in the segment superposition modeling approach is to segment the unit cell. The purpose of segmenting the unit cell is to simplify the geometry by representing the complex curvilinear geometry by a system of linear segments that estimate the shape of the identified unit cell. Two primary factors affect the segmented geometry and function of the unit cell – unit cell geometry and physical constraints. The geometry of the segmented unit cell is determined by representing the geometry of the unit cell with a system of straight bar segments. The exact geometric parameters (lengths, widths, wire diameter, etc.) must be measured from manufactured prototypes in the free-states. While zero external load is applied to the actuator in the free-states, the foundational fiber experiences stresses. The model assumes the initial stresses are accounted for in the free-state calculation, and solves for perturbations from the free-state. Once the geometry has been established any physical constraints that limit the range of motion of the unit cell should be identified. The constraints may be architecturally imposed by adjacent loops within the architecture that limit the range of motion of individual segments or they may be imposed by the applied load to the architecture.

4.1.3. Enumerate Simple Mechanical Effects Models

Once the segmented unit cell has been developed, simple mechanical effect models that predict the deformation of the unit cell from the free states of the actuator in response to an applied load can be derived. The first step to modeling the segmented unit cell is to identify the various localized deformation modes within the knitted architecture. The same segment unit cell should be independently populated for different deformation modes – tension, extension, torsion, bending, and buckling – for each degree of freedom of the architecture. During this step all segments in the architecture should be identified as rigid or with the appropriate deformation mode. Not all deformation modes have a significant impact on the kinetic performance of the active knit

architecture, therefore, the deformation modes that appear to have the greatest impact on performance should be developed first.

4.1.4. Predict Force-Deflection Performance of Simple Effect Models

The affect each model has on kinetic performance can be assessed through the development and analysis of independent force equilibrium interactions. The force equilibrium interactions set the foundation for the predicting the load-extension performance of rib knit pattern active knits. Several assumptions about the active material and the loop architecture are required to realize this modeling approach. The assumptions made in regard to the unit cell, allow the force equilibrium to be analyzed in two dimensions, reducing the complexity of the modeling solution. The unit cell is separated into rigid and elastic segments. The rigid segments are permitted to undergo translation and rotation but are assumed to completely transfer loads without undergoing any deformation. The elastic segments are assumed naturally straight and are subjected to extension, contraction, bending, torsion, or buckling loads that deform the elastic segments. The shape memory effect of the SMA wire is captured in the model by assuming the materials exhibits dual-state behavior in the form of two linear elastic shear moduli. The SMA wire is assumed to be trained to a straight shape that is recoverable upon heating the material above the transformation temperature. Simple mechanical relationships are used to relate the force-deflection behavior to the architectural geometry, material properties of the foundational active material, and external loads that are applied to the actuator and distributed to individual unit cells. The mechanical models predict the performance of the segment unit cell, which is scaled in series and parallel to represent and predict the force-deflection performance of the actuator.

4.1.5. Superimpose Force-Deflection Model

The final step to the segment superposition modeling approach is to superimpose the independent mechanical effects models to predict the performance of the actuator. This approach assumes linearity, which is a significant assumption due to the large changes in geometry the smart material fiber undergoes during deformation, to simplify the modeling process an allow the displacement of each simple mechanical effect model to be added in series for an applied external load. The ability to superimpose individual mechanical effect models is a large assumptions and will not provide an accurate prediction of the behavior of the textile but will invite investigation early in the design process into the effect of each deformation mode and the geometric parameters

on performance. Additional segmented models capturing alternative deformation modes can be developed until the model adequately captures the primary modes of deformation. Superposition of the effects in each state provides the force-deflection behavior for each state of the architecture, which are combined to provide the force-displacement performance of the actuator.

4.2. SEGMENT MODEL OF 2X2 RIB KNIT ACTUATOR ARCHITECTURE

A segment model of the 2x2 rib knit actuator architecture has been developed to demonstrate the segment superposition model approach. The 2x2 rib knit actuator was chosen because the vertically striped architecture produces complex three-dimensional actuation behavior in the form of a corrugated shape with a variable peak-to-peak height during actuation that can act as an embeddable planar lift. The detailed architecture and operation are defined and the segment superposition modeling approach has been followed including identifying the unit cell, segmenting the unit cell, identifying the primary simple mechanical effect, and modeling the force-displacement behavior. During this preliminary investigation of this modeling approach only a

Table 4. Nomenclature for Segment Model of 2x2 Rib Knit Actuator Architecture

Symbol	Description
C	Course (row) height
W	Wale (column) width
l_{bottom}	Length of rigid segments AB and EF of the unit cell
l_{AB}, l_{CD}, l_{EF}	Length of rigid segment
l_{top}	Length of rigid segment CD at top of unit cell
l_{τ}	Length of torsional segment BC or DE
h_{Mcomp}, h_{Aexp}	Height of prototype in the martensite compressed or austenite expanded state
d	Wire diameter
$\pi-\theta_1$	Rotation of active segment BC
$\pi-\theta_2$	Rotation of active segment DE
F^*	Externally applied force to unit cell
τ_1	Torque of active segment BC
T_{Af}, T_{Mf}	Austenite and martensite finish temperature
G_A, G_M	Torsional rigidity of active material in austenite (A) or martensite (M) state
k_A, k_M	Representative stiffness of active torsional segments
μ	Coefficient of friction between knit and plates above and below prototype
N_c	Number of courses in knit textile
N_W	Number of wales in knit textile
J_{τ}	Torsional constant
F_{app}	Externally applied force to knit textile
Subscripts	
A	Austenite phase
M	Martensite phase
0	Initial state with zero external load

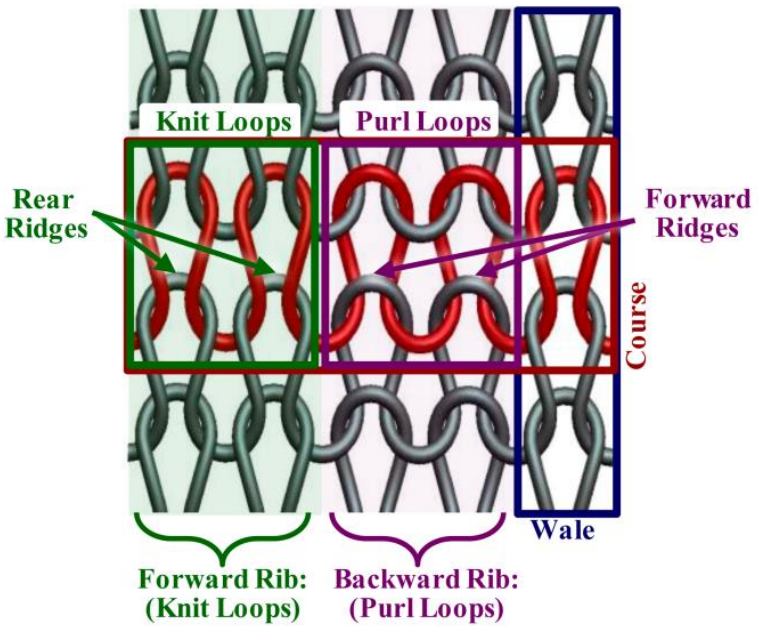

Figure 27. Rib Knit Pattern Architecture.
The 2x2 rib knit pattern is composed of two knit loops alternating with two purl loops forming symmetric columns or raised and lowered ridges.

single mechanical effect model has been developed to explore the potential of this modeling approach, therefore superposition of multiple effects will not be discussed for this architecture. Table 4 lists the various symbols and their descriptions that will be used during the development of the segment model of the 2x2 rib knit actuator architecture.

4.2.1. 2x2 Rib Knit Actuator Architecture and Operation

Rib knit pattern knits leverage the active base material capability to create large strains distributed over a surface through the utilization of a unique rib knit pattern architecture and multi-state operation.

4.2.1.1. 2x2 Rib Knit Architecture

The rib knit pattern is created by alternating knit and purl loops across the first course, or row. As additional rows of the same pattern are added to the textile symmetric wales (columns) are created with smooth columns of the forward ribs composed of knit loops and columns of ridges formed by the backward ribs composed of purl loops. The rib knit pattern architecture can be fabricated by alternating a single knit and a single purl loop, called a 1x1 rib, or by alternating combinations of multiple knit and purl loops (a nxp rib knit pattern alternates n columns of knit loops with p columns of purl loops). The most common rib knit pattern architecture is a 2x2 rib which alternates two adjacent knit loops with two purl loops, creating raised and depressed

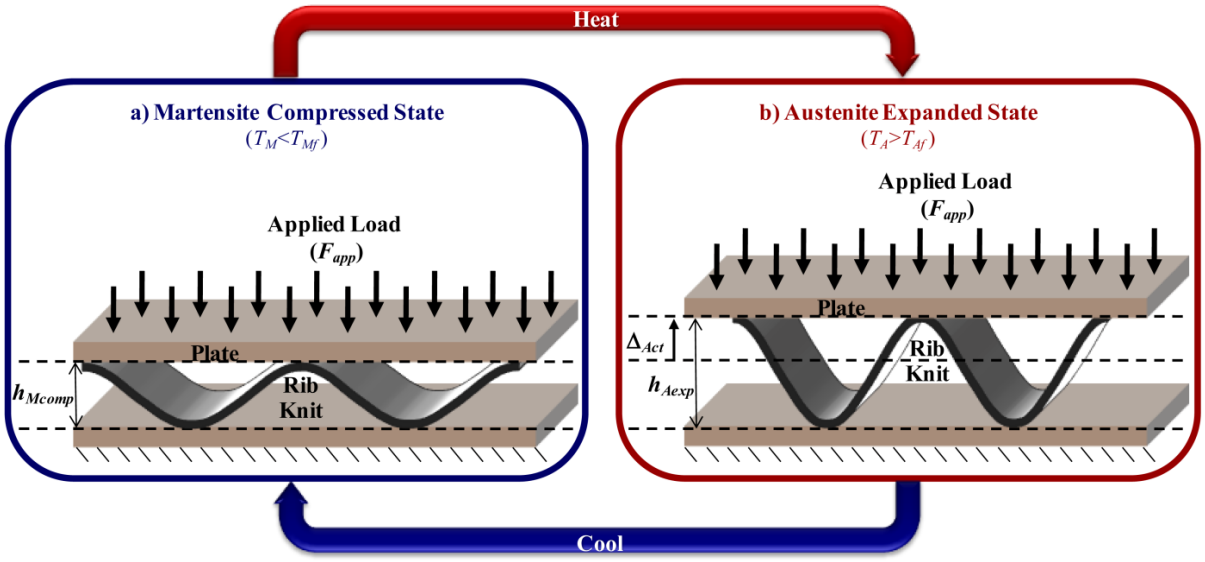

Figure 28. Rib Knit Pattern Operation.
The rib knit pattern embeddable surface actuator cycles between the Martensite Compressed State and the Austenite Expanded State under a constant applied load (F_{app}) via a thermal operational transition between the low temperature Martensite phase (T_M) and the high temperature Austenite phase (T_A).

columns that are two loops wide as shown in Figure 27. Much like the garter knit pattern, the rib knit pattern is geometrically defined by its course height (C), wale width (W), and fiber diameter (d). The course height (C) is the vertical distance between identical reference points of adjacent rows. The wale width (W) is the horizontal distance between identical reference points on adjacent loops within a course. The fiber diameter (d) is the diameter of the foundational wire.

4.2.1.2. Rib Knit Pattern Operation

Rib knit pattern knit textiles go through operational transitions from one state to another resulting in a change in height and stiffness of the textile as depicted in Figure 28. The textile is initially compressed by an applied load (F_{app}) to the Martensite Compressed height (h_{Mcomp}), while the material is in the less stiff Martensite phase. An operational transition occurs when the material is heated above the transition temperature (T_{Af}) into the Austenite phase causing the textile to lift the applied load to the Austenite Expanded height (h_{Aexp}). A second operational transition returns the textile to the Martensite Compressed height (h_{Mcomp}) upon cooling below the Martensite Finish temperature (T_{Mf}), completing the constant load actuation cycle, which cycles between the Martensite Compressed State and the Austenite Expanded State under a constant applied load (F_{app}).

4.2.1.2.1. Martensite Compressed State

The first state, the Martensite Compressed State, is reached when a compressive load, F_{app}, is applied to the textile in the cooled, less stiff state at a temperature below the Martensite Finish temperature (T_{Mf}), compressing the textile to the Martensite Compressed height, h_{Mcomp} (Figure 28a). The textile compresses under the applied load as the contact areas at the peaks and valleys of the textile slip horizontally and the forward ribs at the peaks are pushed down while the backward ribs at the valleys are pushed up. The horizontal slippage of the contact area of adjacent forward and backward ribs increases the distance between the applied loads on the forward ribs and the resultant loads on the backward ribs. The increased distance increases the torsion (and angle of twist) in the vertical sides of the loops, resulting in a less steep transition between forward and backward ribs and a compressed textile height. The torsional loading on vertical sides of the loops decreases the height of the textile because the compliant Martensite material twists to reduce the angle between adjacent legs, compressing to the Martensite Compressed height, h_{Mcomp}. The Martensite Compressed State is the first of two states in the quasi-static cyclic portion of the constant load actuation cycle.

4.2.1.2.2. Austenite Expanded State

The second state in the actuation cycle, shown in the rib knit pattern operation figure (Figure 28b), is reached when the textile is heated under the same applied load, F_{app}, to above the Austenite Finish transition temperature (T_{Af}), recovering the plastic deformations experienced in the Martensite state to become stiffer through utilization of the Shape Memory Effect of the foundational SMA wire. Upon heating, the torsional stiffness of the foundational wire increases and the loops attempt to return to their naturally straight configuration by recovering the twist in the vertical sides of the knit and purl loops. The angle of twist is reduced, increasing the steepness between forward and backward ribs and reducing the distance between the applied load on the forward ribs and the resultant load on the backward ribs. The change in geometry results in an expanded height, the Austenite Expanded height, h_{Aexp}. The combination of the increased stiffness of the material and the reduced torsion of the vertical loop segments cause the legs at the bottom of the loop connecting forward ribs and backward ribs to lift the forward ribs while depressing the backward ribs, raising the prototype to the Austenite Expanded height (h_{Aexp}).

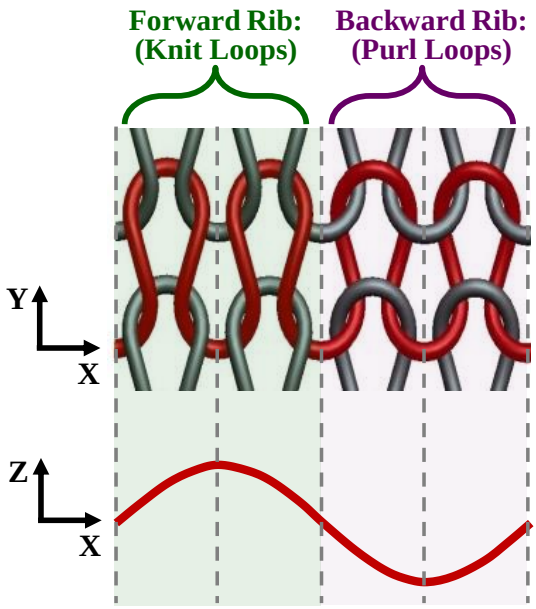

Figure 29. Unit Cell Identification for 2x2 Rib Knit Actuator Architecture.
Each loop in the four loop repeating pattern of the 2x2 rib knit actuator architecture has the same out of plane shape, just in a different orientation. Because of symmetry, the unit cell is a single knitted loop.

4.2.2. Identify Unit Cell of 2x2 Rib Knit Actuator Architecture

The 2x2 rib knit actuator architecture produces a unique accordion-like surface that can support externally applied loads. The externally applied load is evenly distributed through each course, or row, of the architecture. Therefore, the unit cell of the 2x2 rib knit actuator architecture only needs to consider a single course of loops. A quick evaluation of the architecture reveals a four wale (column) repeating pattern of two knit loops and two purl loops (Figure 29). The knit loops arch up through the thickness of the textile while the purl loops arch downward, producing a wavy surface that resembles a full period of a sin wave. Symmetry of this architecture results in a final unit cell of the 2x2 rib knit actuator architecture of a single knitted loop. The single loop can be translated and/or rotated to represent the entire 2x2 rib knit architecture.

4.2.3. Segment Unit Cell of 2x2 Rib Knit Actuator Architecture

The second step in the segment superposition modeling approach is to segment the unit cell. Geometry plays an important role in the development of the segmented model of the 2x2 rib knit actuator architecture. The active fiber can undergo extension, compression, torsion, bending, and even buckling to maintain the curvilinear structure in each state (Figure 30a, c). However, the unit cell can be segmented and represented by five straight segments (Figure 30b, d). Both structure take on the same accordion-like textile geometry (Figure 30e, f), but the complex line path of the

curvilinear architecture is greatly reduced while maintaining the same global textile behavior. The adoption of this simplified segmented unit cell results in an open and angular representation of the entire knit structure (Figure 30f).

The geometry of the unit cell (Figure 31) establishes a connection that represents the physical constraints between the known geometric manufacturing parameters (loop segment lengths – l_{AB}, l_{BC}, l_{CD}, l_{DE}, and l_{EF}, wire diameter – d) and the unknown geometric parameters (wale width – w, and textile thickness – h, torsional spring stiffness, rotational angles – θ_1 and θ_2). All segments are assumed to have a circular cross section with a diameter, d. Due to symmetry within the loop, the length of the bottom segments l_{AB} and l_{EF} are equal and are represented by l_{bot} the length of the torsional segments l_{BC} and l_{DE} are equal and are represented by $l_{T.}$

$$l_{bottom} = l_{AB} = l_{EF} \tag{1}$$

$$l_T = l_{BC} = l_{DE} \tag{2}$$

The top rigid segment, l_{CD}, is approximately twice the length of the bottom segments and is represented by l_{top}.

$$l_{top} = l_{CD} \tag{3}$$

The geometric constraints are developed by analyzing a unit cell of the rib knit pattern architecture. The unit cell is a single knit loop (Figure 31), which can be viewed in the **X-Y** and **X-Z** planes. A complete knit textile can be assembled by rotating and translating the unit cell and connecting loops across a course (row) at points **A** and **F** and across a wale (column) at points **B** and **E** to **C** and **D**. When assembled, the unit cells form a surface of raised peaks and suppressed valleys (Figure 30f). Point **A** originates at the peak of the accordion-like textile. Because segment **AB** is rigid and constrained by symmetry about the **Y-Z** plane, **AB** must remain aligned with the **X**-axis. Torsional segment **BC** extends from **B** in the **Y** direction. During manufacturing the segmented is twisted along its length by angle $\pi-\theta_1$. The rotation along segment **BC** causes the rigid segment **CD** to lie in the **X-Z** plane at an angle of $-\theta_1$ relative to the **X**-axis. Torsional segment **DE** has a diameter, d, which extends in the **–Y** direction and is rotated through an angle $\pi-\theta_2$. The final rigid segment **EF** lies in the **X-Z** plane at $-(\theta_1+\theta_2)$ relative to the X-axis.

The change in height of the textile as a function of applied load and material state is needed to provide predictive capabilities. Geometric constraints that relate the height and width of the

textile to the geometric parameters can be developed by analyzing the X-Z view of the unit cell. The first geometric constraint,

$$\frac{h}{2} = 2d + l_{top} \sin\theta_1 + l_{bottom} \sin(\theta_1 + \theta_2), \quad (4)$$

relates the height of the textile (through the thickness) to the wire diameter, segment lengths, and the rotation angles using trigonometric relationships. Similarly, a second constraint,

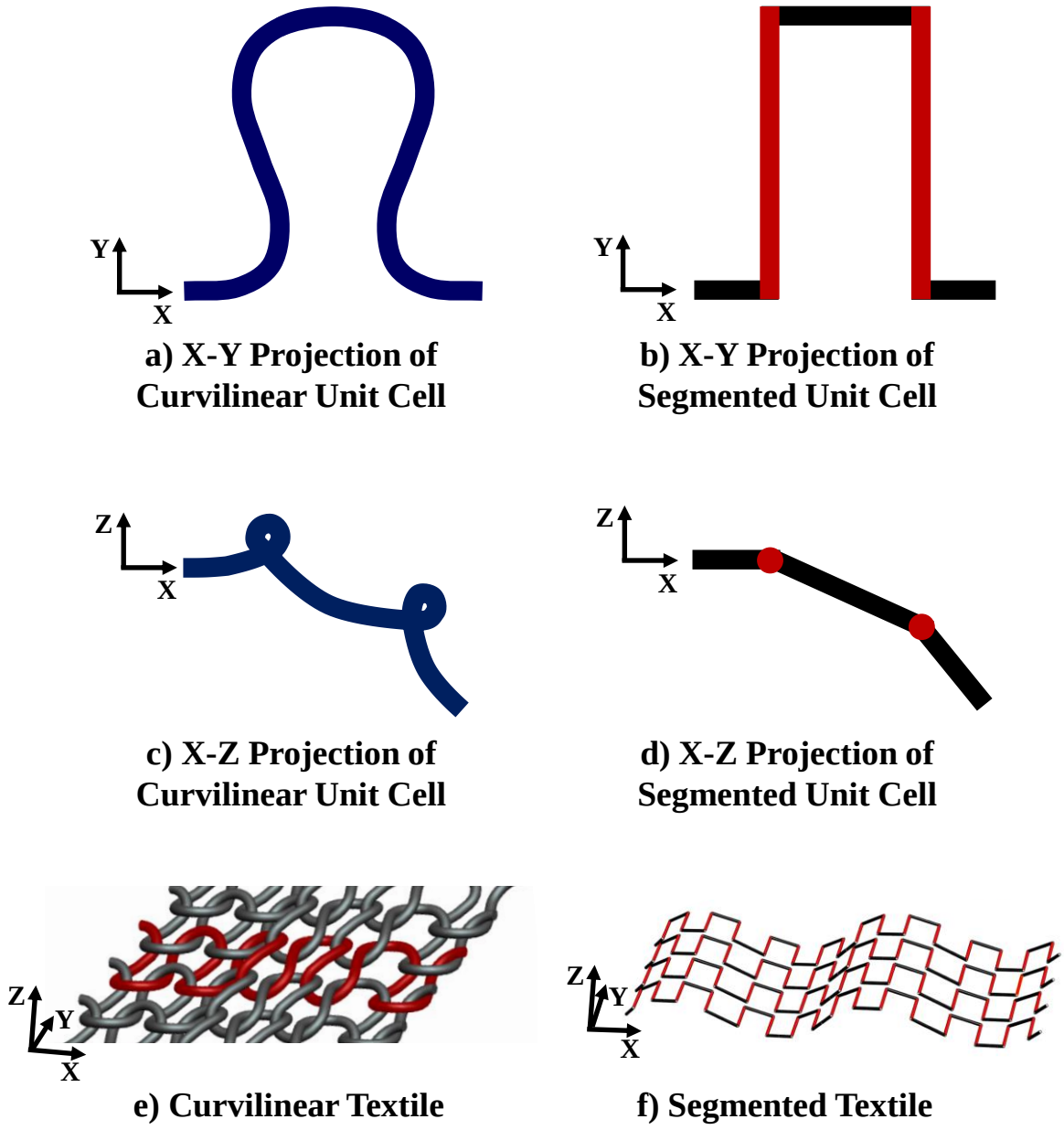

Figure 30. Segmented Unit Cell of 2x2 Rib Knit Actuator Architecture.
X-Y Projections of the a) Curvilinear Unit Cell and the b) Segmented Unit Cell, X-Z Projections of the c) Curvilinear Unit Cell and the d) Segmented Unit Cell, and Representations of the e) Curvilinear Textile and f) Segmented Textile.

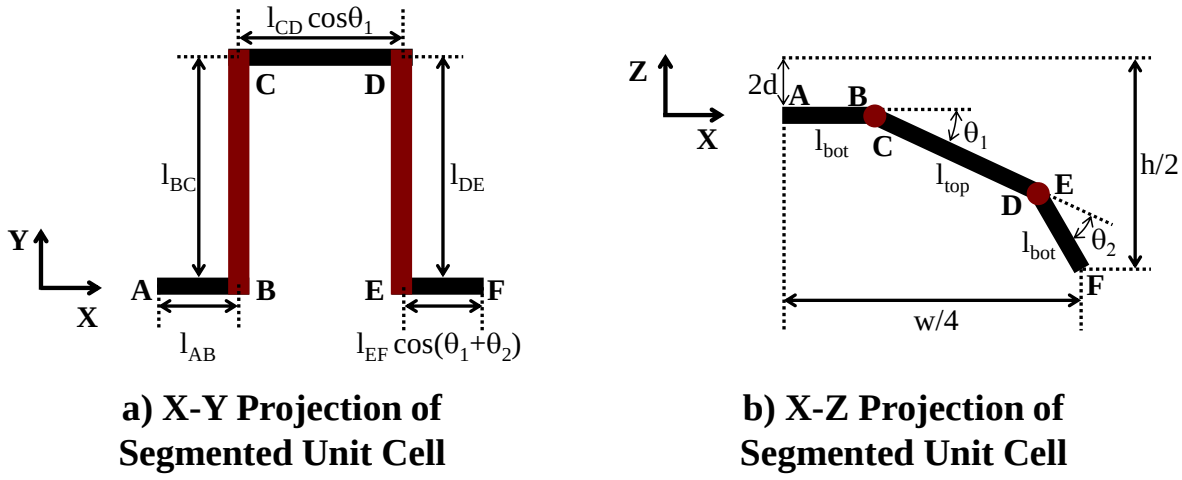

a) X-Y Projection of Segmented Unit Cell

b) X-Z Projection of Segmented Unit Cell

Figure 31. Geometry of segmented 2x2 rib knit unit cell.
The geometry of the 2x2 rib knit pattern unit cell is defined in a) the X-Y plane and b) the X-Z plane.

$$\frac{w}{4} = l_{bottom} + l_{top}\cos\theta_1 + l_{bottom}\cos(\theta_1 + \theta_2) \tag{5}$$

couples the width of the 2x2 segment to the measured segment lengths and the unknown rotation angles.

4.2.4. Enumerate Simple Effect Model of 2x2 Rib Knit Actuator Architecture

The foundational smart material wire in the 2x2 rib knit actuator architecture experiences combined torsion, bending, extension, and compression loading during the manufacturing process. Even when no external load is applied to the textile, internal stresses and strains exist in the foundational wire. Through experimental observation, it was determined that the governing deformation mechanism for the 2x2 rib knit was torsion. During manufacturing, segments BC and DE of the unit cell were twisted and the twist was held in place by adjacent unit cells. Due to the geometric constraints on the unit cell, increased applied loads increase the angle through which each segment rotates. Upon actuation, the dual state material stiffens, recovering some of the induced torsional strains, and the textile lifts the applied load.

The simple torsional model is implemented by considering the segments aligned with the X-axis (black segments in Figure 31) to be rigid and segments aligned with the Y-axis (red segments in Figure 31) to be torsion segments. Rigid segment AB is constrained due to symmetry, torsion segment BC is twisted by the angle $\pi-\theta_1$, rigid segment CD extends at angle θ_1, torsion segment DE is rotated by angle $\pi-\theta_2$, and the final rigid segment, EF, extends angle $\theta_1+\theta_2$.

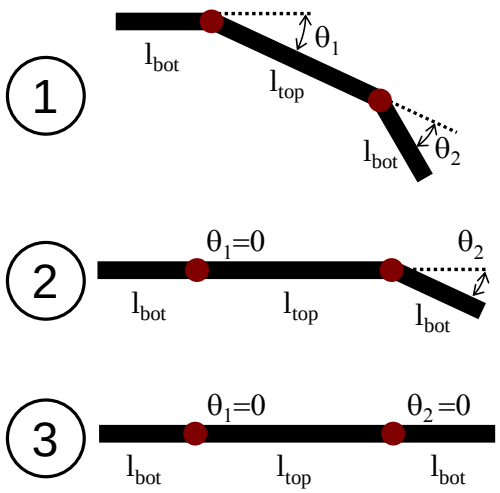

Figure 32. Rib Constraint Regions.
The rib knit unit cell experiences three distinct regions. 1) torsion spring 1 and 2 are both active, 2) only torsion spring 2 is active, and 3) neither torsion spring is active.

The rib model is constructed with three distinct operational constraint regions (Figure 32). For relatively small applied loads both torsions springs are active. As the applied load increases, the first torsion spring can rotate no further due to the plate applied to the top of the prototype and only the second torsion spring is active. As the applied load is furthered increased both torsion springs are confined and the thickness of the textile no longer changes. When torsion spring 1 becomes inactive, the moment arm is greatly decreased resulting in increased stiffness of the structure.

4.2.5. Predict Force-Deflection Performance of Simple Effect Model of 2x2 Rib Knit Actuator Architecture

The foundation for deriving the force-deflection performance of the simple torsional model has been established and a predictive model can be developed for the states and the actuation behavior of the 2x2 rib knit. This section covers some additional assumptions, force-equilibrium, and scaling of the unit cell to represent the entire textile performance.

4.2.5.1. Assumptions

The segmented superposition modeling approach has been created to develop the simplest model that captures the behavior of a given active knit actuation architecture. To simplify the modeling approach as much as possible, several assumptions were made about the active material and the 2x2 rib knit architecture. The unit cell is separated into rigid and elastic segments. The rigid segments are permitted to undergo rotation but are assumed to completely transfer loads without undergoing any deformation. The elastic segments are assumed straight and are subjected

to torsional loading that results in a twist along the length of the center axis. The elastic segments are assumed to be naturally straight, inextensible, incompressible, homogeneous, and experience the shape memory effect. The shape memory effect of the SMA wire is captured in the model by assuming the materials exhibits dual state behavior in the form of two linear elastic shear moduli. The SMA wire is assumed to be trained to a straight shape that is recoverable upon heating the material above the transformation temperature.

4.2.5.2. Force Equilibrium Interactions

The force equilibrium interactions set the foundation for the predicting the load-extension performance of rib knit pattern active knits. The assumptions made in regard to the unit cell, allow the force equilibrium to be analyzed in two dimensions, reducing the complexity of the modeling solution. The equations are state based, and the material properties of the torsional segments are dependent on the material phase, austenite or martensite. The torsional segments are represented by torsions springs.

4.2.5.2.1. Torsional Spring Representation

The torsion segments are represented by torsion springs in the free body diagram (Figure 33). The spring stiffness is determined using a simple torsion equation that relates the torsion to material and geometric properties and the angle of twist. The length of the torsion segment is taken as l_T, the moment of inertia is calculated using the active material diameter, d, and the angle of twist is $\pi-\theta$. Because of the dual state nature of the active material, the shear modulus, $G_{A,M}$,

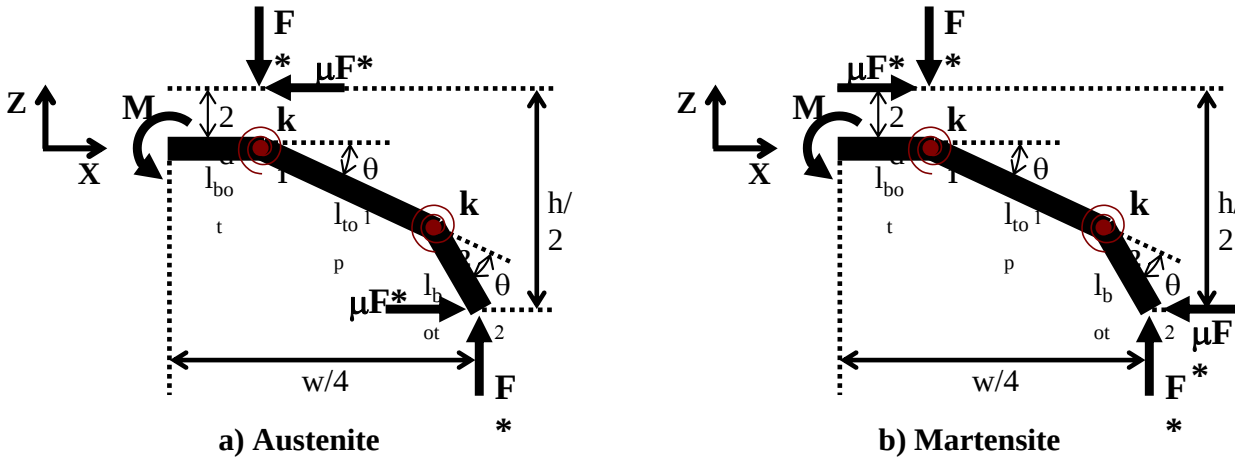

Figure 33. Free body diagram of 2x2 rib knit pattern unit cell.
External forces from the applied load F* per unit cell act on the segmented architecture where friction changes direction between the a) austenite and b) martensite states.

depends on the state of the material, Austenite or Martensite. The torque of each segment can be described using

$$T_1 = \frac{\pi \cdot d^4 \cdot G_{A,M}}{32 \cdot l_T} (\pi - \theta_1) \tag{6}$$

and

$$T_2 = \frac{\pi \cdot d^4 \cdot G_{A,M}}{32 \cdot l_T} (\pi - \theta_2). \tag{7}$$

The torsional stiffness of the two torsion tubes is:

$$k_{A,M} = \frac{\pi \cdot d^4 \cdot G_{A,M}}{32 \cdot l_T} \tag{8}$$

Substituting the stiffness variable into the torsion equations give:

$$T_1 = k_{A,M} (\pi - \theta_1) \tag{9}$$

$$T_2 = k_{A,M} (\pi - \theta_2) \tag{10}$$

4.2.5.2.2. Austenite and Martensite Free States

The initial, unloaded configuration of the knit textile in each state is known as the free-state. When the textile is in the free-state no external loads are applied to the structure. However, internal stresses occur in the wire because interlacing adjacent loops hold the structure in place, retaining some of the stresses induced during manufacturing.

The angles corresponding to the austenite free-state can be calculated by solving the simultaneous equations for the geometric constraints

$$\frac{h_{A0}}{2} = 2d + l_{top} \sin \theta_{1,A0} + l_{bottom} \sin(\theta_{1,A0} + \theta_{2,A0}) \tag{11}$$

$$\frac{w_{A0}}{4} = l_{bottom} + l_{top} \cos \theta_{1,A0} + l_{bottom} \cos(\theta_{1,A0} + \theta_{2,A0}) \tag{12}$$

The torque on each torsion spring in the austenite free-state is given by:

$$T_{1,A0} = k_A (\pi - \theta_{1,A0}) \tag{13}$$

$$T_{2,A0} = k_A (\pi - \theta_{2,A0}) \tag{14}$$

The same process can be followed to calculate the angles and torque corresponding to the martensite free-state.

4.2.5.2.3. Loaded State Heights

The initial angles ($\theta_{1,A0}$, $\theta_{2,A0}$,$\theta_{1,M0}$, and $\theta_{2,M0}$) are a result of the torques in each of the torsion segments that are held in place by interlacing adjacent loops. The prototype changes height as it undergoes changes in the mechanical and thermal loading. The change in each of the angles is a result of the applied load or a transition into a less stiff material state.

As the load applied to the textile increases, the textile is compressed, increasing the angle of twist in the torsion springs. The change in angle results in a change in torque in the torsional spring. The change in torque is related to the applied loads to the structure through a moment balance. The relationship for the torsion spring 2 is given by

$$\Delta T_{2,A} = k_A \left(\theta_{2,A0} - \theta_{2,A}\right) = F^* \cdot l_{bot} \cos(\theta_{1,A} + \theta_{2,A}) + \mu \cdot F^* \cdot l_{bot} \sin(\theta_{1,A} + \theta_{2,A}) \quad (15)$$

A moment balance can also be conducted about spring 1 resulting in the a second relationship,

$$\Delta T_{1,A} = k_A \left(\theta_{1,A0} - \theta_{1,A}\right) = F^*\left(l_{bot} \cos(\theta_{1,A} + \theta_{2,A}) + l_{top} \cos\theta_{1,A}\right) + \mu \cdot F^*(l_{bot} \sin(\theta_{1,A} + \theta_{2,A}) + l_{top} \sin\theta_{1,A} + 2d \quad (16)$$

The same procedure can be used to establish relationships for the martensite state.

$$\Delta T_{2,M} = k_M \left(\theta_{2,M0} - \theta_{2,M}\right) = F^* \cdot l_{bot} \cos(\theta_{1,M} + \theta_{2,M}) - \mu \cdot F^* \cdot l_{bot} \sin(\theta_{1,M} + \theta_{2,M}) \quad (17)$$

$$\Delta T_{1,M} = k_M \left(\theta_{1,M0} - \theta_{1,M}\right) = F^*(l_{bot} \cos(\theta_{1,M} + \theta_{2,M}) + l_{top} \cos\theta_{1,M}) - \mu \cdot F^*(l_{bot} \sin(\theta_{1,M} + \theta_{2,M}) + l_{top} \sin\theta_{1,M} + 2d) \quad (18)$$

The relationships for spring are nearly identical, the only difference is the change in friction direction as a result of the thermal operational transition between the martensite compressed state and the austenite expanded state. The equations are solved for a range of applied loads to determine the load height relationship for the unit cell.

4.2.5.2.4. Textile Performance Prediction

Prediction of the overall knit textile performance from the unit cell model is completed by scaling the performance of the unit cell in the Austenite Expanded and Martensite Compressed States. The unit cell is a single loop; however, the load is transferred from the top of a knit loop through the bottom of an adjacent purl loop. Therefore the total applied load is

$$F_{app} = \frac{N_{Columns}}{2} \cdot N_{rows} \cdot F^* \quad (18)$$

The total height of the textile was incorporated into the unit cell model and no scaling is necessary. The modeling procedure presented in this section produces an analytical model that captures the kinematic and kinetic behavior of each state experienced by this complex actuation architecture.

4.3. RIB KNIT PATTERN EXPERIMENTAL VALIDATION

Several experiments were conducted to fully understand the behavior to this unique actuator architecture and assess the ability of the segment superposition modeling approach to predict the load-extension of each state. The model was coded and executed in MATLAB using the measured initial geometric parameters including the top segment length, bottom segment length, torsion length, wire diameter, and the initial width and height of the structure in the martensite and austenite free states. Additionally, the material properties (shear modulus for each state) were experimentally obtained. The model predictions were compared to experimental results to assess the ability of the model to predict the qualitative and quantitative behavior of 2x2 rib knit pattern active knits.

4.3.1. SMA Material Properties

Shape memory alloys exhibit a complex thermo-mechanical coupling. While elaborate constitutive models exist for SMAs, the goal of this model is to provide modular, tractable, scalable predictive capabilities early in the design process. Because the goal is to keep the model simple, the SMA material is modeled as a dual state material that has a low torsional stiffness in the flexible martensite state and a higher torsional stiffness in the stiff austenite state. Torsional material properties of wire forms are difficult to measure but the shear modulus can be related to the elastic modulus through the relationship $E = 2G(1 + \upsilon)$, where E is the Elastic modulus, G is the Shear Modulus, and υ is Poisson's ratio [91]. SMA has a Poisson's ratio of 0.33 [92]. Dynalloy Flexinol® 90°C wire, the same wire used in the experimental prototypes, was experimentally characterized to determine the Elastic modulus (Figure 35). The austenite elastic modulus was found to be 45.8 GPa, which corresponds to a shear modulus of 17.2 GPa, and the martensite modulus was found to be 16.0 GPa, which corresponds to a shear modulus of 6.0 GPa. Typical values for the shear modulus of the shape memory alloys are 25 to 40 GPa for the austenite phase and 8 to 26 GPa for the martensite phase [93]. Flexinol® 90°C wire undergoes a significant amount of shake down as a result of the manufacturing process, resulting in a softer material

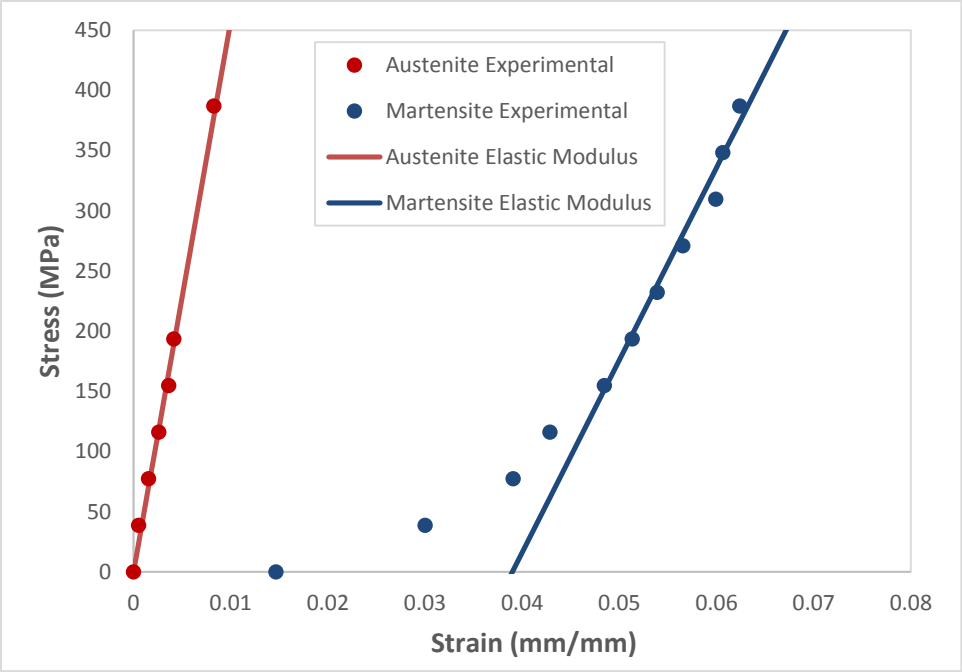

Figure 34. Experimental Material Properties of SMA Wire.
The experimentally obtained material properties of Dynalloy Flexinol® 90°C SMA wire are represented by an Elastic Modulus of 45.8 GPa in the Austenite phase and an Elastic Modulus of 16.0 GPa in the Martensite State.

compared to pure nickel titanium shape memory alloy material [94]. Additionally, 90°C Flexinol® wires exhibits a two-way effect, an offset between austenite and martensite Free States. The offset under zero load is accounted for in the model by using two different initial conditions for the height and width of the textile, one for the martensite free state and one for the austenite free state. The combination of a reduced shear modulus in each state and the incorporation of an independent initial condition for each state, accurately accounts for the unique behavior exhibited by 90°C Flexinol® wire.

4.3.2. Active Knit Prototypes

A knit prototype was fabricated using a Bond America Ultimate Sweater Machine, which uses a bed of needles to manipulate a fiber into a textile. Several cam needle profiles can be selected to change the density of the knitted prototype. The density of the textile decreases with increasing needle profiles (profile 1 creates the densest textile, whereas profile 4 creates the least dense

Table 5. Geometric Parameters of 2x2 Rib Knit Pattern Prototypes
Geometric parameters (d, N_C, N_W, $ltop$, $lbot$, lT) used to create garter knit pattern knit and the measured Austenite Free State textile and unit cell geometries (L_{A0}, $W_{totalA0}$, C_0, W_0, and L).

d (mil)	*Needle Profile*	N_C	N_W	l_{top} (mm)	l_{bot} (mm)	l_T (mm)	$h_{M,0}$ (mm)	$w_{M,0}$ (mm)	$h_{A,0}$ (mm)	w_{A0} (mm)
10	3	24	16	3.31	4.33	9.42	5.0	28.7	6.8	26.1

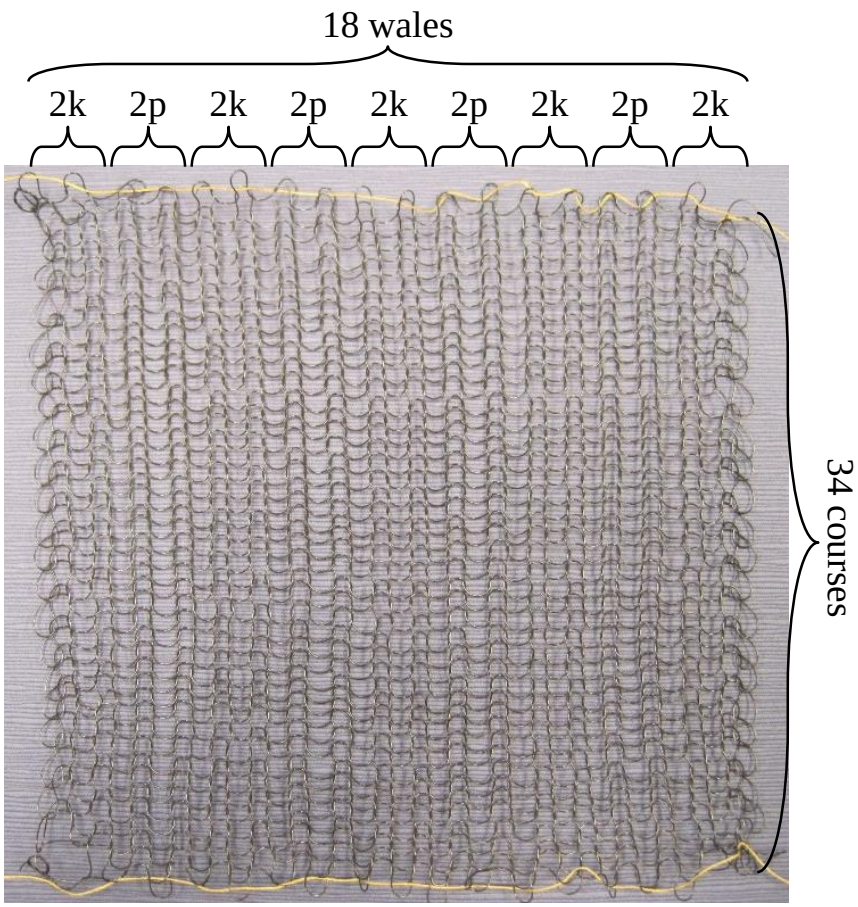

Figure 35. 2x2 Rib Knit Pattern Prototype.
Rib knit pattern prototype in the *Martensite Free State* showing the alternating pairs of knit and purl wales (columns).

textile). The prototype was fabricated with Dynalloy Flexinol® 90°C shape memory alloy wire for 18 wales and a variable number of courses in the 2x2 rib knit pattern. Wire diameters of 8 to 15 mil were chosen to span a range of performance capabilities while staying within the bounds of the knitting machine. The number of courses were varied to meet a minimum prototype depth of 4 inches based on the experimental setup designed for this study. The lengths of the top segment, l_{top}, and the bottom segment, l_{bot}, and the torsion length, l_T, were measured from the prototypes in the martensite free state. The height, $h_{M,0}$ and width, $_{wM,0}$, were measured in the martensite free state as well. The prototype was heated above the material transformation temperature of the SMA wire and the austenite free height, $h_{A,0}$ and width, $w_{A,0}$, were recorded. The geometric parameters of all the prototypes can be found in Table 5.

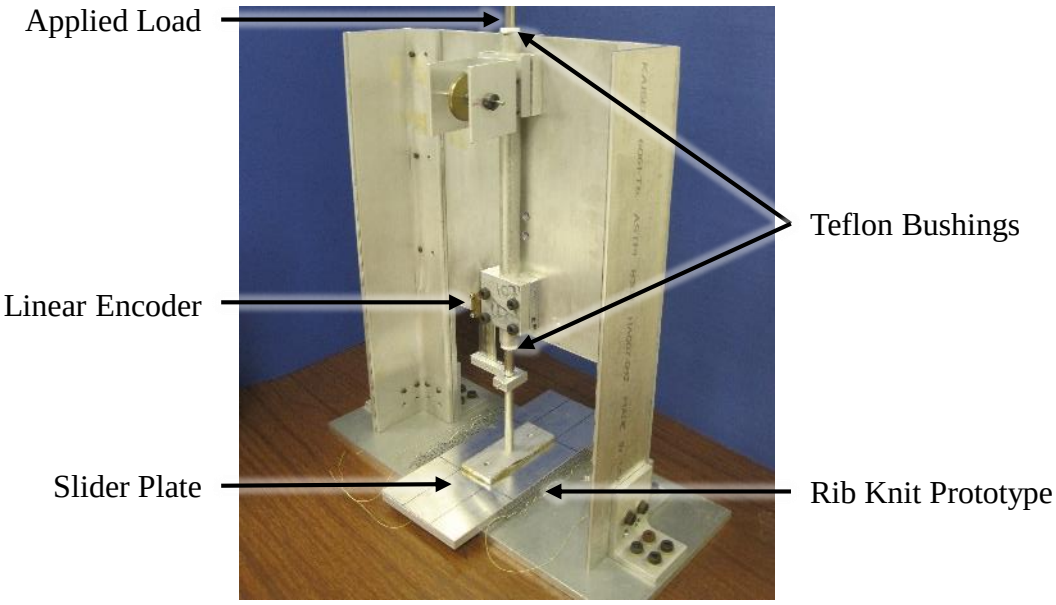

Figure 36. Experimental Setup for Rib Prototypes.
Experimental setup used to determine the load-extension behavior of the Rib Knit Pattern prototypes.

4.3.3. Experimental Method

The experimental setup (depicted in Figure 36) was used to measure the change in height in response to an applied constant load to the rib knit pattern prototypes. The prototype was placed on the smooth aluminum base plate and an aluminum slider plate was placed on top of the prototype. The slider plate moved vertically along a smooth rail that was guided by Teflon bushings. The change in height of the textile was recorded by a linear encoder. The prototype was run through thermo-mechanical cycles (Figure 37) in an Envirotronics FLX300 environmental chamber. A load was applied to the prototype, the chamber was cooled to 10°C, causing slight compression of the prototype. The chamber was heated to 120°C, resulting in a material transition into the stiff austenite phase that lifts the applied load to the austenite expanded height, which was recorded using a US Digital linear encoder strip with 250 divisions per inch. The temperature was reduced to 10°C and the prototype compressed in response to the material transition into the martensite phase, reaching the martensite compressed height. The thermo-mechanical cycle was repeated for increasing applied loads to obtain the load-extension of the textile in each state.

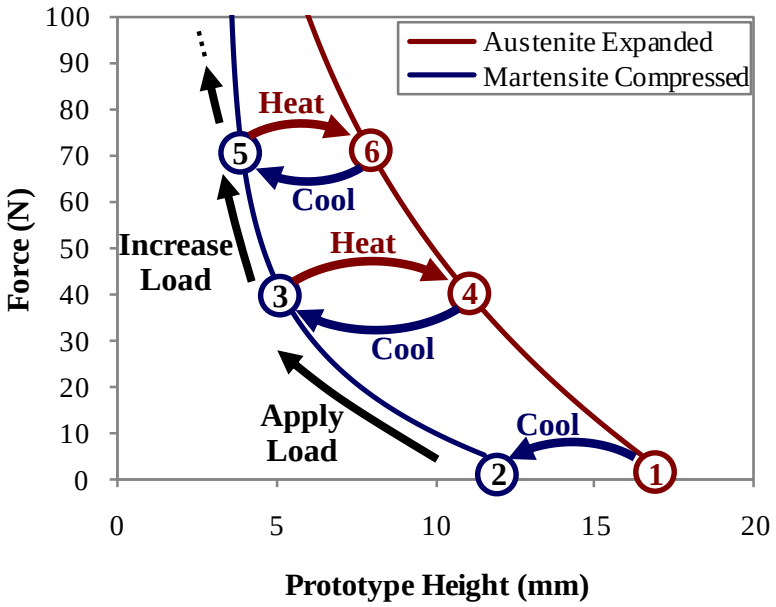

Figure 37. 2x2 Rib Knit Actuator Architecture Experimental Procedure.
Rib knit pattern textiles were experimentally tested in an environmental chamber - a load was applied to the prototype, the environmental chamber was heated to 120°C and the austenite expanded height was recorded, the chamber was then cooled to 10°C wire and the martensite compressed height was recorded. The applied load was increased and the thermo-mechanical testing cycle was repeated to obtain a force-deflection performance curve.

4.3.3.1. Martensite Compressed and Austenite Expanded

The experimental and theoretical results of the martensite compressed and austenite expanded states for prototype 10-3 are shown in Figure 38. The theory and experimental results show the same qualitative results, inverse "J" shaped load-extension curves. For each state, the textile is initially flexible and a small change in applied load greatly compresses the prototype. This flexibility is particularly evident for the martensite compressed prototype, the height of the textile in the martensite compressed state reduces from 4.73 mm to 2.36 mm (49.9% compression) in response to a very small change in applied load (0.19 N to 1.96 N). The flexible behavior for each state corresponds to region 1 of the model constraints (Figure 32), where both torsion segments are active. As the applied load is increased the textile stiffens, resulting in less deformation under the increased applied load, characteristic of region 2 of the model constraints. Region 2 is stiffer because the first torsion segment is no longer active, reducing the moment arm, which simultaneously increases the force and reduces the range of motion of the segment. Finally, the load is increased to a point that the textile is no longer able to be further compressed under increased applied loads (corresponding to region 3 of the model constraints). The theoretical minimum height of the prototype is twice the diameter of the wire. The martensite compressed

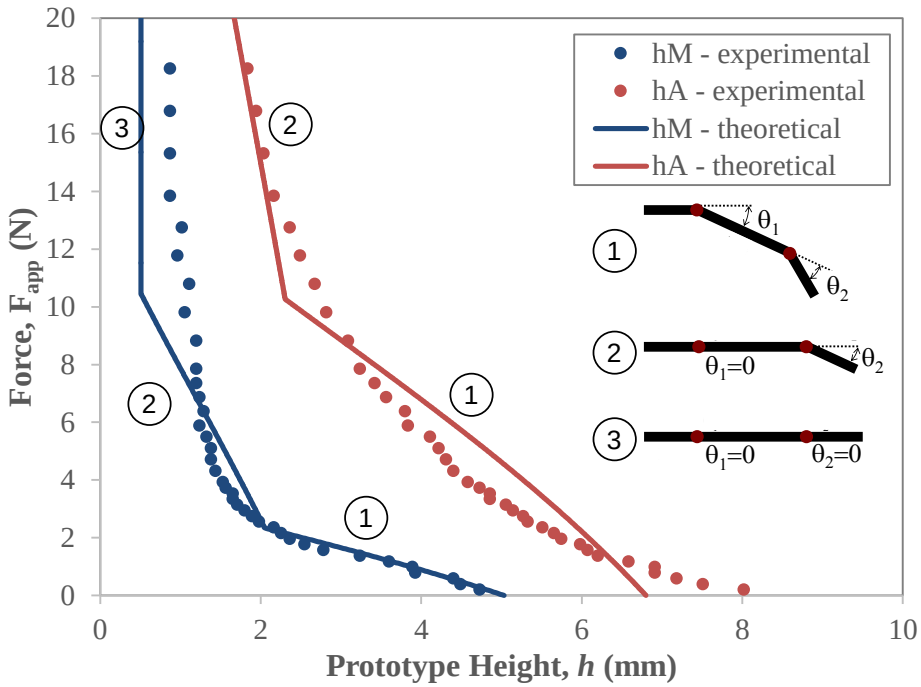

Figure 38. Experimental Results of 2x2 Rib Knit Actuation Architecture.
The theoretical and experimental results for each state exhibit the same qualitative behavior – in Region 1 both torsion segmetns are active and the textile is flexible, in Region 2 only one torsion segment is active resulting in a stiffer textile behavior, and in Region 3 the textile is fully compressed under the applied load. The model predicts the martensite compressed height by 13.6% for Region 1 and 18.8% for Region 2 and the austenite expanded state by 5.1% for Region 1 and 8.0% for Region 2.

prototype compresses to a height greater than the predicted thickness (0.87 mm compared to 0.51 mm) because alternative deformation modes and neglected geometric affects result in a thickness greater than twice the diameter. The prototype was not tested at loads large enough for the austenite compressed state to reach region 3 because it is well beyond the range of loads that produces the maximum actuation displacements.

The model uses the initial geometry of the prototype and the experimentally obtained material properties (shear modulus of 6.0 GPa for the martensite state and 17.2 GPa for the austenite state) to predict the kinetic performance of the textile. The model accurately predicts the martensite compressed height by an average height error of 3.4% for Region 1 and 9.4% for Region 2 and the austenite expanded height by an average height error of 10.0% for Region 1 and 7.5% for Region 2 for the range of applied loads tested. Region 1 of the austenite expanded state has the highest average height error of 10.0%, the error would be reduced with higher manufacturing tolerances. At low loads, small local manufacturing inconsistencies cause non-homogeneous textile behavior in the form of warping of the textile. The non-homogeneous behavior cannot be represented by the unit cell model, therefore the very low force region of the austenite state is not predicted by

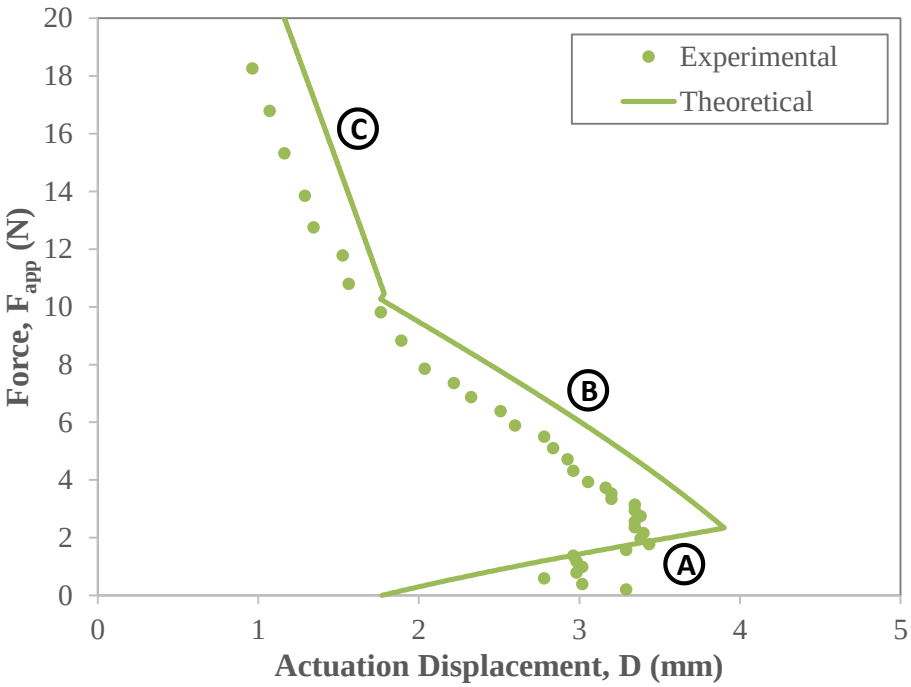

Figure 39. Net Actuation of 2x2 Rib Knit Actuation Architecture.
The qualitative and quantitative behavior of the constant load actuation behavior is captured by the segmented modeling approach. In Region A increased applied loads the actuator produce enhanced actuation displacements to a max displacement point, in Region B increased applied loads result in smaller actuation displacements, and in Region C increased applied loads result in smaller actuation displacements at a slower rate as the martensite prototype is fully compressed and only the austenite expanded state is changing height. The model predicts the peak actuation displacement within 16% and the corresponding force within 14.4%.

the model. While the predicted regions are not straight lines, their minimal curvatures invite comparison to straight line including stiffness of the region. The model predicts a region 1 approximate stiffness of -2.44 Nmm for the austenite expanded state and -0.81 Nmm for the martensite compressed state, compared to -1.43 Nmm and -0.79 Nmm for the experimental straight line slope approximations. The predicted Region 2 stiffness for the austenite expanded state is - 4.46 Nmm and the stiffness for the martensite compressed state is -3.41 Nmm, compared to -4.04Nmm and -2.04 Nmm for the experimental straight line slope approximations. Each region experimentally demonstrates a lower stiffness then predicted by the model because the model only considers a single deformation mode (torsion) and neglects additional deformation modes that contribute to the deformation.

4.3.3.2. Net Actuation

The net actuation performance is the difference between the heights of the prototype in the austenite expanded state and the martensite compressed state under the same applied load. The theoretical and experimental results demonstrate the same qualitative behavior (Figure 39). As the

Table 6. Predictive Capabilities of 2x2 Rib Knit Actuator Architecture Segment Model
The Segment Model of the 2x2 rib knit actuator architecture accurately predicts both the states and actuation performance of the experimental prototype.

	Martensite		Austenite		Max Disp (mm)	Force @ Max Disp (N)	Max Strain (%)	Force @ Max Strain (N)
	Region 1 Avg Slope (Nmm)	Region 2 Avg Slope (Nmm)	Region 1 Avg Slope (Nmm)	Region 2 Avg Slope (Nmm)				
Experimental	-0.79	-2.04	-1.43	-4.04	3.44	1.8	211.8	4.7 N
Theoretical	-0.81	-3.41	-2.44	-4.46	3.9	2.35	-	-

applied load increases, the prototype is able to produce more actuation displacement up to a max displacement point. As the load is further increased, the prototype is not able to produce as much actuation displacement because the prototype in the martensite state stiffens and the rate of compression decreases. This actuation behavior is very similar to that of the planar knit loop and garter knit pattern architecture described in Chapter 3, however the mechanism is different. For 2x2 rib knit actuator architectures the actuation displacement initially increases with increased applied load because the martensite state is compressing more than the austenite state under the same increase in applied load (region A in Figure 39). The increasing actuation displacement with increased applied load occurs until the martensite state begins to stiffen (as it enters Region 2), resulting in the peak actuation displacement. At this point, the martensite compressed state (model region 2) is stiffer than the austenite expanded state (model region 1), resulting in a decrease in actuation displacement with increased applied load (region B). The actuation displacement continues to decrease at a decreased rate with increasing applied loads as the martensite expanded state reaches its minimum height (model region 3) and the austenite expanded state stiffens (model region 2). With further increased applied loads, the austenite compressed state would reach a minimum thickness (model region 3) and the prototype would no longer provide actuation displacement, although the experimental applied loads were not increased to that point because it is beyond the range the prototype provides unprecedented performance. There is an optimal deflection point for 2x2 rib knit actuators where a maximum actuation displacement can be achieved.

The model and experiments are a very good quantitative match considering the various assumptions made during the modeling process. The experimental maximum displacement point was 3.44 mm under an applied load of 1.8 N. The model predicted a 13.4% larger displacement of 3.9 mm under a 30.8% larger load of 2.35 N. Over the entire range of applied loads the model

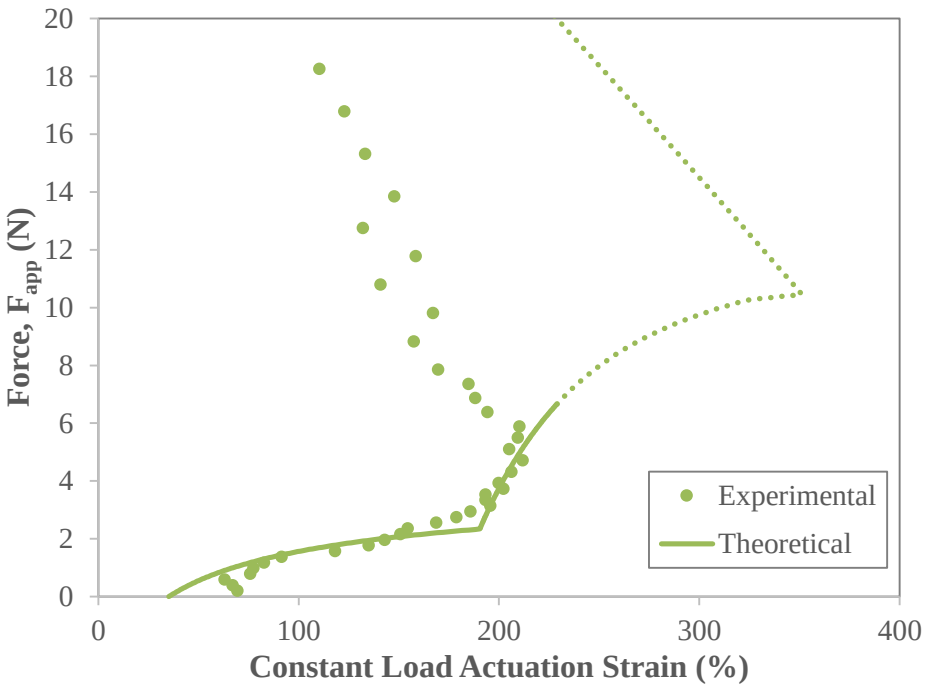

Figure 40. Constant Load Actuation Strain of 2x2 Rib Knit Actuator Architecture.
The constant load actuation strain of the prototype displayed increasing actuation strains with increased applied loads to a peak strain of 211.8% against a 4.7 N applied load. The prototype produced more than 110% constant load actuation strain for a large range of forces 1.5 N to 18.3 N.

resulted in an average absolute displacement error of 0.44 mm, which corresponds to an average displacement error of 14.7%. The error is a result of the numerous assumptions made during the modeling process. One significant source of error is that only a single deformation mode was considered, the torsion of 2 segments. In reality, several other deformation modes contribute to the performance of the actuator. There is combined bending and torsion over the length of the wire and the externally applied load may result in tension, compression, or even buckling of various segments of the loops. The predictive capabilities could be improved through the development of additional segment models that account for alternative deformation modes that result in decreased stiffness of the entire textile. Even with the assumptions the model accurately predicts the actuation form and magnitude, providing a tractable tool for the design of three-dimensional active knit actuators to meet application specifications.

The 2x2 rib knit pattern architecture greatly amplifies the actuation strain of the foundational smart material wire (2 to 8% actuation strain) to provide as much as 211.8% actuation strain under a 4.7 N applied load (Figure 40). The constant load actuation strain is the amount of strain between the martensite compressed state and the austenite expanded state under a constant applied load. The model accurately predicts the actuation strain up to the force of maximum strain within an

average strain of 11.7%. However, at higher loads the model predicts a more compressed martensite compressed height, the reference value for determining the constant load actuation strain, resulting in much higher actuation strains than experimentally observed. The prototype displayed a very large high strain operating region with loads from 1.5 N to the maximum tested load of 18.3 N producing more than 100% constant load actuation strain. The rib knit actuator architecture produces a unique actuation motion in the form of a corrugated structure with a variable peak to peak height that is unavailable with current actuation technologies. The 2x2 rib knit architecture greatly leverages the foundational material properties to provide extremely large strains against application level loads, delivering an advanced actuation capability with the potential to improve current and realize new applications.

4.4. Segment Superposition Three-Dimensional Model Conclusions

This chapter developed a new modeling approach, the segment superposition modeling approach, to establish a framework to predict the kinetic performance of complex three-dimensional active knit architectures. The general modeling procedure was described, the modeling approach was demonstrated with the 2x2 rib knit actuator architecture, and both the modeling approach and the 2x2 rib knit model were experimentally validated.

The segment superposition modeling approach is a five step process that results in modular, tractable, and scalable model results for predicting the kinetic performance of complex knit structures. The modeling approach reduces the complexity of modeling the knit actuator by establishing a clear procedure and representing the architecture with a system of simple mechanical models. The first step is to identify the unit cell, or the smallest repetitive element that can be used to represent the knit architecture or an area of the knit architecture, by recognizing points of symmetry within the knit architecture. The size and complexity of the unit cell increase for higher level of the hierarchy. The second step is to segment the unit cell. Segmenting the unit cell simplifies the geometry by representing the complex curvilinear geometry with a system of linear segments and establishes constraint based on physical limitations of individual segments. The third step is to enumerate individual simple effects models for different deformation modes including tension, extension, torsion, bending, and buckling that have a significant impact on kinetic performance. The fourth step is to predict the force-deflection performance by creating simple mechanical models that relate the architecture to material property approximations and

externally applied loads. The final step is to superimpose the force-deflection of the various individual effects models to predict the performance the individual states and the actuation of the actuator.

To demonstrate the segment superposition modeling approach, the approach was followed to develop a segmented model of the 2x2 rib knit actuator architecture. The corrugated-like structure of the 2x2 rib knit architecture was analyzed to determine the unit cell of the architecture – a single knitted loop. The single loop unit cell was segmented to into five straight segments that were mapped to the geometric properties of the true curvilinear knitted loop. During this step, geometric constraints were developed to mimic physical constraints in the system, including establishing three constraint regions that limit the range of motion of individual segments to best mimic the behavior of the physical textile. A torsion deformation mode was explained and mapped to the appropriate segments in the segmented unit cell. While numerous deformation modes exits, observation of prototypes indicated that the primary deformation mode was in the torsion of the sides of the knitted loops. A simple torsion-based model was developed through force equilibrium analysis to predict the force-displacement performance of the austenite and martensite states. This initial exploration of the segment superposition modeling approached only covered the development of a single simple effects model because the kinetic performance of this particular architecture is dominated by a single physical effect. Future work is needed to establish additional simple effects models and demonstrate the process of superimposing multiple effect models.

The modeling approach and the 2x2 rib knit segmented model was experimentally validated for the ability of the model to predict the force-height relationship for each of the states and the constant load actuation displacement. Based on experimental material characterization, the complex thermo-mechanical material properties of the foundational shape memory alloy wire were simplified to a dual state material with flexible shear modulus of 6.0 GPa in the martensite state and a stiffer shear modulus of 17.2 GPa in the austenite state. A prototype was machine knit using 10 mil diameter Dynalloy Flexinol® SMA wire with a transition temperature of 90°C. The 2x2 rib knit architecture was used for the entire prototype, which consisted of 16 wales and 24 courses. The prototype was experimentally tested in an environmental chamber using a custom designed and built characterization setup that measured the height of the prototype under a range of applied loads as the prototype transitioned from the stiff austenite state to the flexible martensite state. The segmented model accurately predicted the force-height relationship of the prototype in each state

in addition to predicting the actuation performance. The model and experiments correlated very well considering the assumptions made during the modeling process including the material properties and simplified geometry of the structure. The model accurately predicted the martensite compressed height by an average height error of 3.4% for the low force region and 9.4% for the mid force region and the austenite expanded height by an average height error of 10.0% for the low force region and 7.5% for the mid force region for the range of applied loads tested. The theoretical actuation performance was found to match the form and magnitude of the experimental actuation curve with and average absolute displacement error of 0.44 mm, which corresponds to an average displacement error of 14.7%. The segment model of the 2x2 rib knit actuation architecture accurately predicts the qualitative and quantitative performance of the accordion-like actuation behavior of 2x2 rib knit actuators.

The unique actuation motion provided by rib knit pattern actuators has tremendous potential to realize a new form of large strain surface actuation. Not only is the form of actuation useful, the highly leveraged architecture produces very large strains (up to 211%) under usable forces (4.7 N). The architecture not only produces a significant peak actuation strain, it displays significantly enhanced actuation strains over 100% for a wide range of applied loads from 1.5 N to 18.3 N. The performance of the 2x2 rib knit actuation architecture goes beyond what is possible with existing actuators and has the potential to meet the need for large strain actuators in applications.

The experimental validation not only validated the segmented model of the 2x2 rib knit actuation architecture but it also validated the segment superposition modeling approach. The new simplified modeling approach has tremendous potential to provide predictive capabilities for complex knit architectures through the development of modular, tractable, and scalable models. The modeling approach can be easily adapted and expanded to predict the performance of complex three-dimensional active knit actuations with various architectures with different material properties. The approach can also be followed to develop a tool box of modeling elements that can be assembled and implemented to predict the performance of various knit architectures. This chapter establishes the framework need to aid in the design of complex active knit architectures to meet the need for advanced actuators in applications.

.

Chapter 5. FEASIBILITY DEMONSTRATION STUDY

Active knits are a promising actuation architecture that produces unique actuation motions which are unattainable with current technologies, however, the feasibility of using active knits in applications has yet to be demonstrated. This chapter presents a feasibility demonstration study for using rib knit pattern active knits to meet the simultaneous force-deflection performance specifications required for flow control of an aircraft.

Flow control has been of significant interest to the aerospace community because actively manipulating flow characteristics around the wing can enhance high-lift capability and reduce drag by delaying or preventing boundary layer separation; thereby, increasing fuel economy and improving maneuverability and operation over diverse flight conditions which enables longer, more varied missions [1]-[2]. It is predicted that increasing flight efficiency would result in a one percent saving in world consumption of jet fuel worth approximately $1.25 million a day of direct operating costs [92]. Likewise, such fuel savings would lead to reduced environmental impact such as reduced noise and carbon emissions. Engineers have tried numerous tools (wing flaps, spoilers, vortex generators, etc.) to change the effective shape of the wing mid-flight to provide flow control. The simplification of conventional high lift systems by flow control technologies could possibly lead to a 0.3% airplane cost reduction, up to 2% weight reduction and about 3% cruise drag reduction [96]. While wing flaps, spoilers, and vortex generators have provided improvements at the leading and trailing edge of the wing, their large size and weight have prohibited full integration of actuators distributed over the wing surface.

One method that has produced incremental improvement to active flow control using distributed actuation is synthetic jets. Synthetic jets are used to create puffs of air at high frequencies to introduce a nearly constant controlled boundary layer disturbance that prevents or delays separation of the boundary layer across the wing, reducing the wake over the wing and improving efficiency [97]-[100]. Traditional synthetic jets implemented using pneumatics and electromagnetics are robust and provide the necessary airflow but their added design complexity

and the increased manufacturing and operating costs of the system has constrained their use [97]-[100]. While piezoelectric jets offer a compact and lightweight solution, current approaches exhibit failure of the diaphragm due to debonding and cracking at the high operating frequencies, restricting their adoption on aircraft [98]-[100].

A second approach to flow control is to vary wing surface conditions, via small to medium scale distributed actuation, to minimize drag and maximize efficiency while maintaining a continuous, smooth, aerodynamic structure. Surface contour bumps, a local change in the shape of the wing, have been computationally shown to reduce drag by 15% under transonic flow conditions [101]. Experimentally replicating the improved flow characteristics of contour bumps is difficult because varying the bump height and creating larger gradual bump surfaces pose technical difficulties [101]. Shape modification can also be accomplished using surface texturing to create small dimples that can produce vortices of prescribed strength and duration for the real time control of aerodynamic flows [102]-[103]. Generally, aircraft fly in turbulent flow regimes with 50% of cruise drag arising from skin friction [104]. A layer of harmonically forced dimples have the potential to generate span-wise travelling vortices that are known to reduce turbulent skin friction drag by as much as 30% [102]-[103]. Another form of flow control can come from ribs dispersed over a wing surface to reduce shear stress on the wings by obstructing span-wise movement of the fluid. Optimal rib shape and arrangement can lead to shear stress reductions of 9.9% [101]. These flow control approaches need to be actively actuated mid-flight as not to disrupt the flow over the wing during normal flight conditions for which the original wing has been designed. In order to achieve this in-flight surface change, actuators that are capable of large three-dimensionally complex distributed motions and that can be embedded in the wing must be developed.

This chapter provides the result of a feasibility demonstration study that investigates the potential of active rib knit pattern actuators to produce the simultaneous forces and displacements required to realize contour bumps for flow control applications. The orientation and configuration of rib knit pattern textiles are described. A rib knit pattern active knit prototype is created and tested using a specially designed experimental rig. Series and parallel combinations of identical rib knit pattern prototypes are experimentally explored to meet the technical specification required by the contour bump application. The measured knit performance is on the scale of the necessary aerodynamic pressures and displacements; thus, the rib knit pattern active knit is promising as a

technical solution for distributed actuation of local surface profiles in flow control. This feasibility demonstration study shows that active knit pattern textiles have the potential meet kinematic and kinetic specifications of new applications by exploiting their unique performances.

5.1. RIB KNIT PATTERN ARCHITECTURE, OPERATION, AND CONFIGURATIONS

Rib knit pattern knits leverage the active base material capability to create large strains distributed over a surface through the utilization of a unique rib knit pattern architecture, multi-state operation, and structural architectural configurations.

5.1.1. Architecture

All knit architectures are created using two types of loops – knit loops and purl loops. Both types of loops are characterized by a unit cell containing a loop, ridge, and two legs (Figure 41a). The tear drop shaped upper portion of the unit cell is the loop, which extends providing the legs which attach unit cells to one another. The ridge is the uppermost portion of the loop from the previous course (row of loops), which intersects with the loop and divides the loop from the legs. Knit and purl loops are differentiated by the location of the ridge relative to the loops and legs. Knit loops have backward arching loops with ridges in the back. The legs of the knit loop interlock with the ridge then extend behind the ridge, maintaining the curvature of the loop. The purl loop is the opposite of the knit loop with a forward arching loop with forward ridges and legs that extend to the front. A knit loop on one side of a textile appears as a purl loop on the other. Different combinations of the two basic loop structures enable myriad architectures to be created.

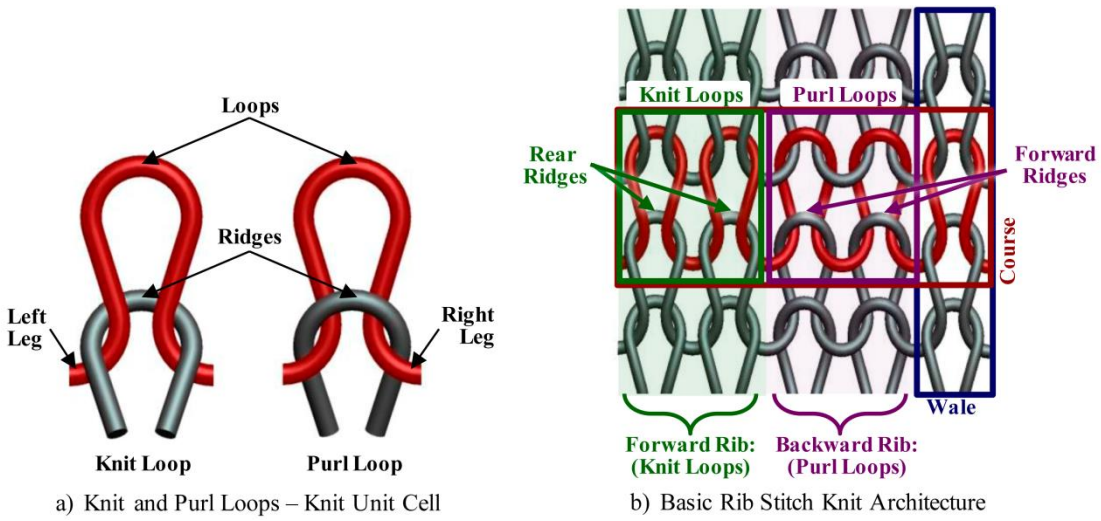

Figure 41. Rib Knit Architecture.
Knit textiles are composed of two basic unit cells, knit and purl, which can be combined to form different architectural patterns. The rib knit pattern architecture is comprised of two knit loops alternating with two purl loops forming symmetric columns.

The combination of knit and purl loops of particular interest for flow control applications is the rib knit pattern architecture (Figure 41b). The rib knit pattern is created by alternating knit and purl loops across the first course, or row. After the first course is completed, knit loops are purled and purled loops are knit in each additional course. The alternation of the fundamental unit cell produces symmetric wales (columns), alternating between smooth columns of the forward ribs comprised of knit loops and columns of ridges formed by the backward ribs comprised of purl loops. The rib knit pattern architecture can be fabricated by alternating a single knit and a single purl loop, called a 1x1 rib, or by alternating combinations of multiple knit and purl loops. The most common rib knit pattern architecture is a 2x2 rib which alternates two adjacent knit loops with two purl loops, creating raised and depressed columns that are two loops wide as shown in Figure 41b.

5.1.2. Operation

SMA rib knit pattern knit textiles go through operational transitions from one state to another resulting in a change in height and stiffness of the textile as depicted in Figure 42. The textile is initially compressed by an applied load (F_{app}) to the Martensite Compressed height (h_{Mcomp}), while the material is in the less stiff Martensite phase. An operational transition occurs when the material is heated above the transition temperature (T_{Af}) into the Austenite phase causing the textile to lift the applied load to the Austenite Expanded height (h_{Aexp}). A second operational transition returns the textile to the Martensite Compressed height (h_{Mcomp}) upon cooling below the Martensite Finish

temperature (T_{Mf}), completing the typical actuation cycle (Figure 42), which cycles between the Martensite Compressed State and the Austenite Expanded State

5.1.2.1. Martensite Compressed State

The first state, the Martensite Compressed State, is reached when a compressive load, F_{app}, is applied to the textile in the cooled, less stiff state at a temperature below the Martensite Finish temperature (T_{Mf}), compressing the textile to the Martensite Compressed height, h_{Mcomp} (Figure 42a). The textile compresses under the applied load as the contact areas at the peaks and valleys of the textile slip horizontally and the forward ribs at the peaks are pushed down while the backward ribs at the valleys are pushed up. The applied load normal to the plane of the knit applies off-set forces in the normal direction between adjacent courses at the interaction points that result in force couples at each interaction point in the knit structure. Figure 43 shows two different sets of force couples: the first set is a pair of balanced force couples at the top of a knit loop in the forward rib column that create moments of equal magnitude that balance in different directions (one clockwise the other counterclockwise). The second set is a pair of unbalanced force couples at the bottom of a loop that connects a knit loop to a purl loop that creates two moments of equal magnitude in the same direction. The legs connecting forward ribs to backward ribs connect knit and purl loops on either side and have a clockwise moment applied to each constrained end (Figure 43). The torsional loading on the leg encourages the compression of the textile because the compliant Martensite material twists to horizontally flatten the leg, compressing to the Martensite Compressed height, h_{Mcomp}. The Martensite Compressed State is the first of two states in the quasi-static cyclic portion of the typical actuation cycle.

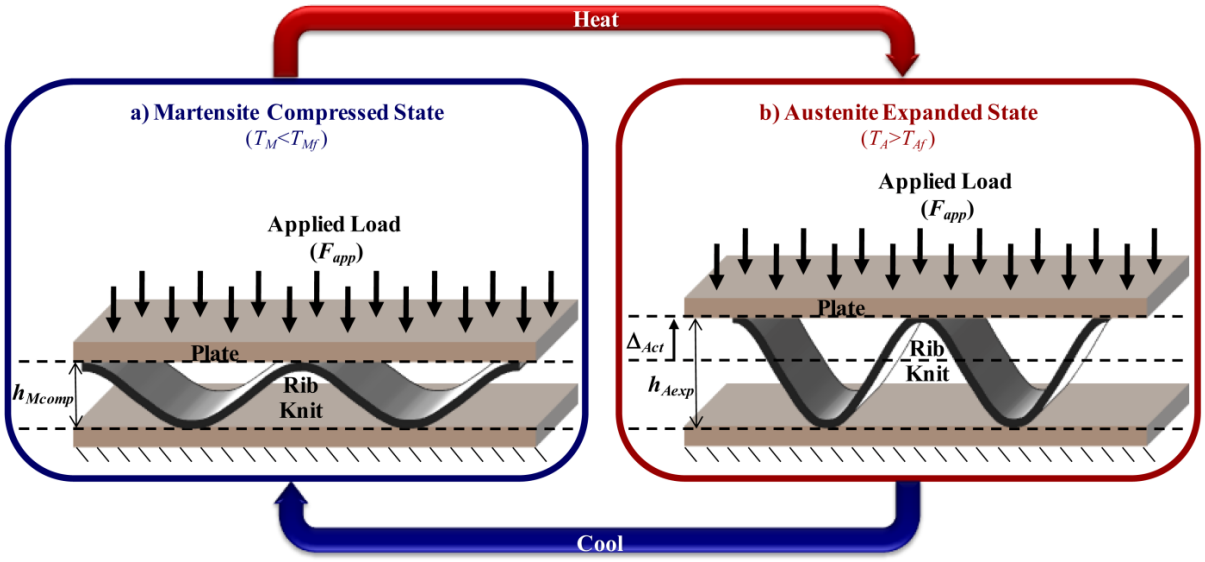

Figure 42. Rib Knit Pattern Operation.
The rib knit pattern distributed actuator cycles between the Martensite Compressed State and the Austenite Expanded State under a constant applied load (F_{app}) via a thermal operational transition between the low temperature Martensite phase (T_M) and the high temperature Austenite phase (T_A).

5.1.2.2. Austenite Expanded State

The second state in the actuation cycle, shown in the rib knit pattern operation figure (Figure 42b), is reached when the textile is heated under the same applied load, F_{app}, to above the Austenite Finish transition temperature (T_{Af}), recovering the plastic deformations experienced in the Martensite state to become stiffer through utilization of the Shape Memory Effect of the foundational SMA wire. The rib knit pattern textile is comprised of bent loops of SMA wire which is trained to a straight shape by the manufacturer. Upon heating, the loops attempt to return to their naturally straight configuration, increasing the width of individual loops while decreasing the loop height. The structural force couples between interacting adjacent courses, described in the previous section, are still present in the actuated structure. The combination of the increased stiffness of the material and the unbalanced force couples cause the legs at the bottom of the loop connecting forward ribs and backward ribs to lift the forward ribs while depressing the backward ribs, raising the prototype to the Austenite Expanded height (h_{Aexp}).

5.1.3. Rib Knit pattern Architectural Configurations

The rib knit pattern architecture is extremely versatile, and numerous combinations of loops can be used to slightly modify the knit pattern architecture. Performance enhancing modifications

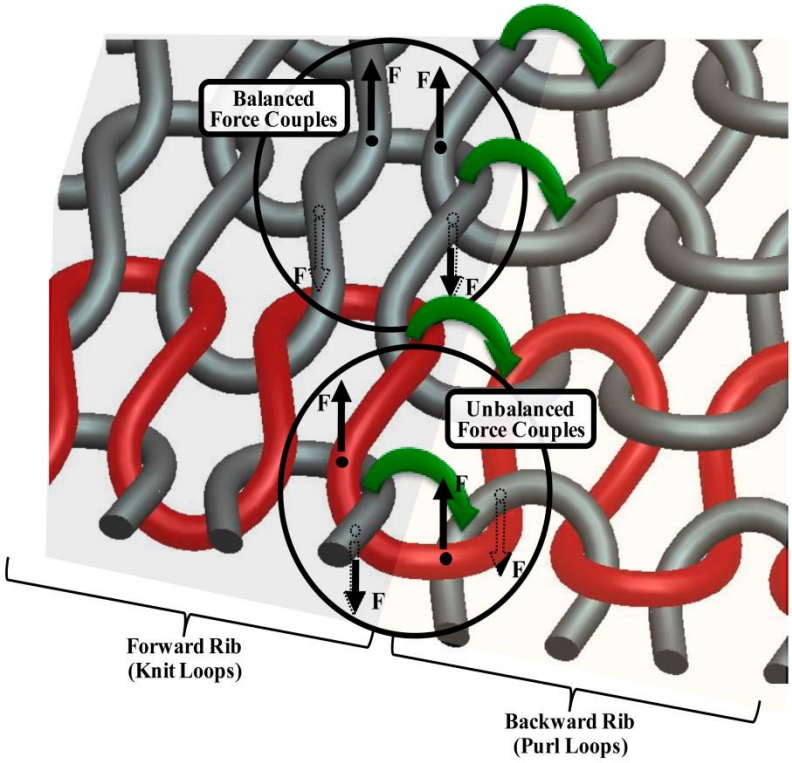

Figure 43. Rib Knit Pattern Actuation Mechanism.
The unique accordion actuation behavior of the rib knit pattern architecture is a result of the unbalanced force couples in each course between forward and backward ribs that lifts columns of forward ribs upward while depressing columns of backward ribs downward.

can be made by creating architectural configurations using multiple individual rib knit pattern textiles such as stacking (series) and nestling (parallel).

5.1.3.1. Stacking

Stacking is an architectural configuration obtained by placing multiple individual rib knit pattern textiles on top of each other, where each textile is separated by a thin, rigid plate (Figure 44a shows two stacked textiles). The individual rib knit pattern textiles work in series, the applied load is transferred through each individual textile while each textile is free to expand or compress in response to a thermal operational transition. The stacked architecture maintains the original height of each individual textile while scaling the total height by the number of stacked textiles in the actuator. The stacked architectural configuration results in a final actuator with the same footprint and a scaled volume compared to an individual actuator that produces scaled displacement under the same applied load.

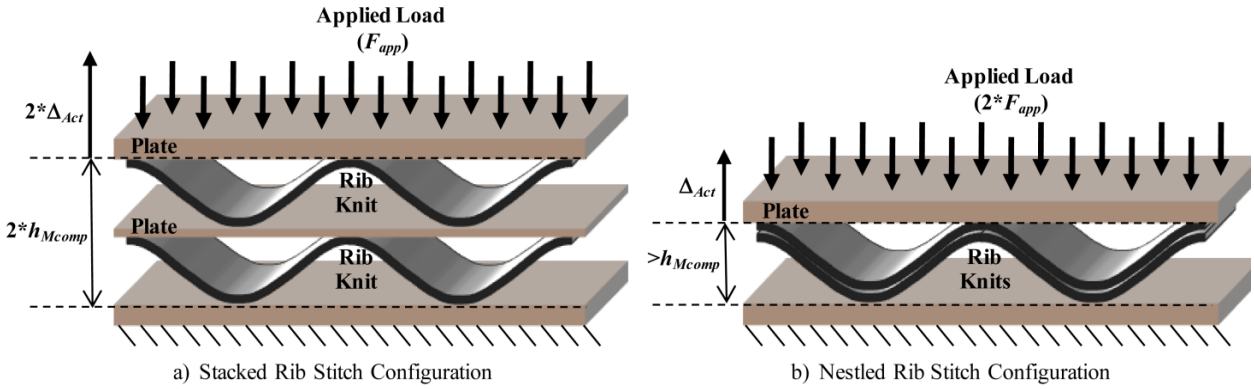

Figure 44. Architectural Configurations.
The stacked rib knit pattern configuration (two identical individual rib knit pattern prototypes separated by a thin rigid plate) provides additive displacement, acting in series. The nestled rib knit pattern configuration (two identical rib knit pattern prototypes placed directly on top of each other while matching the peaks and valleys) provides additive force, acting in parallel.

5.1.3.2. Nestling

The second architectural configuration, nestling, requires the entire top surface of one rib knit pattern textile to contact the bottom surface of another rib knit pattern textile (two nestled textiles are shown in Figure 44b). The textiles are placed on top of each other such that the forward and backward rib columns of each of the textiles are aligned. The nestled rib knit pattern textiles work in parallel, each textile undergoes the same displacement throughout the actuation cycle while supporting twice the load as each individual textile supports the same load. Nestling doubles the thickness of the textile, resulting in an actuator with a slightly larger height while maintaining the footprint of the actuator.

5.2. RIB KNIT PATTERN EXPERIMENTAL EVALUATION

An experimental evaluation was conducted to quantitatively compare the force-displacement performance capability of the rib knit pattern architecture and architectural configurations to the local surface modification specifications for flow control applications. This section develops the force-deflection specifications for the contour bump application, discusses prototype fabrication and experimental testing, and assesses the ability of the rib knit pattern actuator to meet the application specifications.

5.2.1. Contour Bump Specifications

Flow control approaches using local surface shape changes have shown significant theoretical improvements to flight efficiency under specific off-design flight conditions, however, the actuator technology needed to realize flow control approaches does not currently exist. Large transonic

aircraft fly up to a ceiling height (maximum altitude) of 10 to 20 km in the compressible flow regime. Using basic compressible flow equations and published pressure coefficients across the wing, the pressures on aircraft wings can be determined [105]. The average free-stream pressures range from approximately 10 to 16.5 kPa at the ceiling altitudes, e.g. F-22 Raptor at a ceiling altitude of 9.8 km experiences pressures of 10.1 kPa [106]. At these high pressures, surface displacements ranging from 10 to 30 mm acting are needed to act against aerodynamic pressures. To assess the ability for the active rib knit pattern knit to meet this realm of operation, experiments were conducted to characterize the quasi-static force-displacement performance of five forms of the rib knit pattern configurations: individual, stacked, nestled, two sets of stacked-nestled, and three sets of stacked-nestled.

5.2.2. Rib Knit Pattern Prototype Fabrication

Individual rib knit pattern knit prototypes (textiles) were fabricated by hand knitting 20 mil Dynalloy Flexinol® 70°C shape memory alloy wire with 6 mm traditional knitting needles for 14 courses (rows) and 16 wales (columns) using a 2x2 rib knit pattern architecture (Table 7, Figure 45). The first course of the 2x2 rib knit pattern architecture was created by casting on a single knit loop, alternating two purl loops and two knit loops, and ending with a single knit loop. In each subsequent course, knit loops were purled and purl loops were knit to create the final rib knit pattern. The textiles contained 7 complete ribs that occupied 2 wales, and two single wale ribs on either side of the textiles. All ribs extended through all 14 courses. Six individual rib knit pattern textiles were made, each weighed 19.6 g and measured 140.0 mm in width by 72.1 mm in length for a surface area of 0.010 mm^2. Six total prototypes were manufactured and experimentally tested in different architectural configurations. Two prototypes were individually tested to determine their force-deflection and actuation behavior. The same two prototypes were experimentally tested in both the stacked and nestled configurations. An additional two prototypes were incorporated in a new arrangement by stacking two sets of nestled prototypes on top on each other to create a stacked-nestled configuration. The final two prototypes were incorporated in the arrangement to form a three level stacked-nestled configuration.

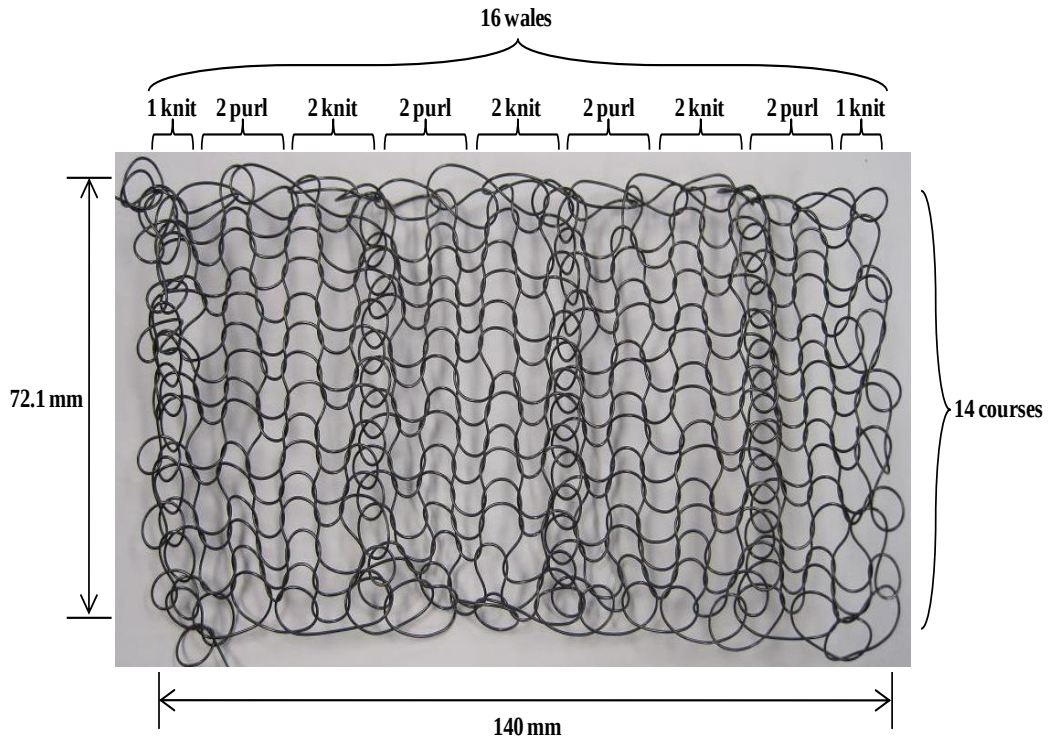

Figure 45. Rib Knit Pattern Prototype.
Rib knit pattern textile knit with 20 mil Flexinol® 70°C wire on 6 mm knitting needles for 14 courses and 16 wales in a 2x2 rib knit pattern.

5.2.3. Experimental Setup and Procedure

To determine the expansive distributed surface actuation performance of the rib knit pattern architecture, the following setup (Figure 46) and procedure (Figure 47) was used to measure the actuation height in response to an applied constant load. Each prototype in its Martensite state was placed on a smooth aluminum base plate and heated until fully actuated in austenite state under no load using a Milwaukee Digital Heat Gun Model 3300 to ensure proper phase transition upon cooling. Another smooth aluminum plate, the slider plate, was placed on top of the rib knit pattern prototype, compressing it slightly. The slider plate moved vertically (parallel to the base plate) on Teflon bushings along an orthogonally aligned parallel precision ground stainless steel guide rail. The prototype was run through thermo-mechanical cycles (Figure 42) in an Envirotronics

Table 7. Rib Knit Pattern Prototype Parameters.
Material (transition temperature), Geometric (wire diameter, needle diameter, number of course and wales) and Architectural (rib pattern) parameters used in rib knit pattern prototypes fabrication and the resulting physical measurements of the knits (width, length, area, and mass).

Wire diameter (mil)	Transition Temperature (°C)	Needle Diameter (mm)	Number Courses	Number Wales	Rib Pattern	Width (mm)	Length (mm)	Area (mm^2)	Mass (g)
20.0	70.0	6.0	14	16	2x2	140.0	72.0	0.010	19.6

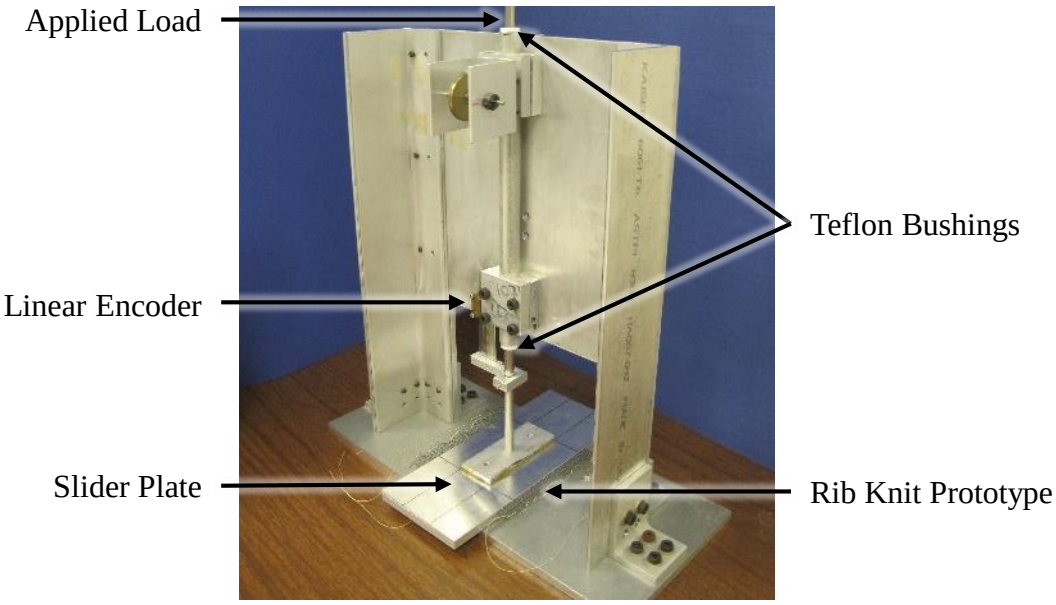

Figure 46. Experimental Setup for Rib Knit Pattern Prototypes.
The rib knit pattern prototype expands from the Martensite Compressed State to the Austenite Expanded State to lift the slider plate against applied loads.

EnviroFLX 300 environmental chamber. The environmental chamber and the prototype were cooled to 10°C and the initial Martensite compressed height was measured using a US Digital linear encoder strip with 500 divisions per inch. A weight was applied to the top of the precision ground stainless steel guide rail, compressing the prototype. The environmental chamber and the prototype were heated to 100°C causing the material to transition into the Austenite phase and the prototype to expand into raised rows of arches (Figure 42b), characteristic of the Austenite Expanded State, with a recorded height, h_{Aexp}. The temperature was reduced to 10°C, the prototype compressed in response to the material transition into the Martensite phase, and the sample returned to the Martensite Compressed State with a height of h_{Mcomp} (Figure 42a) Additional weight was applied to the prototype and the thermo-mechanical testing cycle was repeated to obtain a force-deflection performance curve.

5.2.4. Experimental Results

Each of the rib knit pattern prototypes and the architectural configurations display the same operational states and form (Figure 42). The initially compressed nearly planar prototype expands vertically by creating a series of raised and lowered semi-cylindrical ridges as the temperature increases above the austenite finish temperature. Upon cooling, the prototype compresses, completing the actuation cycle. Every prototype produced very large displacements under

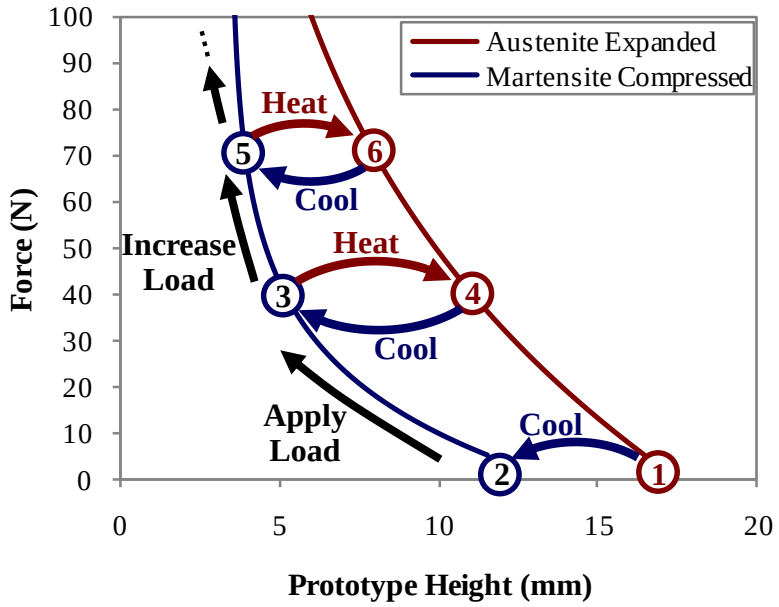

Figure 47. Rib Knit Pattern Experimental Procedure.
Rib knit pattern textiles were experimentally tested in an environmental chamber - a load was applied to the prototype, the environmental chamber was heated to 100°C and the austenite expanded height was recorded, the chamber was then cooled to 10°C wire and the martensite compressed height was recorded. The applied load was increased and the thermo-mechanical testing cycle was repeated to obtain a force-deflection performance curve.

significant applied loads. As the applied load increased the net actuation increased to a maximum then decreased under increased applied loads.

5.2.4.1. Single Rib Knit Pattern Prototypes

Two single rib knit pattern knit prototypes were experimentally tested individually. The first individual prototype was actuated against an applied load of 24.7 N (approximately equivalent to 2.5 kPa calculated as a distributed pressure over the footprint of the prototype in the Martensite Compressed State) to the Austenite Expanded height (h_{Aexp}) of 13.1 mm (red curve in Figure 48a). The material was cooled to the Martensite phase causing the prototype to compress under the applied load to the Martensite Compressed height (h_{Mcomp}) of 6.8 mm (blue curve in Figure 48a). The 6.3 mm net actuation motion of the individual rib knit pattern prototype, Δ_{act}, was calculated as the difference between the actuated height of the Austenite Expanded State and the compressed height of the Martensite Compressed State ($\Delta_{act}=h_{Aexp}- h_{Mcomp}$) and plotted against the constant applied load in Figure 48b. This process was repeated for a range of applied loads, producing an actuation curve (Figure 48b) characteristic of knitted actuators (as described in Chapter 3 and Chapter 4) that provides increasing net actuation under increasing applied loads to a maximum

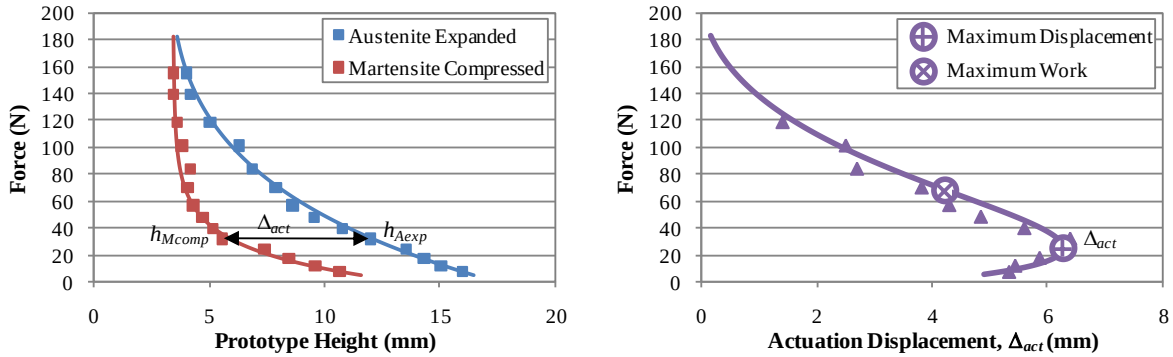

a) Height of a Single Rib Prototype in Martensite and Austenite

b) Actuation Performance of a Single Rib Prototype

Figure 48. Experimental Results of the Single Rib Knit Pattern Prototype.
The performance of a single rib knit pattern prototype (knit with 20 mil Flexinol® 70°C wire on 6 mm knitting needles for 14 courses and 16 wales in a 2x2 rib knit pattern) was experimentally determined for the a) height in each state and b) the actuation performance. The experimental data is fit with double exponential curves to highlight general performance trends including the maximum displacement (marked with a +) and the maximum work (marked with a x).

peak actuator displacement (peak marked with a cross in Figure 48b) then decreased net actuation under further increased applied loads. The initial increase in actuation displacement under increased applied loads is a result of the larger applied loads greatly decreasing the height of the prototype in the Martensite Compressed State, which is recovered upon actuation to the Austenite Expanded State. As larger loads are applied, the height of the prototype in the Martensite Compressed State continues to decrease but the material is no longer able to recover the strain when actuated into the Austenite Expanded State, resulting in smaller net actuation displacement for increased applied loads. This actuation behavior implies that there is an optimal point for designing actuators to provide the maximum deflection possible. The first individual prototype provided a maximum displacement of 6.3 mm under a 2.5 kPa applied load, highlighted with the cross in Figure 48b. Likewise, there is a similar point on the actuation curve at a larger applied load which provides the maximum work, 286.2 Nmm, producing 4.2 mm of displacement under a 6.7 kPa applied load, highlighted with an ⊗ in Figure 48b.

The experimental process was repeated for the second individual rib knit pattern prototype, revealing that the actuation performances of the two individual prototypes (green and purple curves in Figure 49) were kinetically very similar with an average displacement error of 7.7% over the range of applied loads, inferring small inconsistencies in the hand knit prototypes have little influence on the mechanical behavior of the actuator. The second individual rib knit pattern

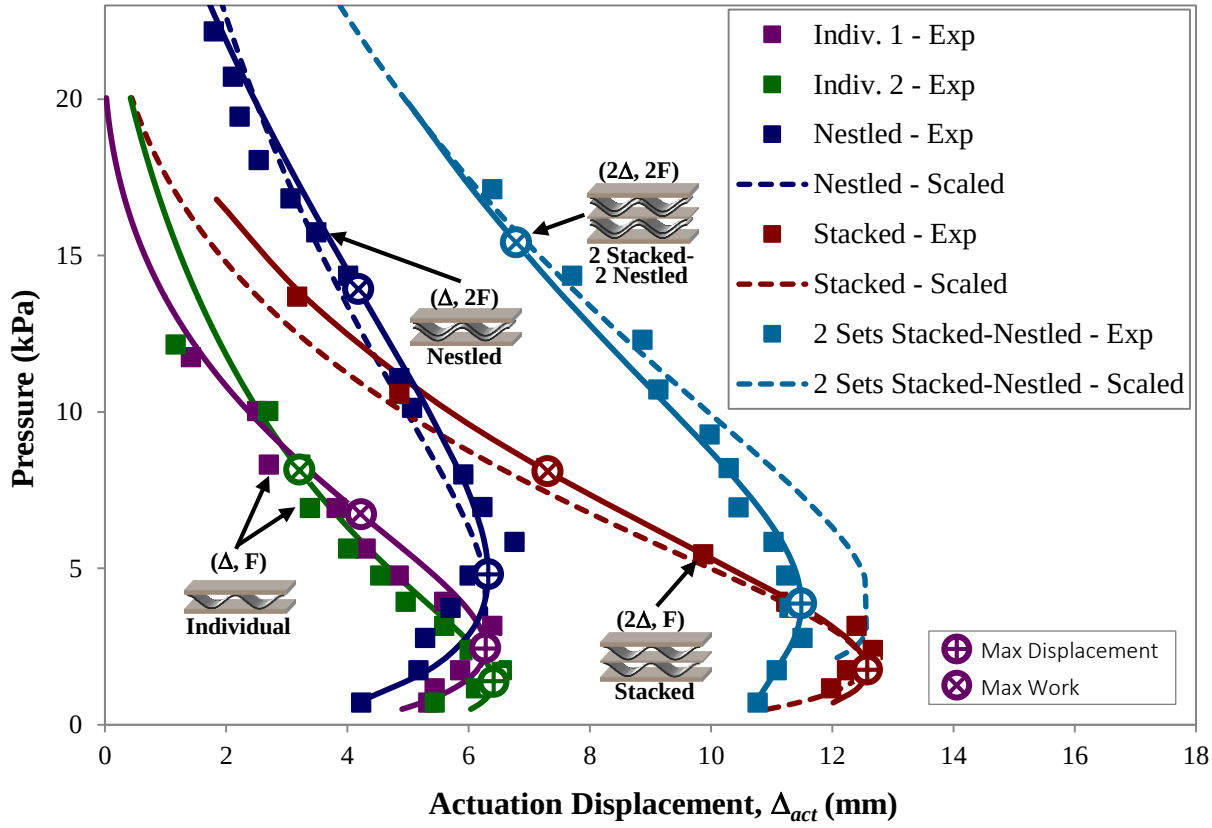

Figure 49. Experimental Results of Rib Knit Pattern Architectural Configurations.
Rib knit pattern prototypes (knit with 20 mil Flexinol® 70°C wire on 6 mm knitting needles for 14 courses and 16 wales in a 2x2 rib knit pattern) were combined by stacking and nestling, resulting in series and parallel combinations with enhanced displacements and forces over individual prototypes.

prototype produced a net actuation displacement of 6.4 mm under an applied load of 13.7 N (Figure 49), which is equivalent to a pressure of 1.4 kPa, calculated as a distributed pressure over the entire footprint of the prototype in the Martensite Compressed State. The maximum work, 263.5 Nmm, occurred under an enhanced pressure, 8.1 kPa, due to the unique load-displacement performance. As the individual samples were knit using identical geometric and architectural parameters, they each weighed 19.6 g and had a surface area of 0.010 m^2, providing very close maximums for specific work (29.2 J/kg and 26.9 J/kg) and work density (7.1 kJ/m^3 and 5.9 kJ/m^3) at the same applied load as the maximum work performance point. The individual prototypes produce displacements and pressures in the same order of magnitude as required for flow control applications and can be used as a building block to produce the required displacements under aerodynamic loads.

5.2.4.2. Stacked Rib Knit Pattern Prototype

Stacking of two individual rib knit pattern textiles was investigated to increase the actuation displacement of the rib knit pattern actuator. The two individual rib knit pattern portions were separated by a thin rigid aluminum plate and work in series. The applied load was transferred through each individual textile while each textile was free to expand and/or compress against the applied load. The experimental behavior of the stacked prototype (shown with red squares with a solid red line in Figure 49) closely matches the predicted behavior obtained by adding the displacements of the individual prototypes for an applied load (shown with red dashed line in Figure 49) with an average displacement error of 5.5% over the range of applied loads. This confirms the additive displacement series behavior of the stacked architectural configuration. The experiments verified this behavior with twice the maximum actuation displacement (12.6 mm for stacked compared to 12.5 mm for the additive displacements of the individuals) under the same applied load (stacked actuated under 17.7 N or 1.8 kPa while the predicted applied load under max displacement was 19.2 N or 1.9 kPa). The maximum work was also increased by stacking the individual textiles: more than twice the maximum work (595.9 Nmm) was produced compared to a single rib knit pattern knit architecture (286.2 Nmm and 263.5 Nmm) as the displacement corresponding to the maximum work was increased from 4.2 mm and 3.2 mm of the individual prototypes to 7.3 mm for the stacked actuator. The enhanced maximum work corresponds to similar maximum specific work (30.4 J/kg for stacked compared to 29.2 J/kg and 26.9 J/kg for individuals) and work density (7.7 kJ/m^3 for stacked compared to 7.1 kJ/m^3 and 5.9 kJ/m^3 for individuals) as both the mass and volume of the prototype doubled while producing twice the actuation displacements. The stacked architectural configuration doubles the actuation displacement, resulting in useable displacements to adequately change the shape of the wing to improve flow control.

5.2.4.3. Nestled Rib Knit Pattern Prototype

Two rib knit pattern textiles were nestled, placed directly on top of each other matching the peaks and valleys of the forward and backward ribs, to actuate against larger loads compared to individual prototypes. The nestled prototype acts as two individual textiles in parallel, for the same actuation displacement each individual rib knit pattern knit textile carries the same load as the individual experimental tests. The parallel additive force behavior of the nestled architecture is confirmed by the experimental behavior of the nestled prototype (shown with blue squares in

Figure 49) matching the added forces of two individual textiles under the same displacement (shown with the dashed blue line in Figure 49) with an average displacement error of 5.0%. The nestled architectural configuration more than doubles the load (48.4 N or 4.8 kPa for the nestled configuration compared to 24.7 N or 2.5 kPa and 13.7 N or 1.4 kPa for individuals) under which the prototype provides the same max displacement (6.3 mm for nestled compared to 6.3 mm and 6.4 mm for the individual prototypes). The enhanced stiffness of the nestled actuator provides twice the work (586.7 Nmm) as the single rib knit pattern knit actuators (286.2 Nmm and 263.5 Nmm) at double the aerodynamic load (13.9 kPa for the nestled compared to 6.7 kPa and 8.1 kPa for the individuals) while providing the nearly the same actuation displacement (4.2 mm for nestled compared to 4.2 mm and 3.2 mm for individuals). The nestled architecture provides essentially the same maximum specific work (29.6 J/kg compared to 29.24 J/kg and 26.9 4 J/kg for individuals) because the force and total mass have doubled. The nestled architectural combination doubles the work density (13.0 kJ/m^3 compared to 7.1 kJ/m^3 and 5.9 kJ/m^3 for individuals) since twice the work was done in nearly the same package size. Nestling two individual samples increases the pressure at which the actuator can do usable work, actuating against aerodynamic level loads.

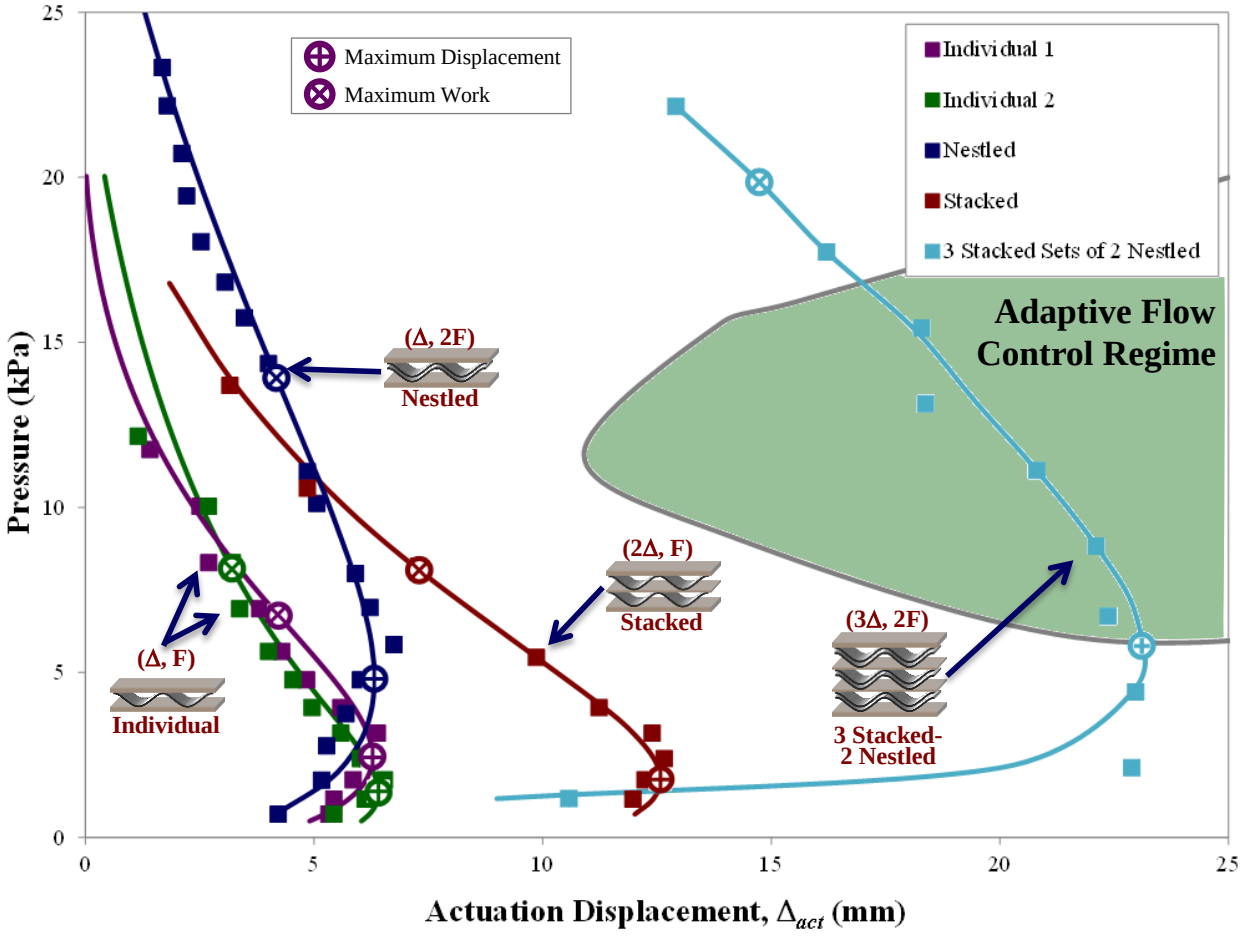

Figure 50. Experimental Results of Rib Knit Pattern Actuators for Flow Control Application.
Three stacked sets of nestled prototypes meet the simultaneous force and displacement application specification region for flow control applications.

5.2.4.4. Stacked-Nestled Rib Knit Pattern Prototypes

These experiments confirm that stacking increases displacement additively and nestling increases force additively, with both in the realm of necessary to realize flow control applications. By combining the two types of rib knit pattern knit architectural configurations (stacking and nestling), the specifications for the displacement and loading for flow control can be reached. Four individual rib knit pattern knit textiles were arranged by stacking two sets of two nestled textiles on top of one another. The stacked-nestled prototype produces increased displacements under increased loading (shown with teal circles in Figure 49) that corresponds to an average displacement error of 5.8% compared to the theoretical performance obtained by doubling the actuation displacement of the theoretical nestled behavior of the two individual rib knit pattern knit textiles (shown with a dashed teal line in Figure 49). The stacked-nested architectural configuration produces a maximum of 11.5 mm of displacement under a 39.0 N or 3.9 kPa, nearly

doubling the displacement of the individuals (6.4 mm and 6.3 mm) under the additive loading at max displacement for the individual textiles (13.7 N or 1.4 kPa and 24.7 N or 2.5 kPa), meeting the displacement criteria for flow control applications. At the optimal operating point, the maximum work production point, the stacked-nestled rib knit pattern knit actuator produces 6.8 mm of displacement under a pressure of 15.4 kPa, realizing the load (10 to 16.5 kPa) and approaching the deflection (10 to 30 mms) requirements for distributed flow control devices. While both of these maximum performance points are just outside the application specification region, a large portion of the predicted pressure displacement curve between the max displacement and max work point meet the application specifications.

By stacking a third nestled prototype on top of the current stacked-nestled configuration it is possible to reach the specified load and displacement simultaneously. It was predicted that three stacked two nestled prototypes would produce 18.8 mm of actuation motion under a 3.1 kPa applied load at the maximum displacement point and 11.1 mm of actuation motion under a 14.5 kPa applied load at the maximum work point. The experimental results (Figure 50) of three sets of stacked and nestled prototypes exceeded the prediction, producing 23.0 mm displacement under a 4.4 kPa applied load at the maximum displacement point and 14.7 mm of displacement under a 19.85 kPa applied load. While neither the maximum displacement nor the maximum work occur in the adaptive flow control regime, the three sets of stacked nestled prototypes are able to exceed the necessary displacements between 6 kPa and 16 kPa. The three sets of stacked-nestled prototypes simultaneously meets the force-deflection application specifications needed to provide local surface modification in some flow control applications.

Table 8. Rib Knit Pattern Experimental Results.
Experimental results of Individual, Stacked, Nestled, and Stacked-Nestled Rib Knit Pattern Prototypes comparing performance at maximum displacement and maximum work operating points.

Prototype	Max Disp (mm)	Strain @ Max Disp (%)	Force @ Max Disp (N)	Pressure @ Max Disp (kPa)	Max Work (Nmm)	Pressure @ Max Work (kPa)	h_{Mcomp} @ Max Work (mm)	Disp @ Max Work (mm)	Max Specific Work (J/kg)	MaxWork Density (kJ/m^3)
1	6.3	91.7	24.7	2.5	286.2	6.7	4.0	4.2	29.2	7.1
2	6.4	80.7	13.7	1.4	263.5	8.1	4.4	3.2	26.9	5.9
Stacked	12.6	86.5	17.7	1.8	595.9	8.1	7.7	7.3	30.4	7.7
Nestled	6.3	61.5	48.4	4.8	586.7	13.9	5.1	4.2	29.9	11.4
2 Sets Stacked & Nestled	11.5	64.5	39.0	3.9	1053.9	15.4	11.1	6.8	36.2	9.4
3 Sets Stacked & Nestled	23.0	75.1	44.4	4.4	2949.8	19.85	14.7	14.7	75.3	19.9

5.3. FEASIBILITY DEMONSTRATION STUDY CONCLUSIONS

This chapter investigated the potential of active knits to produce the simultaneous forces and displacements for an application requiring distributed surface actuation: a contour bump for flow control. Contour bumps have the potential to enhance flight efficiency by delaying separation of or by reattaching the boundary layer; however, no actuators currently exist to provide the desired actuation motion during flight. The goal of this chapter is to demonstrate the feasibility of active knits by identifying a potential application, defining the technical specifications for the application, choosing a knit architecture to meet the kinematic motion needs of the application, and experimentally testing active knit prototypes to meet the kinetic force-displacement technical specifications.

The specific application, a contour bump for flow control over an airfoil, was chosen and the technical specifications (displacements on the order of 10-25 mm under aerodynamic level loads of 10-16 kPa) of the application were determined by analyzing existing literature on the theoretical study of transonic contour bumps. The rib knit pattern was chosen for the flow control feasibility demonstration study because it produces large surface displacements under significant applied loads by transforming from a nearly planar surface to a series of raised and lowered ridges. The rib knit pattern actuator could be used as an embedded surface actuator that is placed beneath the skin of the wing and the actuation displacement can be used to create local shape modification by contouring the surface of the wing.

Individual, stacked, nestled, two sets of stacked-nestled, and three sets of stacked-nestled rib knit pattern prototypes were experimentally tested to determine their actuation performance capabilities compared to flow control specifications. Six individual rib knit pattern prototypes were created using a 2x2 rib knit pattern with 20 mil 70°C Flexinol® wire on 6.0 mm knitting needles for 14 loops and 16 rows. The six prototypes were experimentally tested, individually and in configurations, to obtain the actuation displacement in response to an applied constant load. Each of the individual prototypes and configurations displayed the same behavior as displayed by garter knit pattern active knit actuators discussed in Chapter 3, as the applied load was increased the actuation displacement increased up to a maximum actuator displacement then further increased applied loads resulted in decreased actuation displacements. The individual prototypes provided nearly identical performance (average displacement error of 7.7%), producing maximum actuation displacements of 6.3 and 6.4 mm against loads of 2.5 and 1.4 kPa. The individual textiles were stacked on top of each other, creating the stacked prototype, and acted in series to double the actuation displacement to 12.6 mm under an applied pressure of 1.8 kPa. An additional architectural configuration, nestling, enhanced the operational pressure by allowing the textiles to work in parallel, producing 6.3 mm deflection under 4.8 kPa. A stacked-nestled prototype was shown to simultaneously improve the pressure (from 1.8 kPa to 3.9 kPa) and deflection (from 6.3 mm to 11.5 mm) over each the stacked and the nestled configurations. The displacement was further increased through a configuration of three sets of stacked-nestled prototype. The enhanced configuration produced an enhanced maximum deflection of 23.0 mm under a similar pressure (4.4 kPa compared to 3.9 kPa) over the stacked-nestled configuration. By leveraging the individual prototype performance through series and parallel combinations, an actuator was created that simultaneously meet the displacement and loading requirements for some flow control applications.

This feasibility demonstration study was designed to determine if the rib knit actuation architecture has the actuation authority to meet the force-deflection specifications for the contour bump application. Many research issues would need to be addressed before the active knit architecture could be implemented in a device. For example, during this experimental study the prototypes were actuated in an environmental chamber. Most applications, including the contour bump application, would require actuation control in the form of embedded heaters or resistive heating. Regardless of the method of actuation, thermal actuation would require significant power

consumption that would be difficult to satisfy in applications. Additionally, attachment of the actuator within a device would need to be explored and the resulting multi-axis loading and constraint conditions of the device and application would need to be characterized. These are just a few of the implementation issues that would need to be addressed to realize the contour bump and other complex applications.

This feasibility demonstration study has shown that rib knit pattern active knits can meet the force-deflection performance specifications required for flow control of an aircraft. The rib knit pattern, which expands out-of-plane, provides a new actuation motion that is unattainable with current technologies. The out-of-plane expansion produces very large actuation motions on the order of 100%, under large, application level loads. Additionally, an amplification scheme that improves kinetic performance was identified. The stacked and nestled architectural configurations enhanced the performance of the rib knit pattern through series and parallel connections of prototypes. Beyond the immediate results, this case study investigates an effective way to use the unique motions created by active knits and demonstrates the ability to create large actuation motions under application level loads. The series and parallel connections approach can be used to improve the kinetic performance of all knit architectures by identifying the manner in which the load is transferred and the motion is created. The approach of identifying an application that could be improved, identifying the motion required to achieve the application, choosing an active knitted architecture to produce the desired motion, and using amplification techniques such as series and parallel connections to meet the application specifications could be implemented for other applications. This case study has demonstrated the potential of the rib knit pattern to meet the technical specifications for this flow control application and shows that active knits are a promising technology to meet the kinetic and kinematic requirements of modern applications by producing simultaneous radical forces and displacements in the form of complex distributed motions in a small package.

Chapter 6. CONCLUSIONS

The active knitted actuation architecture provides unprecedented actuation performance that is unattainable with other means of actuation. The architecture has limitless potential to realize a variety of applications that require advanced actuation capabilities. The goal of this research was to develop the fundamental scientific understanding of the active knit actuation architecture to enable the design, analysis, and synthesis of simultaneous large force and strain actuators that produce complex three-dimensionally distributed actuation motions in a compact package. Four research objectives were crucial to meeting this goal.

1. **Hierarchical Knit Architecture Classification.** Established a formal language and a hierarchical classification structure that identified the actuation mechanism and linked the kinematic actuation motion to the hierarchical level, enabling exploration of the full breadth of possible actuator motions and providing a foundation for the modeling effort, an understanding for design, and insight into feasibility for applications.
2. **Fundamental Knitted Loop Modeling.** Developed predictive capabilities for the fundamental knitted loops (knit and purl) that capture the kinematic and kinetic performance of the knitted loop and two-dimensional knit patterns by accounting for the dual state nature of active knits and friction between interlacing adjacent loops, providing a tractable tool for prediction, design, and tailoring of planar contractile active knits.
3. **Three-Dimensional Knit Architecture Modeling.** Developed, demonstrated, and experimentally validated a new modeling approach, the segment superposition modeling approach, which isolates individual deformation modes to capture out-of-plane motions and predict kinematic and kinetic performance of complex three-dimensional active knits.
4. **Feasibility Demonstration.** Evaluated the applicability of active knits and their supporting models through a design case study that investigated the ability of active knits to create the desired kinematic actuation motions under application-level kinematic loads while addressing application implementation issues.

It was necessary to address all these objectives to set the foundation for design, analysis, and synthesis of the active knit actuation architecture and realize active knits as an enabler to numerous applications that require distributed complex three-dimensional actuation motions. This chapter reviews the outcomes and contribution of this research.

6.1. RESEARCH OVERVIEW

Diverse applications from morphing aircraft, active flow control, deployable space structures, implantable medical devices, and advanced automotive applications require enhanced actuation capabilities. Of particular interest are actuators that are capable of simultaneous large forces and strains that produce complex, three-dimensionally distributed actuation motions. In Chapter 1, a review of the current state-of-the-art revealed that conventional actuators, which are robust and have significant actuation authority, have difficulty producing complex shape change. Smart materials are a promising technological solution because, as a material based actuator, they are inherently distributed. However, they have difficulty generating complex motions with simultaneous large forces and displacements. To address this difficulty, numerous actuation architectures have been investigated. While architectural approaches have made great advances beyond the base material, no architectures have been successful in meeting the need of simultaneous radical forces and strains in the form of complex distributed actuation motions. This research established a hierarchical actuation architecture, the active knit architecture, which leverages the foundational smart material wire to produce complex, three-dimensionally distributed actuation motions capable of simultaneous large forces and strains. To fulfil the goals of this research and establish the science base for active knit actuation architectures the research objectives were addressed through four primary tasks: establishing an Active Knit Hierarchy, deriving an analytical model of the planar knitted loop and garter knit pattern architecture, developing a modeling approach to predict three-dimensional actuation performance, and conducting a feasibility design study related to an Air Force flow control application.

6.1.1. Active Knit Hierarchy

This dissertation developed the active knit actuation architecture as a new actuation approach that has the potential to enable myriad applications. During the broad exploration of the active knit architecture several research issues emerged. To create actuators capable of complex three-dimensional actuation motions, the conceptual foundation for a new genre of smart material

actuators that leverage a hierarchical architecture was developed. To describe the actuation motion in relation to the actuator architecture, a hierarchical classification scheme was established. To understand the breadth of potential actuation motions, a catalog of architectures and their resulting motions was created. To facilitate discussion of the architectural influence on actuation performance, a language that blends traditional textile terminology with engineering concepts and smart material fundamentals was defined. Additionally, a systematic method of identifying the actuation mechanism was necessary to provide a starting point for predictive capabilities.

To address the range of research issues related to the active knit actuator architecture, an active knit hierarchy was developed. The active knit hierarchy leveraged the hierarchical approach of traditional and engineering textiles to develop a more sophisticated classification scheme that accounts for 1) multiple types of unit cells, 2) homogeneous distribution of unit cells across the knitting grid, 3) heterogeneous distribution of unit cells across the knitting grid of the textile, and 4) non-planar orthogonal knitting grids. The active knit hierarchy includes four levels that demonstrate the advancing complexity of actuation motions at higher levels of the hierarchy through experimental examples. The first level of the hierarchical architecture, knitted loops, acts as the unit cell of the knitting grid and produces large strains as the bent loops leverage the strain of the foundational wire. The second level of the hierarchy, knit patterns, forms homogeneous patterns of adjacent knit and purl loops across the knitting grid that interact to provide three-dimensional actuation motions such as rolling, contraction, accordion, and arching. The third level, grid patterns, combines multiple knit patterns to form heterogeneous patterns across the knitting grid which affords complex and controlled three dimensional actuation motions across different areas of the textile such as arching in one area and accordioning in another. The fourth level, restructured grids, restructures the knitting grid by forming both uniquely shaped and three dimensionally structured textiles that leverage the behavior of knit patterns and grid patterns to provide new three-dimensional actuation motions distributed across a surface and throughout a structure such as deployable tubes, contractile belts, coiling tubes, triangular actuators, and twisting surfaces. Chapter 2: Active Knit Hierarchical Architecture developed the conceptual foundation for hierarchical architecture, established a hierarchical classification scheme, created a catalog of architectures and motions, defined a language, and provided a starting point for identifying the unit cell, delivering insight in the understanding, modeling, and design of this new actuation paradigm to meet growing actuation needs.

6.1.2. Two-Dimensional Analytical Knitted Loop Model

To provide a foundation for design, analysis, and synthesis of planar active knit actuators, a model was derived that relates the geometric parameters, dual state nature of the foundational wire, large rotations of the wire in the formed knitted loop, and friction between interlacing adjacent loops to the force-deflection performance of the actuator. To accurately account for the thermal and mechanical operational transitions that influence the load path and the interlacing loop friction that match the experimental conditions, the states of a planar knit actuator operation were defined. A typical actuation cycle for planar active knits begins in the unloaded *Austenite Free State*, transitions to the *Austenite Extended State* under an applied external load, then cycles between the cold *Martensite Extended State* and the hot *Austenite Contracted State* for constant load actuation. To simplify the modeling process, the first level of the active knit hierarchy – the knitted loop – was modeled. By investigating geometric and loading symmetry within the knitted loop, it was determined that the smallest repetitive element, or the unit cell, was a quarter of the knit loop, which greatly simplified the modeling process. Geometric constraints were developed and force equilibrium analysis of the unit cell were completed while assuming different friction conditions (stick or slip) during the operational transition depending on the loading and the initial state of the textile. Elastica Theory and Euler Bernoulli beam bending were used, in addition to the knit geometry and the force equilibrium, to develop governing differential equations that were solved to determine the deflection from the *Austenite Free State* of the textile and thus the relative displacement between the *Martensite Extended* and *Austenite Contracted States* for constant load actuation. A set of fully analytical transcendental algebraic equations (as opposed to a set of coupled differential equations) describe the deflections experienced within a unit cell for each operational state. To relate the performance of an individual element to performance of an entire textile, the load-extension performance of the unit cell was scaled in series and parallel.

To demonstrate the model's ability to predict the force-displacement performance, an experimental validation was performed in which the load-deflection and actuation performance of a knitted prototype was compared to theory for the same geometry and loading conditions. A garter knit pattern prototype was fabricated from 70°C Dynalloy Flexinol® wire with a diameter of 8 mil using 5.5 mm knitting needles for 10 loops and 15 rows. The prototype was cycled through the defined sequence of operational states under a range of increasing applied loads from 0 to 12 N. The experimental results correlated well with the theoretical results, resulting in just 4.1% to 6.1%

average relative displacement error for each extended state, 2.8% average relative displacement error for the contracted state, and 2.0 mm absolute displacement error for the actuation performance. The model demonstrated the ability to predict predicts the qualitative and quantitative performance of planar contractile garter knit pattern active knits, providing an excellent match to the experimental results particularly considering the modeling assumptions: dual stiffness, linear-elastic material with prescribed friction states.

To investigate the capability of the garter knit pattern to produce unprecedented strains, the unique actuator performance was analyzed. Contractile garter knit pattern actuators demonstrate a unique actuation curve, where, at low loads, increased applied loads result in increased net displacement to a maximum displacement peak. As the load is further increased the net displacement is decreased. The highly leveraged garter knit pattern architecture generates large strains (51%) at moderate forces (1.22 N) and usable strains (4.1%) at enhanced forces (12 N) over the material alone (4% strain at 5.8 N). The garter knit pattern actuator provides large strain distributed planar contractile actuation motions, which are beyond what is possible with conventional and smart material actuators. The unique actuation also provides the opportunity for tailoring geometric parameters such as loop size, wire diameter, and the number of courses and wales within the textile to optimally match the specific needs of a particular application. The development of the active planar loop and garter knit pattern model provides the ability to predict actuation motions for the large stroke, large force garter knit pattern actuation architecture, enabling the design of planar contractile active knitted architectures for a wide range of applications and providing the foundation for models of more complex knitted architectures that produce three-dimensional actuation motions.

6.1.3. Three-Dimensional Analytical Reduced Order Knit Pattern Model

To develop a modeling approach to produce modular, tractable, and scalable models of complex three-dimensional active knit architectures to provide insight early in the design process, a segment superposition modeling approach was developed. The modeling approach reduces the complexity of modeling complex knit structures by establishing a clear procedure and representing the architecture with a system of simple mechanical models. The segment superposition modeling approach establishes a framework to predict the kinetic performance using a five step process. The first step is to identify the unit cell by analyzing symmetry in the architecture. The second step is

to segment the unit cell by replacing the curvilinear geometry with a system of linear segments. The third step is to enumerate the individual simple effects models for different possible deformation modes such as tension, extension, torsion, bending, and buckling. The fourth step is to predict the force-deflection performance in response to a single deformation mode using simple mechanical equations. The fifth step is to superimpose the force-deflection or the various individual models to predict the performance of the actuator.

To demonstrate the segment superposition modeling approach, the approach was followed to develop a segmented model of the 2x2 rib knit actuator architecture. The first four steps of the segment superposition modeling approach were followed to develop the segment model of the 2x2 rib knit actuator architecture. The unit cell was identified as a single knit loop by analyzing symmetry of the knit architecture. The loop was segmented into five straight segments by matching the geometric properties of the curvilinear loop onto the segment loop. Several deformation modes were mapped to the segmented unit cell. The primary deformation mode was identified a torsion of the sides of the knitted loops, therefore a simple torsion model was developed to predict the force-displacement performance of the austenite expanded and martensite compressed states. While this work focused on developing a single simple effects model because the 2x2 rib knit actuator is dominated by a single physical effect, the process established by the segment superposition modeling approach efficiently guided the development of the segmented model of the 2x2 rib knit actuator architecture.

To validate the segment model of the 2x2 rib knit actuator architecture, an experimental validation was performed. A 2x2 rib knit architecture prototype was machine knit using 10 mil diameter Dynalloy Flexinol® SMA wire with a transition temperature of 90°C. The 2x2 rib knit architecture was used for the entire prototype, which consisted of 16 wales and 24 courses. The prototype was experimentally tested in an environmental chamber using a custom designed experimental setup, cycling from 10°C to 120°C under a series of increasing applied loads to obtain the force-deflection performance of each state and the constant load actuation performance. Geometric parameters were measured from the prototype and the SMA material was assumed to be a dual state material with flexible shear modulus of 6.0 GPa in the martensite state and a stiffer shear modulus of 17.2 GPa in the austenite state. To assess the predictive capability of the model, the model and experimental results were analyzed. The model accurately predicted the martensite compressed height by an average height error of 3.4% for Region 1 and 9.4% for Region 2 and the

austenite expanded height by an average height error of 10.0% for Region 1 and 7.5% for Region 2 for the range of applied loads tested. The theoretical actuation performance was found to match the form and magnitude of the experimental actuation curve with and average absolute displacement error of 0.44 mm, which corresponds to an average displacement error of 14.7%. The segment model of the 2x2 rib knit actuation architecture accurately predicts the qualitative and quantitative performance of the accordion-like actuation behavior of 2x2 rib knit actuators.

6.1.4. Feasibility Design Study

To demonstrate feasibility of active knits meeting the simultaneous force and displacement specifications for applications, an Air Force case study was conducted. The Air Force case study focused on meeting the actuation needs for a contour bump application that has the potential to enhance flight efficiency by delaying separation of or by reattaching the boundary layer during flight. To determine the application specifications for the contour bump case study, the theoretical results on the drag reduction in response to an active bump were combined with geometric and flight information from aircraft that fly in the transonic regime to determine the pressure-deflection actuation requirements. The specifications require displacements on the order of 10-25 mm under aerodynamic level loads of 10-16 kPa. The feasibility design study was conducted using rib knit pattern active knits, which actuate normal to the surface, producing span-wise discrete periodic arrays that have the potential to withstand aerodynamic forces while supplying the necessary displacement for flow control.

To investigate the ability of rib knit actuators to meet the application specifications, rib knit actuators were experimentally tested over a range of applied loads. Six individual rib knit pattern prototypes were created using a 2x2 rib knit pattern with 20 mil diameter 70°C Dynalloy Flexinol® wire on 6.0 mm knitting needles for 14 loops and 16 rows. Each of the individual prototypes displayed the same actuation behavior as the planar contractile active knits in Chapter 3 and the rib knit active knits in Chapter 4, as the applied load was increased the actuation displacement increased up to a maximum actuator displacement then further increased applied loads resulted in decreased actuation displacements. The individual prototypes provided nearly identical performance (average displacement error of 7.7%), producing maximum actuation displacements of 6.3 and 6.4 mm against loads of 2.5 and 1.4 kPa. To meet the enhanced the kinetic actuation specifications required by the contour bump application, architectural configurations were

developed to leverage systems of prototypes in series and parallel. Stacking two individual textiles on top of each other created a stacked prototype that acted in series to double the actuation displacement 12.6 mm under an applied pressure of 1.8 kPa. Nestling two actuators by matching the peaks and valleys of the rib architecture, enhanced the operational pressure by allowing the prototypes to work in parallel, 6.3 mm deflection under 4.8 kPa. A system of three sets of nestled prototypes stacked on top of each other was shown to simultaneously improve the pressure (from 1.8 kPa to 6.7 kPa) and deflection (from 6.3 mm to 23.0 mm) over each the stacked and the nestled configurations. The feasibility demonstration study showed that rib knit actuators can meet the actuation needs for the flow control application, although numerous research issues would need to be addressed before a flow control device could be created. The case study demonstrated the potential of the rib knit pattern to meet the technical specifications for this flow control application and shows that active knits are a promising technology to meet the kinetic and kinematic requirements of modern applications by producing simultaneous radical forces and displacements in the form of complex distributed motions in a small package.

6.2. CONTRIBUTIONS

Active knits are a new hierarchical architectural paradigm with the potential to revolutionize actuators by producing simultaneous radical forces and displacements, in the form of complex three-dimensional actuation motions distributed throughout a structure, all in a small package size. The ability to create complex shape change will enable applications across diverse fields including aerospace, biomedical, and consumer devices. While a significant amount of research has been conducted on smart materials based actuation architectures, existing architectures lack the sophistication to produce truly complex actuation motions. The active knitted actuation architecture has been identified as a promising approach to creating shape change, however, several research issues had to be addressed before the active knit architecture can be implemented in devices. This research establishes the scientific basis for active knitted actuators.

Active knit actuation architectures produce unprecedented actuation through a hierarchically arranged structure. A hierarchical classification scheme was established to explore the breadth of actuation motions and a language was developed to describe the knitted architectures and their corresponding kinematic actuation behaviors. The classification scheme produced a catalog of different active knit motions and provides an understanding of the relationship between

hierarchical level and kinematic actuation behavior. Insight from the hierarchy aids in the identification of the actuation mechanism and provides a starting point for the derivation of models that predict kinematic and kinetic performance.

Predictive capabilities are provided by analytical models of two- and three-dimensional active knit architectures. Two different modeling approaches – a high fidelity model of two-dimensional active knits and a low fidelity model of three-dimensional active knits for design – address the need for predictive capabilities with different levels of accuracy. The two-dimensional analytical model considers the large rotation bending of the wire and incorporates the dual state nature of the active material and the friction between interlacing loops to accurately predict the cyclic actuation performance of planar actuating active knits. The segment superposition modeling approach provides a modular, tractable, and scalable modeling approach to predict complex, out-of-plane actuation motions to provide insight early in the design process. A modeling procedure is outlined for each approach. Regardless of the fidelity of the model, the initial modeling steps include identifying the smallest repetitive element, establishing geometric relationships, and developing force equilibrium interactions. The models predict the unique performance of the various active knit architectures while highlighting important design points including maximum displacement, strain, and work. The modeling approaches set the foundation for design of actuators and enable performance tailoring to meet application specifications.

The feasibility demonstration study shows effective ways to use the unique actuation motions of active knits to enable applications. The procedure used in the feasibility demonstration study – identifying potential application, defining technical specifications, choosing active knit architecture to produce desired kinematic motion, and experimentally testing for quasi-static kinetic performance – can be followed to realize other applications. Additionally, the feasibility demonstration study shows that even more architectural configurations can be developed to further leverage the hierarchical nature of the active knit architecture. The active knit architecture can be used as a building block architecture to leverage performance in series and parallel combinations to meet application specifications. The feasibility demonstration study shows that this new actuation architecture can be used as an enabling technology to realize a variety of applications.

The contribution of this research will extend beyond active knitted actuators. The expanded knit hierarchy can be used to design complex architectures for traditional and engineering textile

applications and the models can be used to enhance predictive capabilities. The improved handling of friction in the two-dimensional model could be used to predict hysteretic friction behavior, a capability not currently available. Additionally, the modeling approach could be expanded to work with other active/passive material combinations and activation stimuli that may provide different performance characteristics (force, speed, frequency). This foundational research on active knits provides the foundation for further development and use in structural applications.

This research provides the fundamental knowledge needed to develop active knits to meet the demand for advanced actuators. The radical forces and strains and complex, distributed, three-dimensional behaviors of these architectures go well beyond anything currently accessible through traditional actuation or conventional smart material actuation architectures. This novel technology will enable advancements in current applications (shape morphing, flow control, deployable structures, safety mechanisms, medical devices, etc.), as well as open the door to applications yet imagined.

6.3. CLOSING

Research on active knits began in order to investigate the ability of the architecture to create simultaneous large force and strain actuators that produce complex, three dimensionally distributed actuation motions across a surface and throughout a structure. Smart materials have long held to promise of expanding actuation authority, and countless actuation architectures have been explored to leverage the underlying behavior of the foundational smart material. However, existing smart materials actuator architectures frequently fell short of the radical shape change needed to realize new applications. This work on active knits establishes a new hierarchical architectural paradigm that leverages the foundational smart material fiber through hierarchically organized unit cells. The research on active knits was approached a technological solution to providing enhanced kinematic and kinetic actuation capabilities that are unattainable with current actuation technologies.

The goal of this dissertation was to develop the fundamental scientific understanding of active knit actuation architectures to enable the design, analysis, and synthesis of simultaneous large force and strain actuators that produce complex three-dimensionally distributed actuation motions in a compact package. The knowledge base that resulted from this work can be used not only to develop an actuators to meet specific kinematic and kinetic application specifications, but it sets the

foundation to thoroughly explore the design space for a new actuation architecture that can meet a variety of actuation needs. This dissertation shares the active knit architecture as a promising solution to the ever increasing demand for enhanced actuators. The novel active knit actuation architecture may enable advancements in current applications, as well as open the door to applications not yet imagined.

REFERENCES

[1] NASA Fact Sheet: Opening the Door to a New Era in Flight, FS-2001-04-63-LaRC, NASA Langley Research Center.

[2] Reich, G., Sanders, B., 2007, "Introduction to Morphing Aircraft Research," Journal of Aircraft, 44(4), pp. 1059.

[3] Rodriguez, A. R., 2007, "Morphing Aircraft Technology Survey," AIAA Aerospace Sciences Meeting and Exhibit, 1258, pp.1-16.

[4] McKnight, G., Doty, R., Keefe, A., Herrera, G., Henry, C., 2010, "Segmented Reinforcement Variable Stiffness Materials for Reconfigurable Surfaces," Journal of Intelligent Material Systems and Structures, 21, pp. 1783-1793.

[5] Collis, S.S., Joslin, R.D., Seifert, A., and Theofilis, V., 2004, "Issues in Active Flow Control: Theory, Control, Simulation, and Experiment," Progress in Aerospace Science, 40, pp. 237–289.

[6] McLean, J.D., Crouch, J.D., Stoner, R.C., Sakurai, S., Seidel, G.E., Feifel, W.M., and Rush, H.M., 1999, "Study of the application of separation control by unsteady excitation to civil transport aircraft," NASA Technical report CR–1999–209338.

[7] Milholen, W.E., Owens, L.R., 2005, "On the application of contour bumps for transonic drag reduction," AIAA Aerospace Sciences Meeting and Exhibit, 462, pp. 1-12.

[8] Dearing, S., Lambert, S., and Morrison, J., 2007, "Flow Control with Active Dimples," Aeronautical Journal, 111, pp.705-714.

[9] Todoroki, A., Kumagai, K., Matsuzaki, R., 2009, "Self-deployable Space Structure using Partially Flexible CFRP with SMA wires," Journal of Intelligent Material Systems and Structures, 20, pp. 1415-1424.

[10] Ganesh Raja, M., Narayanan, S., 2009, "Simultaneous Optimization of Structure and Control of Smart Tensegrity Structures," Journal of Intelligent Material Systems and Structures, 20, pp. 109-117.

[11] Sofla, A.Y.N., Elzey, D.M., Wadley, H.N.G., 2007, "A rotational joint for shape morphing space truss structures," Smart Material and Structures, 16, pp. 1277-1284.

[12] Yoo, E., Roh, J., Han, J., 2007, "Wrinkling control of inflatable booms using shape memory alloy wires," Smart Materials and Structures, 16, pp. 340-348.

[13] Yoon, H., Washington, G., 2010, “An optimal method of shape control for deformable structures with an application to a mechanically reconfigurable reflector antenna,” Smart Materials and Structures, 19, pp. 1-9.

[14] Kiper, G., Soylemez, E., 2009, "Deployable Space Structures," International Conference on Recent Advances in Space Technologies, 4, pp.131-138.

[15] Ronert, M., Hofheinz, H., Manassa, E., Asgarouladi, H., Olbrisch, R., 2004, “The Beginning of a New Era in Tissue Expansion: Self-Filling Osmotic Tissue Expander-Four-Year Clinical Experience,” Plastic & Reconstructive Surgery, 114, pp.1025-1031.

[16] Veeramani, A.S., Buckner, G.D., Owen, S.B., Cook, R.C., Bolotin, G., 2008, “Modeling the dynamic behavior of a shape memory alloy actuated catheter,” Smart Materials and Structures, 17, pp. 1-14.

[17] Utter, B., Barnes, B., Luntz, J., Brei, D., Teitelbaum, D., Okawada, M., Miyasaka, E., 2010, “Design of an SMA Actuated Mechanotransductive Implant for Correcting Short Bowel Syndrome,” Proc. of ASME SMASIS, 1, pp. 875-892.

[18] Browne, A., Rober, K., Johnson, N., Brown, J., “Pivotally Deployable air dam utilizing active material actuation,” Patent 7,775,582 B2. 17 August 2010.

[19] Browne, A., Johnson, N., Sears, I., “On demand morphable automotive body moldings and surfaces,” Patent 7,252,313. 7 August 2007.

[20] Palley, I., Nanying, J., Pulver, R., Trask, C., 2003, “Mechanisms of passenger kinetic energy absorption during collision and role of SECURUS fiber,” SAE Transactions, 112, pp. 498-506.

[21] Huber, J., Fleck, N., and Ashby, M., 1997, “The selection of mechanical actuators based on performance indices,” Proc. R. Soc. London A, 453, pp. 2185-2205.

[22] Wada, T., Lee, C. C.,Chen, H. H., Kusaka, M., and Taya, M., 2003, "Design of Spring Actuators made of Ferromagnetic Shape Memory Alloys and Composites", Proc. of SPIE, 5054, pp. 125-134.

[23] Sutou, Y., Oikawa, K., Kainuma, R., Ishida, K., and Taya, M., 2003, "Martensitic Transformation behavior under magnetic field of Co-Ni-Al Ferromagnetic Shape Memory Alloys", Proc. of SPIE, 5053, pp. 159-168.

[24] Liang, Y., Taya, M., and Kuga, Y., 2003, "Design of Diaphragm actuator based on Ferromagnetic Shape Memory Alloy Composite", Proc. of SPIE, 45, pp. 45-52.

[25] Taya, M., Wada, T., Lee, C.C., 2004,"Design of Torque actuators based on ferromagnetic shape memory alloy composites," Proc. of SPIE, 5390, pp. 309-316.

[26] Spinks, G.M., Wallace, G.G., Ding, J., Dezhi, Z., Xia, B., Scott, T., and Truong, V., 2003, “Electroactive Polymer Actuator Devices (EAPAD).” Proc. of SPIE, 5051, pp. 21-28.

[27] Metz, P., Alici, G., and Spinks, G., 2006, “A finite element model for bending behaviour of conducting polymer electromechanical actuators.” Sensors and Actuators A: Physical, 130-131, pp. 1-11.

[28] Alici, G., and Huynh, N.M., 2006, “Predicting force outputs of trilayer polymer actuators.” Sensors and Actuators A: Physical, 132, pp. 616-625.

[29] Fernandez, D., Moreno, L., and Baselga, J., 2005, “A bioinspired EAP actuator design methodology,” Proc. of SPIE, 5759, pp. 361-370.

[30] Bar-Cohen, Y., Sherritl, S., and Lih, S., 2001 “Characterization of the Electromechanical Properties of EAP materials,” Proc. of SPIE, 4329, pp. 319-327.

[31] Bar-Cohen, Y., 2002, “Electro-active polymers: current capabilities and challenges,” Proc. of SPIE, 4695, pp.1-7.

[32] Park, J., Carman, G. P., Thomas Hahn, H., 2000, ‘‘Design and Testing of a Mesoscale Piezoelectric Inchworm Actuator with Microridges,’’ Journal of Intelligent Material Systems and Structures, 11, pp. 671–684.

[33] Uchino, K., 1998, “Piezoelectric ultrasonic motors: overview,” Smart Materials and Structures, 7, pp. 273-285.

[34] Wallaschek, J., 1995, “Piezoelectric Ultrasonic Motors,” Journal of Intelligent Material Systems and Structures, 6, pp. 71-83.

[35] Mitrovic, M., Carman, G., Straub, F., 1999, “Electromechanical characterization of piezoelectric stack actuators,” Proc. SPIE, 3668, pp. 586-601.

[36] Carpi, F., Salaris, C., De Rossi, D., 2007, “Folded dielectric elastomer actuators,” Smart Materials and Structures, 16, pp. S300-S305.

[37] Barnes, B., Brei, D., Luntz, J., Strom, K., Browne, A., Johnson, N., 2008, “Shape memory alloy resettable spring lift for pedestrian protection,” Proc. SPIE, 6930, pp. 1-13.

[38] Ervin, J.D. and Brei, D., 1998, ‘‘Recurve Piezoelectricstrain- Amplifying Actuator Architecture,’’ IEEE/ASME Transactions on Mechatronics, 3, pp. 293–301.

[39] Moskalik, A.J., Brei, D., 1998, ‘‘Parametric Investigation of the Deflection Performance of Serial Piezoelectric Cblock Actuators,’’ Journal of Intelligent Material Systems and Structures, 9, pp. 223–231.

[40] Onitsuka, K., Dogan, A., Tressler, J.F., Xu, Q., Yoshikawa, S., Newnham, R.E., 1995, ‘‘Metal-ceramic Composite Transducer, the ‘Moonie’,’’ Journal of Intelligent Material Systems and Structures, 6, pp. 447–455.

[41] Dogan, A., Fernandez, J.F., Uchino, K., Newnham, R.E., 1996, ‘’’Cymbal’ Electromechanical Actuator,’’ Proc. IEEE International Symposium on Applications of Ferroelectrics, 1, pp. 213–216.

[42] Hall, S.R., Tzianetopoulou, T., Straub, F., and Ngo, H., 2000, ‘‘Design and Testing of a Double X-frame Piezoelectric Actuator,’’ Proc. of SPIE, 3985, pp. 26–37.

[43] Carpi, F., Rossi, D., Kornbluh, R., “Dielectric Elastomers as Electromechanical Transducers: Fundamentals, Materials, Devices, Models and Applications of an Emerging Electroactive Polymer Technology," Elsevier, 2008.

[44] Canfield, S., Frecker, M., 2000, “Topology optimization of compliant mechanical amplifiers for piezoelectric actuators,” Structural and Multidisciplinary Optimization, 20, pp. 269-279.

[45] Ramrakhyani, D.S., Lesieutre, G. A., Frecker M., Bharti S., 2005, “Aircraft Structural Morphing Using Tendon-Actuated Compliant Cellular Trussess.” Journal of Aircraft, 42, pp. 1615-1621.

[46] Bharti, S., Frecker, M., 2007, “Compliant Mechanical Amplifier Design using Multiple Optimally Placed Actuators,” Journal of Intelligent Material Systems and Structures, 18, pp. 209-217.

[47] Johnson, T., Frecker, M., Abdalla, M., Gurdal, Z., Lindner, D., 2009, "Nonlinear Analysis and Optimization of Diamond Cell Morphing Wings," Journal of Intelligent Material Systems and Structures, 20, pp. 815-824.

[48] Lee, H.J., Lee, J.J., 2000, "Evaluation of the characteristics of a shape memory alloy spring actuators," Smart Materials and Structures, 9, pp. 817-823.

[49] Williams, K., Chiu, G., Bernhard, R., 2005, "Dynamic modelling of a shape memory alloy adaptive tuned vibration absorber," Journal of Sound and Vibration, 280, pp. 211-234.

[50] Reedlunn, B., Churchill, C., Nelson, E., Daly, S., Shaw, J., 2011, “Bending of Superelastic Shape Memory Allow Tubes,” Proc. of SMASIS, 1, pp. 249-258.

[51] Pei, Q., Posenthal, M., Stanford, S., Prahlad, H., Pelrine, R., 2004, "Multiple-degrees-of-freedom electroelastomer roll actuators," Smart Materials and Structures, 13, pp. N86-N92.

[52] Baz, A., Chen, T., Ro, J, 2000, “Shape Control of NITINOL - Reinforced Composite Beams,” Composites Part B, 31, pp. 631-642.

[53] Kugel, V.D., Chandran, S., Cross, L.E., 1997, ‘‘Comparative Analysis of Piezoelectric Bending-mode Actuators,” Proc. of SPIE, 3040, pp. 70-80.

[54] Jonnalagadda, K., Sottos, N. R., 2003, “Influence of Adhesion on Micromechanical Behavior of SMA Composites,” Proc. SPIE, 2442, pp. 143-151.

[55] Choi, S., Lee, J.J., 1998, "The shape control of a composite beam with embedded shape memory alloy wire actuators," Smart Materials and Structures, 7. pp. 759-770.

[56] Williams, R.B., Park, G., Inman, D., Wilkie, W., 2002, "An overview of composite actuators with piezoceramic fibers," Proceeding of IMAC, pp. 421-427.

[57] Pulliam, W., McKnight, G., Carman, G., 2002, “Recent advances in magnetostrictive particulate composite technology,” Proc. of SPIE, 4698, pp. 271-281.

[58] Alexander, P., Brei, D., Halloran, J., 2007, "DEPP functionally graded piezoceramics via micro-fabrication by co-extrusion," Journal of Materials Science, 42, pp. 5805-5814.

[59] Huang, W., Lee, C., Teo, H., 2006, "Thermomechanical Behavior of a Polyurethane Shape Memory Polymer Foam," Journal of Intelligent Material Systems and Structures, 17, pp. 753-760.

[60] Shaw, J., Michailidis, P., Triantafyllidis, N., Grummon, D., 2009, “Superelasticity, Shape Memeory and Stability of Nitinol Honeycombs under In-plane Compression," MRS Proceedings, 1188-LL05-04.

[61] Postle, R., Munden, DL., 1967, “Analysis of the dry-relaxed knitted loop configuration – Part II: three-dimensional analysis.” J Text Inst, 58(8), pp. 352-65.

[62] Postle, R., Munden, DL, 1967, “Analysis of the dry relaxed knitted loop configuration – Part I: two-dimensional analysis.” J Text Inst, 58(8), pp. 329-51.

[63] Leaf, GAV, 1960, “Models of the plain- knitted loop,” J Text Inst, 51(2), pp. T49-58.

[64] Leaf, GAV, Glaskin, A., 1953, “The geometry of a plain knitted loop,” J Text Inst, 44(8), pp. T587-605.

[65] Peirce, FT., 1947, “Geometrical principles applicable to the design of functional fabrics,” J Text Inst, 17(3), pp. 123-47.

[66] Hearle, J. W. S., Grosberg, P. & Backer, S., *Structural Mechanics of Fibers, Yarns, and fabrics.* Wiley Interscience, New York, 1969, pp. 80.

[67] Peirce, F.T., 1937, “The Geometry of Cloth Structure,” J Textile Inst, 28 (3), pp. T45-96.

[68] Munden, DL, 1959, “The geometry and dimensional properties of plain-knit fabrics,” J Text Inst, 50, pp. T448-71.

[69] Smirfitt, JA., 1965, “Worsted 1x1 rib fabrics – Part I: dimensional properties” J Text Inst, 56, pp. T248-59.

[70] de Jong, S., Postle, R., 1977, “Energy analysis of knitted-fabric mechanics by means of optimal control theory – Part I: the nature of loop-interlocking in the plain-knitted structure,” J Text Inst, 68(10), pp. 307-15.

[71] de Jong, S., Postle, R. 1977, “Energy analysis of knitted-fabric mechanics by means of optimal control theory – Part II: relaxed-fabric dimensions and tensile properties of the plain-knitted structure,” J Text Inst., 68(10), pp. 316-23.

[72] de Jong, S., Postle, R., 1977, “Energy analysis of knitted-fabric mechanics by means of optimal control theory – Part III: the 1x1 rib-knitted structure,” J Text Inst, 68(10), pp. 324-9.

[73] Shanahan, WJ, Postle, R.,1974, "A theoretical analysis of the tensile properties of plain-knitted fabrics – Part I: the load-extension curve for fabric extension parallel to the courses," J Text Inst, 65, pp. 200-12.

[74] Hong, H., de Araujo, M.D., Rangueiro, R., and Ciobanu, O., 2002, "Theoretical Analysis of Load-Extension Properties of Plain Weft Knits Made from High Performance Yarns for Composite Reinforcement," Textile Research Journal, 72(11), pp. 991-995.

[75] Padaki, N. V., Alagirusamy, R., Sugun, B.S., 2006, "Knitted Preforms for Composite Applications," Journal of Industrial Textiles, 35(4), pp. 295-321

[76] Love, A., "A treatise on the mathematical theory of elasticity," Cambridge, University Press, 1927.

[77] Ramakrishna, S., 1997, "Characterization and modeling of the tensile properties of plain weft-knit fabric reinforced composites" Composite Science and Technology, 57, pp. 1-22.

[78] Leong, K. H., Ramakrishna, S., Huang, Z. M., Bibo, G. A., 2000, "The potential of knitting for engineering composites – a review," Composites: Part A, 31, pp. 197-220.

[79] Wu, WL, Hamada, H., Kotaki, M., Maekawa, Z., 1995, "Design of knitted fabric reinforced composites," J Reinf Plast Comp, 14, pp. 786-98.

[80] Huang, Z.M., Ramakrishna, S., Leong, K.H., 2002, "Modeling the Tensile Behavior of Milano Rib Knit Fabric Composites," Journal of Reinforced Plastics and Composites, 21(12), pp. 1123-1146.

[81] Luo, Y., Verpoest, I., 2002, "Biaxial tension and ultimate deformation of knitted fabric reinforcements," Composites: Part A, 33, pp. 197-203.

[82] Venkat Rao, M., Mahajan, P., Mittal, R.K., 2008, "Effect of architecture on mechanical properties of carbon/carbon composites," Composite Structures 83, pp. 131–142.

[83] Takano, N., Yasutomo, U., Kashiwagi, Y., Zako, M., 1999, "Hierarchical modelling of textile composite materials and structures by the homogenization method" Modelling Simul. Mater. Sci. Eng., 7, pp. 207-231.

[84] Kononova, O., Krasnikovs, A., Dzelzitis, K., Kharkova, G., Vagel, A., Eiduks, M., 2011, "Modelling and experimental verification of mechanical properties of cotton knitted fabric composites," Estonian Journal of Engineering, 17, pp. 39–50.

[85] Lim, T., 2003, "A three-level hierarchal approach in modeling sheet thermoforming of knitted-fabric composites," International Journal of Mechanical Sciences, 45, pp. 1097-1117.

[86] Lomov, S.V., Huysmans, G., Verpoest, I., 2001, "Hierarchy of Textile Structures and Architecture of Fabric Geometric Models," Textile Research Journal, 71, pp. 534-543.

[87] Dynalloy inc., "Specs on various sizes of Flexinol®," http://www.dynalloy.com/pdfs/MWPBv4.00_FlexSpecs.pdf, 5/26/2009.

[88] Shaw, J. 2002, "A thermomechanical model for a 1-D shape memory alloy wire with propagating instabilities" International Journal of Solids and Structures 39 (2002) pp. 1275–1305

[89] Weber, R.L., Manning, K.V.; White, M.W. *College Physics- 4th Edition*. USA: McGraw-Hill, 1965: pp. 66.

[90] Engineer's Handbook, "Coefficient of Friction Reference Table" http://www.engineershandbook.com/Tables/friction coefficients.htm,5/24/2006.

[91] Barber, J.R. Intermediate Mechanics of Materials. McGraw-Hill Higher Education, 2001.

[92] Churchill, C.,B., Shaw, J.,A., Iadicola, M.A., 2010, "Tips and Tricks for Characterizing Shape Memory Alloy Wire: Part 4 – Thermo-mechanical Coupling," Experimental Techniques, 34(2), pp. 63-80.

[93] An, A., Ryu, J., Cho, M., Cho, K., 2012, "Engineering design framework for a shape memory alloy coil spring actuator using a static two-state model," Smart Materials and Structures, 21, pp. 1-16.

[94] Churchill, C. Shaw, J., 2008, "Shakedown Response of Conditioned Shape Memory Alloy Wire," Proc. of SPIE, 6929, pp.1-12.

[95] Collis, S.S., Joslin, R.D., Seifert, A., Theofilis, V., 2004, "Issues in Active Flow Control: Theory, Control, Simulation, and Experiment," Progress in Aerospace Science, 40, pp. 237–289.

[96] McLean, J.D., Crouch, J.D., Stoner, R.C., Sakurai, S., Seidel, G.E., Feifel, W.M., Rush, H.M., 1999, "Study of the application of separation control by unsteady excitation to civil transport aircraft," NASA Technical report CR–1999–209338.

[97] Smith, B.L., Glezer, A., 1998, "The formation and evolution of synthetic jets," Physics of Fluids, 10, pp. 2281–2297.

[98] Cattafesta, L.N., Garg, S., Shukla, D., 2001, "Development of Piezoelectric Actuators for Active Flow Control," AIAA, 39, pp. 1562-1568.

[99] Crook, A., Sadri, A.M., Wood, N.J., 1999, "The Development and Implementation of Synthetic Jets for the Control of Separated Flow", AIAA, 99–3176, pp. 1-11.

[100] Rathnasingham, R., Breuer, K.S., 1997, "System Identification and Active Control of a Turbulent Boundary Layer", PhD Thesis, MIT.

[101] Milholen, W.E., Owens, L.R., 2005, "On the application of contour bumps for transonic drag reduction," AIAA, 2005-462, pp. 1-19.

[102] Dearing, S., Lambert, S., Morrison, J., 2007, "Flow Control With Active Dimples," Aeronautical Journal, 111, pp.705-714.

[103] Udovidchik, N.., Morrison, J., 2006, "Investigation of Active Dimple Actuators for Separation Control," AIAA, 2006-3182, pp. 1-9.

[104] Wadsworth, D.C., Muntz, E.P., Blackwelder, R.F., Shiflett, G.R, 1993, "Transient Energy Release Pressure Driven Microactuators for Control of Wall-Bounded Turbulent Flows," AIAA, 93-3271, pp. 1-15.

[105] Anderson, J.D., 2001, "Fundamentals of Aerodynamics," McGraw Hill Publishers.

[106] Miller, J., 2005, "Lockheed Martin F/A-22 Raptor, Stealth Fighter," Aerofax Aviation Books.

[107] Abel, J., Luntz, J., Brei, D, 2009, "Two-Dimensional Analytical Model and Experimental Validation of Garter Stitch Knitted Shape Memory Alloy Actuator Architecture," Proc. of ASME SMASIS, 1426, pp. 1-16.

[108] Shaw, J, Kyriakides, S, "Thermomechanical aspects of NiTi," Journal of the Mechanics and Physics of Solids, vol. 43, no. 8, pp. 1243-1281, 1995.